



---

SCHOOL OF ENGINEERING

**Project Technical Report:  
Modelling CO<sub>2</sub> Decomposition In A  
Surface-Confined Plasma Reactor**

Name: Uzair Abdullah

Student ID: u2103892

Module: ES327 Individual Project

Supervisor: Prof. Evgeny Rebrov

**School of Engineering**

University of Warwick

2024-2025

---

## Abstract

Plasma technology for CO<sub>2</sub> conversion is gaining traction due to its ability to operate under mild conditions, such as room temperature and atmospheric pressure, and effectively utilise intermittent renewable energy. Plasma, an ionised gas composed of electrons, ions, and both excited and neutral molecules, creates a reactive environment ideal for converting inert CO<sub>2</sub>, particularly when confined to a surface by an applied electric field, which enhances density and reactivity. This project used Fortran-based scientific computing to develop a comprehensive model of CO<sub>2</sub> decomposition in a surface-confined plasma reactor, systematically investigating key design parameters such as electrode configuration, gas flow rates, and AC supply characteristics to capture transient reactive species and complex reaction kinetics. Findings indicate that optimising operational parameters, notably higher AC voltages, tailored frequency settings, and precise electrode geometry control, can significantly improve conversion rates and energy efficiency, though further advances in material durability and reactor scalability are needed. Overall, the model offers practical guidance for refining plasma-assisted CO<sub>2</sub> conversion processes and lays a robust foundation for sustainable industrial applications.

---

## Acknowledgments

*I would like to express my deepest gratitude to my Project Supervisors, Professor Evgeny Rebrov, Dr Nima Pourali, and Dr Pradeep Lamichhane, for their unwavering support, encouragement, and invaluable guidance throughout this project. Their expertise, insightful advice, and constructive feedback have been instrumental in shaping the direction and outcomes of my research. Their enthusiasm for advancing the field of plasma-assisted gas decomposition has been a constant source of inspiration.*

*I want to personally acknowledge Professor Rebrov for providing critical insights into the theoretical and computational aspects of the project, as well as ensuring I had access to the necessary resources and reading materials. Our meetings were a constant source of crucial guidance and cheerful motivation, unexpectedly re-igniting a deep passion for physical chemistry and plasma physics. His patience in explaining complex concepts and his unwavering support throughout the research process were invaluable. I am deeply grateful for his mentorship, which not only enhanced my understanding of the subject matter but also inspired me to pursue further exploration in this fascinating field.*

*Furthermore, I would like to sincerely thank Dr. Peter Brommer for sparking my interest in scientific computing and inspiring me to explore the computational tools and methodologies underpinning this project. His influence has significantly shaped my academic journey and my passion for applying computational techniques to solve complex problems.*

*This project is dedicated to the ongoing pursuit of sustainable technologies and innovative solutions to combat climate change. I hope that the insights gained from this research will contribute meaningfully to the advancement of plasma-based carbon conversion and inspire future efforts in creating a more sustainable world.*

---

## Program Instructions

### Installation

#### Fortran

Ensure that **gfortran** is installed on the machine.

```
gfortran --version
```

If it is not, follow the instructions on the Fortran website.

[https://fortran-lang.org/learn/os\\_setup/install\\_gfortran](https://fortran-lang.org/learn/os_setup/install_gfortran)

### Program

Ensure that the files **2103892\_ES327\_Code.f90**, **CO2Modelling**, **CO2ratesF.dat**, **CO2ratesB.dat**, **O2ratesF.dat**, and **O2ratesB.dat** are downloaded to the preferred working directory.

If downloading via web browser, right-click the file link and choose “Save As...” then select the desired folder.

## Setting Up

### Open the Terminal

On **macOS** or **Linux**, open the “Terminal” application.

On **Windows**, open “Command Prompt”, “PowerShell”, or a terminal provided by the Fortran environment (such as Git Bash or the MinGW terminal).

### Navigate to working directory

```
cd ~/ProjectDirectory
```

## Running the Program

### Compile the Fortran code (Optional)

```
gfortran 2103892_ES327_Code.f90 -o CO2modelling
```

### Run the Program

```
./CO2modelling
```

### Verify Output (Optional)

List the directory contents and find **plotdata.dat**.

```
ls
```

---

## Abbreviations

### Environmental

Bio-Energy with Carbon Capture and Storage	BECCS
Carbon Capture, Utilisation, and Storage	CCUS
Direct Air Carbon Capture and Storage	DACCS
Greenhouse Gas	GHG

### Mathematics

Zero-Dimensional	0D
Ordinary Differential Equation	ODE
Partial Differential Equation	PDE
Fourth-Order Runge-Kutta	RK4

### Physics

Alternating Current	AC
Dielectric Barrier Discharge	DBD
Direct Current	DC
Electron Energy Distribution Function	EEDF
Non-thermal Plasma	NTP
Optical Emission Spectroscopy	OES
Specific Energy Input	SEI
Vibrational-Translational	VT
Vibrational-Vibrational	VV

### Financial & Markets

Enhanced Oil Recovery	EOR
Capital Expenditures	CAPEX
Operational Expenditures	OPEX

---

# Project Logbook Link

[https://livewarwickac-my.sharepoint.com/:f/:r/personal/u2103892\\_live\\_warwick\\_ac\\_uk/Documents/ES327\\_2103892\\_Logbook\\_2024-25?csf=1&web=1&e=cefxbZ](https://livewarwickac-my.sharepoint.com/:f/:r/personal/u2103892_live_warwick_ac_uk/Documents/ES327_2103892_Logbook_2024-25?csf=1&web=1&e=cefxbZ)

## Contents

<b>Abstract</b>	<b>i</b>
<b>Acknowledgments</b>	<b>ii</b>
<b>Program Instructions</b>	<b>iii</b>
<b>Abbreviations</b>	<b>iv</b>
<b>List of Figures</b>	<b>vii</b>
<b>List of Tables</b>	<b>vii</b>
<b>1 Introduction</b>	<b>1</b>
<b>2 Literature Review</b>	<b>3</b>
2.1 Sources of Carbon Dioxide . . . . .	3
2.1.1 Direct Air Carbon Capture and Storage . . . . .	3
2.1.2 Bio-Energy with Carbon Capture and Storage . . . . .	4
2.1.3 Opportunities for CO <sub>2</sub> Utilisation . . . . .	4
2.2 Techniques for CO <sub>2</sub> Decomposition . . . . .	5
2.2.1 Thermochemical Methods . . . . .	5
2.2.2 Photochemical Methods . . . . .	5
2.2.3 Electrochemical Methods . . . . .	6
2.2.4 Plasma-Chemical Methods . . . . .	7
2.2.5 Comparative Analysis . . . . .	7
2.3 The Dielectric Barrier Discharge Reactor . . . . .	7
2.3.1 Key Reactor Components . . . . .	8
2.3.2 Operating Principle . . . . .	9
2.3.3 Reactor Configurations . . . . .	9
2.3.4 Mechanisms . . . . .	9
2.3.5 Applications in CO <sub>2</sub> Decomposition . . . . .	10
2.4 Financial Analysis . . . . .	11
2.4.1 Current Industrial Methods . . . . .	11
2.4.2 Challenges and Opportunities . . . . .	13
2.4.3 Plasma-Based CO <sub>2</sub> Decomposition . . . . .	13
2.4.4 The Value of CO . . . . .	15

---

2.4.5	Economic Viability & Future Directions . . . . .	15
2.5	The Problem . . . . .	16
<b>3</b>	<b>Methodology</b>	<b>17</b>
3.1	Non-thermal Plasma Chemistry . . . . .	17
3.1.1	Reactions & Species . . . . .	17
3.1.2	Reversibility and Equilibrium Considerations . . . . .	18
3.2	Mathematical Modelling . . . . .	19
3.2.1	Numerical Methods . . . . .	19
3.2.2	Reaction Kinetics . . . . .	20
3.3	Computational Implementation . . . . .	26
3.3.1	Program Design . . . . .	26
3.3.2	Simplified Model . . . . .	27
<b>4</b>	<b>Results &amp; Analysis</b>	<b>29</b>
4.1	Plasma Composition . . . . .	29
4.2	Parametric Studies . . . . .	30
4.2.1	Pressure Variation . . . . .	30
4.2.2	Electrode Gap Variation . . . . .	31
4.2.3	Volumetric Flow Rate Variation . . . . .	32
4.2.4	AC Voltage Variation . . . . .	33
4.2.5	AC Frequency Variation . . . . .	34
4.3	Production Rates and Energy Efficiency . . . . .	35
4.4	Technical Analysis . . . . .	36
<b>5</b>	<b>Conclusion</b>	<b>37</b>
<b>A Appendices</b>		<b>I</b>
<b>A Financial</b>		<b>I</b>
<b>B Derivations</b>		<b>II</b>
B.1	Electrodynamics . . . . .	II
B.2	Thermal-Energy Balance . . . . .	IV
<b>C Supplementary Results</b>		<b>VII</b>
C.1	Reduced Electric Field and SEI . . . . .	VII
<b>D Code</b>		<b>IX</b>
D.1	Diagram . . . . .	IX
D.2	Listings . . . . .	X

---

## List of Figures

1.1	Atmospheric CO <sub>2</sub> concentration in parts per million . . . . .	1
1.2	Average CO <sub>2</sub> intensity of global electricity generation . . . . .	2
2.1	Illustration of the DACCS process . . . . .	3
2.2	Illustration of the BECCS process . . . . .	4
2.3	Photochemical decomposition of CO <sub>2</sub> with Triethanolamine . . . . .	6
2.4	Electrochemical reduction of CO <sub>2</sub> to formic acid . . . . .	6
2.5	DBD non-thermal plasma reactor high-voltage electrode . . . . .	7
2.6	Cylindrical DBD non-thermal plasma reactor . . . . .	8
2.7	Annual CO <sub>2</sub> utilisation, products, and downstream applications . . . . .	11
2.8	The Fischer-Tropsch process . . . . .	15
3.1	Evolution of the $\frac{E}{N}$ and temperatures, with spikes of $T_{\text{exc}}$ at DBDs . . . . .	21
3.2	Evolution of $V_{\text{input}}$ and $I_{\text{input}}$ . . . . .	22
3.3	Normalised species concentration evolution for a simplified model . . . . .	27
4.1	Normalised species concentration evolution for a complex model . . . . .	30
4.2	Effects of pressure change on the formation of O <sub>2</sub> from CO <sub>2</sub> . . . . .	31
4.3	Effects of pressure change on the formation of CO from CO <sub>2</sub> . . . . .	31
4.4	Effects of electrode gap change on the formation of CO from CO <sub>2</sub> . . . . .	32
4.5	Effects of electrode gap change on the formation of O <sub>2</sub> from CO <sub>2</sub> . . . . .	32
4.6	Effects of volumetric CO <sub>2</sub> flow rate $\dot{V}$ on the formation of CO from CO <sub>2</sub> . . . . .	33
4.7	Effects of AC supply voltage change on the formation of CO from CO <sub>2</sub> . . . . .	34
4.8	Effects of AC supply frequency change on the formation of CO from CO <sub>2</sub> . . . . .	34
4.9	Production rates for species of interest compared to power input efficiency . . . . .	35
C.1	Effects of electrode gap change on the reduced electric field $\frac{E}{N}$ and SEI . . . . .	VII
C.2	Effects of electrode gap change on the reduced electric field $\frac{E}{N}$ and SEI . . . . .	VII
C.3	Effects of volumetric CO <sub>2</sub> flow rate $\dot{V}$ change on specific energy input SEI . . . . .	VII
C.4	Effects of AC supply voltage change on the reduced electric field $\frac{E}{N}$ and SEI . . . . .	VIII
C.5	Effects of AC supply frequency change on the reduced electric field $\frac{E}{N}$ and SEI . . . . .	VIII
D.1	Flow diagram showing the program structure . . . . .	IX

## List of Tables

2.1	Financial summary of industrial CO <sub>2</sub> decomposition techniques . . . . .	13
2.2	Financial summary of DBD plasma-based CO <sub>2</sub> decomposition . . . . .	14
3.1	Species in the complex model . . . . .	18
3.2	Reaction profile of the complex model . . . . .	18
3.3	List of key constants, parameters, and variables . . . . .	20
3.4	Species in a simplified model . . . . .	28
3.5	Reaction profile of a simplified model . . . . .	28
4.1	Initial baseline conditions for model testing . . . . .	29
A.1	Financial summary of EOR . . . . .	I
A.2	Financial summary of chemical conversion . . . . .	I
A.3	Financial summary of biological conversion . . . . .	I
A.4	Financial summary of mineralisation . . . . .	I

---

## 1 Introduction

The global environment is in crisis due to rising greenhouse gas (GHG) emissions from human activities like fossil fuel combustion and deforestation, disrupting Earth's carbon cycle. Carbon dioxide ( $\text{CO}_2$ ), now exceeding 420 parts per million, accounts for 75% of anthropogenic GHG emissions [1], intensifying the greenhouse effect and causing rising temperatures, melting ice caps, ocean acidification, biodiversity loss, and extreme weather. Without swift intervention, these impacts may become irreversible, threatening ecosystems, economies, and livelihoods.

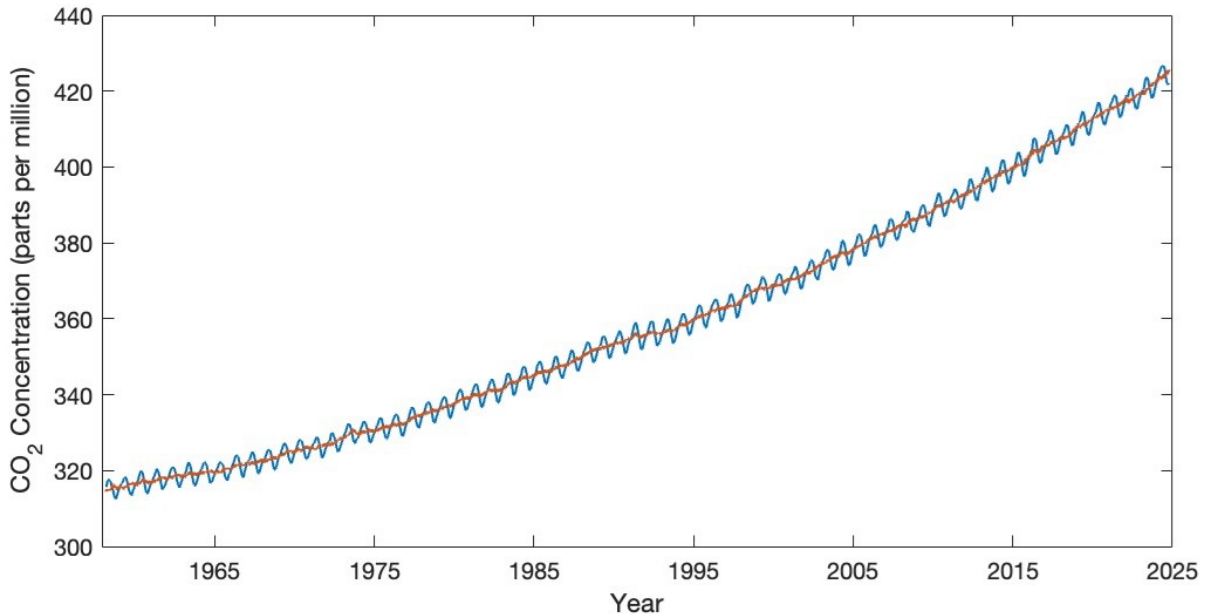


Figure 1.1: Atmospheric CO<sub>2</sub> concentration in parts per million, adapted from [1]

Efforts to combat this crisis intensified with the 2015 Paris Agreement, where nearly 200 countries committed to limiting global temperature increases to below 2°C, aiming for 1.5°C. Nationally determined contributions focus on renewable energy, efficiency, and innovative technologies, however, current commitments are insufficient, requiring more ambitious targets and rapid adoption of low-carbon solutions from industry [2].

The UK leads with a legally binding Net Zero goal by 2050, targeting a 68% emissions reduction by 2030 and 78% by 2035, relative to 1990 levels [3]. The UK's Industrial Decarbonisation Strategy emphasises reducing emissions in energy-intensive sectors using electrification, hydrogen, and Carbon Capture, Utilisation, and Storage (CCUS) [4]. Beyond environmental goals, this strategy addresses economic concerns by fostering green innovation to retain industries domestically and create opportunities for reshoring outsourced manufacturing.

Among emerging technologies, plasma-assisted CO<sub>2</sub> decomposition offers promise. Dielectric barrier discharge (DBD) reactors enable efficient decarbonisation of hard-to-electrify industries. Operating under non-equilibrium conditions, these reactors use energetic electrons to dissociate CO<sub>2</sub> without heating the bulk gas, requiring far less energy than traditional thermal methods.

---

Additionally, they produce valuable by-products like carbon monoxide (CO) and oxygen (O<sub>2</sub>), which can be used for synthetic fuels and materials [5].

However, the complexity of non-thermal plasma (NTP) environments, including electron-molecule interactions and chemical reaction pathways, necessitates advanced computational tools. Zero-dimensional (0D) time-dependent models efficiently capture the temporal evolution of plasma reactions, enabling parameter optimisation such as plasma density, electrode geometry, and specific energy input to maximise CO<sub>2</sub> conversion while minimising energy use [6].

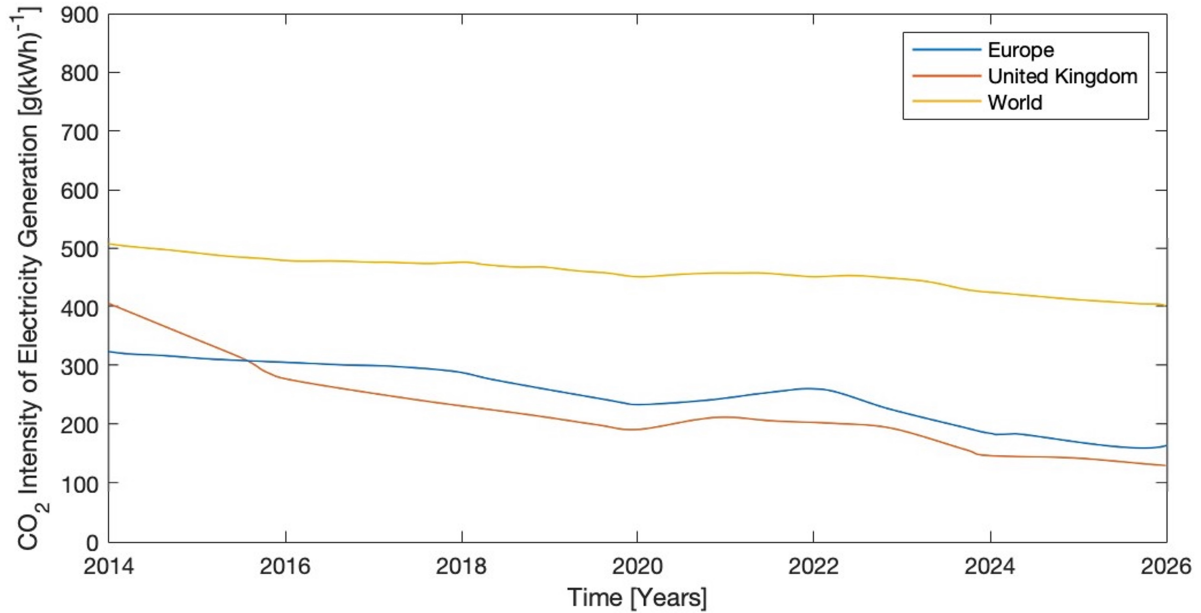


Figure 1.2: Average CO<sub>2</sub> intensity of global electricity generation, adapted from [5].

This study examines the influence of various process parameters, such as pressure, volume, and gas flow rate, on the conversion of CO<sub>2</sub> in surface-confined DBD plasma reactors. Central to this investigation is the development of a computational model in Fortran, which integrates both a kinetic model and a DBD plasma model. By utilising chemical kinetics, the study provides a detailed analysis of energy distributions across translational, rotational, and vibrational modes, thereby yielding valuable insights into optimising reactor performance to achieve high conversion rates with minimal energy consumption. This approach aims to bridge the current experimental gap in understanding the input–output relationships in DBD plasma decomposition processes, ultimately paving the way for an open-source tool to simulate reactions.

Academically, this study deepens the understanding of plasma-assisted CO<sub>2</sub> decomposition by elucidating the effects of key parameters on conversion efficiency and energy input. From an industrial perspective, it informs the design of energy-efficient NTP reactors that support the UK's decarbonisation agenda, thereby fostering innovation in domestic manufacturing and reshoring opportunities [3]. On a global scale, it offers a transformative pathway towards sustainable carbon management, contributing to the advancement of a circular economy and the transition to a low-carbon future.

## 2 Literature Review

### 2.1 Sources of Carbon Dioxide

#### 2.1.1 Direct Air Carbon Capture and Storage

Direct Air Carbon Capture and Storage (DACCs) is a cutting-edge technology designed to capture CO<sub>2</sub> from ambient air. This process typically involves using solid sorbents or liquid solvents that bind to CO<sub>2</sub> in air. Once saturated, the sorbent or solvent is regenerated through heating or pressure changes, releasing a concentrated stream of CO<sub>2</sub>. This purified CO<sub>2</sub> can be compressed and transported for either geological storage or industrial utilisation [7].

DACCs presents several key advantages. It primarily offers remarkable flexibility in deployment, as DACCs systems can be set up in various locations, independent of their proximity to CO<sub>2</sub> emission sources. This versatility allows them to operate effectively in regions rich in renewable energy resources, driving down logistical costs. DACCs systems also produce high-purity outputs, with the concentrated CO<sub>2</sub> stream being of a quality suitable for a wide array of industrial applications or long-term storage solutions [4]. Lastly, there is considerable potential for renewable integration, as DACCs systems powered by renewable energy sources have a minimal carbon footprint, significantly enhancing their sustainability.

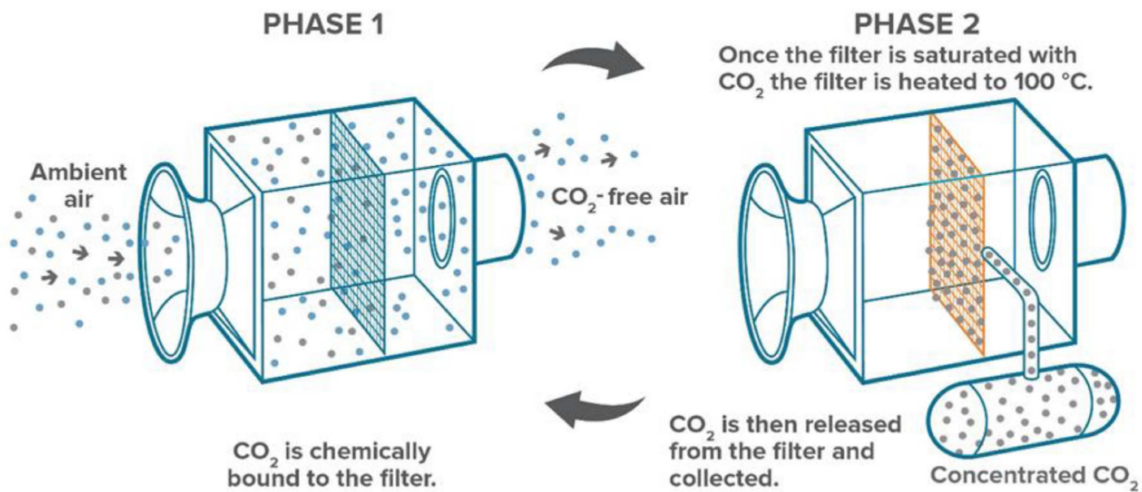


Figure 2.1: Illustration of the DACCs process, from [8]

However, the technology is not without its challenges. DACCs is energy-intensive, with current systems consuming between 1.0 and 2.0 MWh per tonne of CO<sub>2</sub> captured [5]. The financial cost of DACCs is estimated to range from £197.50 to £473.50 per tonne of CO<sub>2</sub> captured, depending on factors such as system efficiency, scale of deployment, and energy source. These costs remain a significant barrier to widespread adoption, although ongoing research aims to reduce these figures by improving efficiency and developing advanced materials. Despite the high costs, the market value of CO<sub>2</sub> can offset some expenses. Captured CO<sub>2</sub> is valued between £16.00 and £31.50 per tonne for enhanced oil recovery (EOR) applications, with higher valuation potential in speciality chemical markets [9].

### 2.1.2 Bio-Energy with Carbon Capture and Storage

Bio-Energy with Carbon Capture and Storage (BECCS) combines biomass energy production with CO<sub>2</sub> capture and storage, offering a dual benefit of renewable energy generation and negative emissions. Biomass, derived from sources such as agricultural residues, forestry by-products, or dedicated energy crops, is combusted or gasified to produce heat, electricity, or biofuels. During this process, CO<sub>2</sub> is captured before it is released into the atmosphere, resulting in a net-negative emission profile if the biomass feedstock is sustainably sourced [2].

Simultaneous energy production and CO<sub>2</sub> removal is the first key benefit of BECCS, as it provides a sustainable energy source while actively working to reduce atmospheric CO<sub>2</sub> levels. Secondly, BECCS utilises waste biomass, such as agricultural and forestry residues, as feedstock. This reduces land use competition and contributes to enhanced sustainability. Finally, BECCS allows for carbon sequestration, with captured CO<sub>2</sub> permanently stored in geological formations, ensuring long-term climate benefits.

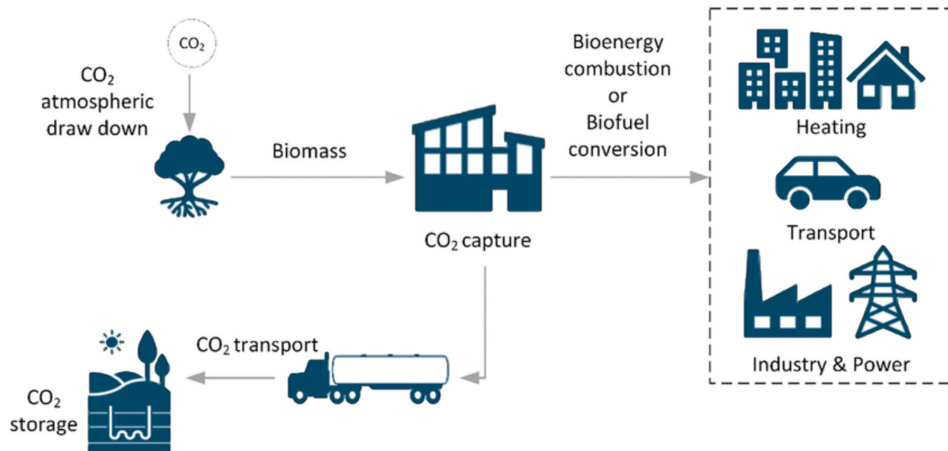


Figure 2.2: Illustration of the BECCS process, from [10]

Despite its potential, BECCS faces challenges related to land use, feedstock availability, and logistical complexities. Large-scale BECCS deployment could require significant land area for biomass cultivation, raising concerns about food security and biodiversity loss. Additionally, the cost of BECCS is estimated to range from £39.50 to £158.00 per tonne of CO<sub>2</sub> removed, with variations depending on feedstock type and capture efficiency [11]. The economic viability of BECCS is further influenced by the market value of CO<sub>2</sub>, as well as government incentives and carbon pricing mechanisms.

### 2.1.3 Opportunities for CO<sub>2</sub> Utilisation

The concentrated CO<sub>2</sub> streams produced by DACCS and BECCS are commonly compressed and injected into geological reservoirs for storage, ensuring long-term atmospheric removal. However, this approach lacks economic value, limiting its appeal to private investors. In contrast, CO<sub>2</sub> utilisation offers a pathway to generate value from captured CO<sub>2</sub>, enhancing the

---

economic viability of these technologies [12]. Plasma-based CO<sub>2</sub> conversion, a promising utilisation method, employs NTP to dissociate CO<sub>2</sub> into CO and O<sub>2</sub>, which can serve as feedstocks for synthetic fuels like methanol and valuable chemicals such as polymers. Plasma reactors provide unique advantages: they operate flexibly with variable electricity supplies, are catalyst-free, eliminating the need for expensive materials and offer scalability and modularity to meet diverse industrial demands.

Integrating plasma-based conversion with DACCS and BECCS could create synergistic systems capable of capturing, converting, and utilising CO<sub>2</sub>, thereby addressing challenges of cost, scalability, and energy efficiency. Captured CO<sub>2</sub>, valued at £16.00-£32.00 per tonne, can be converted into CO with a market value of approximately £316.00 per tonne [13], significantly enhancing the economic feasibility of these technologies. This integration not only supports broader decarbonisation goals but also provides compelling economic incentives for stakeholders, making plasma-based conversion a valuable complement to existing negative emission technology.

## 2.2 Techniques for CO<sub>2</sub> Decomposition

When comparing plasma-chemical methods to alternative or current technologies, thermochemical processes stand out for their effectiveness in large-scale applications but are hindered by their substantial energy demands. Electrochemical methods, on the other hand, provide moderate energy efficiency and operating conditions but are constrained by the reliance on expensive catalysts and concerns over long-term durability. Photochemical methods, though environmentally appealing due to their dependence on solar energy, are limited by their low conversion efficiencies and significant space requirements, making them less feasible for widespread application.

### 2.2.1 Thermochemical Methods

Thermochemical methods decompose CO<sub>2</sub> at high temperatures, typically between 500°C and 1,000°C. These processes are often employed in industrial operations where thermal energy, sourced from concentrated solar power or other energy inputs, facilitates the splitting of CO<sub>2</sub> into CO and O<sub>2</sub>.

Thermochemical methods are particularly effective for large-scale applications, achieving high conversion rates. This makes them suitable for industrial processes requiring significant CO<sub>2</sub> processing capacities. However, their high energy requirements limit their feasibility for smaller or decentralised applications [14]. Furthermore, the elevated temperatures necessary for these reactions demand robust reactor materials and significant energy investments, which may challenge their overall sustainability when not paired with renewable energy sources.

### 2.2.2 Photochemical Methods

Photochemical methods utilise sunlight as an energy source to activate catalysts, enabling the decomposition of CO<sub>2</sub> into CO and O<sub>2</sub> or other intermediates. These methods are considered environmentally friendly as they rely on renewable solar energy and do not require external

---

heating or electrical inputs.

Despite their sustainability, photochemical methods face critical limitations, including low conversion efficiencies and reliance on intermittent sunlight. Large surface areas are often required to capture sufficient solar energy, which poses challenges for scalability. Although research into advanced light-absorbing materials continues to improve the feasibility of photochemical methods, they remain largely uncompetitive with other approaches for large-scale, continuous CO<sub>2</sub> decomposition [15].

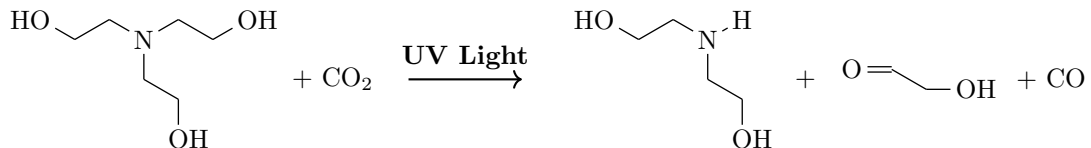


Figure 2.3: Photochemical decomposition of CO<sub>2</sub> with Triethanolamine

### 2.2.3 Electrochemical Methods

Electrochemical approaches involve the reduction of CO<sub>2</sub> into value-added products like CO or formic acid (HCOOH) using electricity as the driving force. These reactions occur under moderate conditions of temperature and pressure, and they rely on advanced electrode materials and catalysts to enable the conversion [16].

Electrochemical methods are advantageous for their ability to operate at lower temperatures compared to thermochemical methods, with the potential for integration into renewable electricity systems. However, their reliance on highly specialised and expensive catalysts, such as platinum or iridium, presents significant cost challenges. Furthermore, achieving high selectivity for specific CO<sub>2</sub> products, such as CO, remains an ongoing technical hurdle [17]. The long-term durability of electrochemical systems also requires further optimisation to enable scalability for industrial applications.

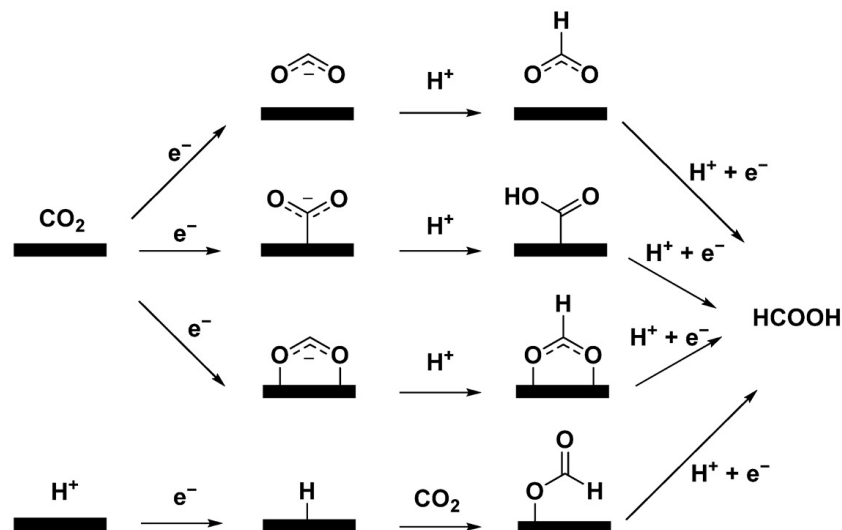


Figure 2.4: Electrochemical reduction of CO<sub>2</sub> to formic acid, from [18]

#### 2.2.4 Plasma-Chemical Methods

Plasma-chemical methods, particularly those involving NTP in DBD reactors, provide a novel approach to CO<sub>2</sub> decomposition. These systems operate at ambient temperatures and atmospheric pressure, offering a significant advantage over thermochemical and electrochemical processes. High-energy electrons generated in the plasma directly dissociate CO<sub>2</sub> molecules into CO and O<sub>2</sub> without requiring costly catalysts or extreme operational conditions.

The ability of plasma reactors to integrate seamlessly with intermittent renewable energy sources, such as wind and solar power, makes them particularly attractive in the context of future low-carbon energy systems. However, challenges remain in improving the energy efficiency of plasma-chemical methods, especially for scaling beyond laboratory settings [19]. Additionally, plasma reactors are less established than thermochemical or electrochemical systems in industrial environments, which could slow their adoption in large-scale CO<sub>2</sub> management initiatives.

#### 2.2.5 Comparative Analysis

Each of these methods presents distinct trade-offs in terms of scalability, energy efficiency, and practicality for CO<sub>2</sub> decomposition. Thermochemical approaches excel in large-scale industrial applications but require significant energy inputs. Electrochemical systems are more energy-efficient but face challenges related to cost and durability. Photochemical methods offer sustainable and environmentally friendly solutions but are hindered by low efficiencies. Plasma-chemical methods, while still in their early stages of development, show promise for decentralised applications due to their mild operating conditions and compatibility with renewable energy sources [20].

By leveraging the strengths of these approaches, researchers can explore hybrid systems that combine the advantages of multiple methods. For example, plasma-chemical methods could be paired with thermochemical or electrochemical techniques to enhance overall efficiency and scalability. Understanding and addressing the limitations of each method is essential for advancing CO<sub>2</sub> decomposition technologies and achieving sustainable carbon management solutions [21].

### 2.3 The Dielectric Barrier Discharge Reactor

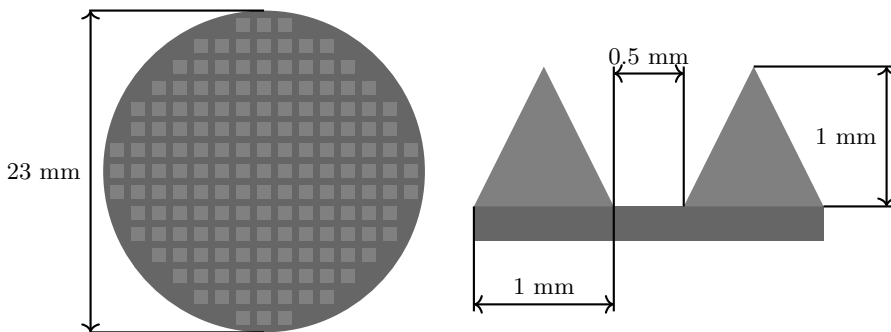


Figure 2.5: DBD non-thermal plasma reactor high-voltage electrode, adapted from [22]

### 2.3.1 Key Reactor Components

#### 1. Electrodes

The DBD reactor comprises two electrodes, typically metal, which serve as the source of the high-voltage electric field required to generate plasma. One electrode is connected to a high-voltage AC power supply, while the other is grounded. These electrodes can take various forms depending on the reactor configuration, such as flat parallel plates or cylindrical designs. The surface geometry may be changed to create regions of higher electric field strength, such as by introducing sharp points [22].

#### 2. Dielectric Barrier

A dielectric material, such as quartz, glass, or ceramic, coats at least one of the electrodes. This barrier plays a crucial role in the reactor's operation by preventing a direct current discharge and avoiding the formation of damaging arcs. Instead, the dielectric allows for a uniform and stable glow discharge, creating a highly effective plasma for the gas decomposition process [23].

#### 3. Reaction Zone

The space between the electrodes constitutes the reaction zone, where the gas flows and plasma is generated. The gap between the electrodes is typically narrow, in the order of millimetres, ensuring efficient interaction between the gas molecules and the plasma [24].

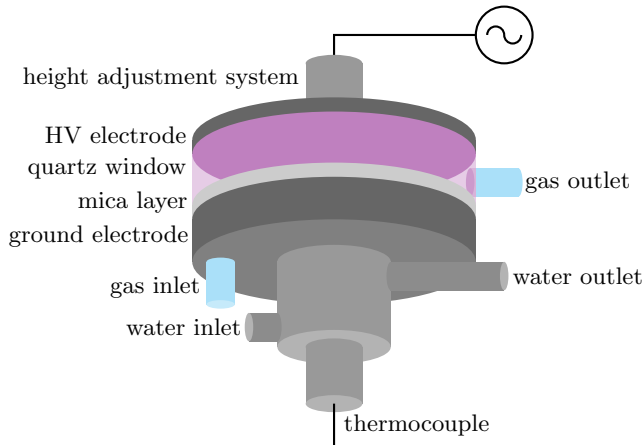


Figure 2.6: Cylindrical DBD non-thermal plasma reactor, adapted from [22]

#### 4. Gas Inlet and Outlet

Gases, such as CO<sub>2</sub>, are introduced into the reactor through a dedicated inlet. The gas flows through the reaction zone and is exposed to the plasma, undergoing decomposition into products such as CO and O<sub>2</sub> before exiting via the outlet. Precise control of the gas flow is essential to ensure uniform exposure and maximise the conversion efficiency.

#### 5. High-Voltage Power Supply

A high-voltage AC power supply is required to create the electric field necessary for plasma

---

generation [25]. The power supply typically operates in the kilovolt range and drives the alternating electric field that ionises the gas within the reaction zone.

### 2.3.2 Operating Principle

The application of high-voltage AC power between the electrodes ionises the gas molecules, creating a plasma consisting of electrons, ions, and reactive neutral species. These energetic species interact with the gas, breaking molecular bonds and facilitating chemical reactions [26]. In the case of CO<sub>2</sub> decomposition, the plasma splits CO<sub>2</sub> into CO and O<sub>2</sub> through high-energy electron collisions and subsequent reaction pathways.

The dielectric barrier limits the current and prevents the formation of a continuous arc discharge, maintaining the plasma in a non-thermal state [27]. This feature ensures that the energy input is distributed effectively, promoting uniformity in the plasma and enhancing the overall efficiency of the process.

### 2.3.3 Reactor Configurations

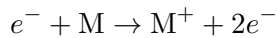
DBD reactors can be designed in various geometries, each optimised for specific applications or operational requirements. One common configuration is the planar DBD reactor, which consists of parallel plate electrodes separated by a dielectric layer [28]. This arrangement provides a uniform electric field and consistent plasma distribution, making it suitable for applications where precise control of plasma uniformity is essential.

Another widely used design is the cylindrical DBD reactor, where a cylindrical dielectric tube houses an internal electrode, while the outer surface is surrounded by a second electrode [29]. This geometry is particularly advantageous for continuous gas flow applications, as it facilitates efficient interaction between the plasma and the gas. The concentric design ensures stable plasma formation, enhancing reactor performance in processes such as CO<sub>2</sub> decomposition. In cylindrical configurations, the central rod electrode and surrounding dielectric tube create a controlled environment for gas flow, while the external grounded electrode promotes effective plasma generation [30]. This design supports high conversion rates and energy efficiency by maximising the contact between gas molecules and the plasma region.

### 2.3.4 Mechanisms

In NTPs, interactions among electrons, ions, radicals, and neutral species under an electric field dictate the fundamental pathways of production, transformation, and consumption of chemical species. The following reactions depend strongly on the electron energy distribution function (EEDF), applied reduced electric field ( $\frac{E}{N}$ ), and specific reaction cross-sections [31].

#### **Ionisation**



Ionisation occurs when an electron with sufficient energy collides with a neutral species, M,

---

ejecting an additional electron and forming a positive ion. This process replenishes free electrons, sustaining the plasma by balancing electron loss mechanisms.

### Dissociative Ionisation



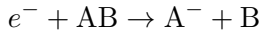
Dissociative ionisation proceeds similarly to ionisation but involves a diatomic or polyatomic species, AB. The incoming electron has enough energy not only to ionise AB but also to break it into its constituent parts, producing both a positive ion  $A^+$  and a neutral fragment B.

### Electron Attachment



In certain energy regimes, free electrons can attach to a neutral species, M, forming a negative ion. This mechanism typically becomes important at lower electron energies and can significantly affect the charge balance and overall reactivity of the plasma.

### Dissociative Electron Attachment



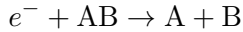
Dissociative attachment occurs when an electron collides with a molecule, AB, and forms a negative ion ( $A^-$ ), while the remaining fragment (B) is released as a neutral species. This pathway can be especially influential in controlling radical concentrations and the distribution of charged species.

### Excitation



Excitation involves an electron transferring part of its energy to a neutral species, M, elevating it to an excited state (M<sup>\*</sup>). These excited species can undergo further reactions, such as ionisation or dissociation, depending on their energy levels and collision probabilities.

### Dissociation



Dissociation takes place when the electron imparts enough energy to break the bond in a diatomic or polyatomic molecule, AB, yielding neutral fragments, A and B. This process is a primary source of radical species, which can drive subsequent reactions in the plasma.

Each of these mechanisms is governed by the local plasma conditions, including electron temperature, electron density, and gas composition [31]. Their collective effect underpins the reactive environment in non-thermal plasma systems, ultimately shaping the pathways and efficiency of chemical transformations.

#### 2.3.5 Applications in CO<sub>2</sub> Decomposition

The DBD reactor is highly suited to CO<sub>2</sub> decomposition due to its ability to operate under mild conditions and its compatibility with intermittent renewable energy sources. By optimising operational parameters such as the applied voltage, frequency, and gas flow rate, significant

conversion of CO<sub>2</sub> to CO and O<sub>2</sub> can be achieved with minimal energy input [32]. Furthermore, the non-thermal nature of the plasma ensures that the reaction is not dependent on elevated temperatures, distinguishing DBD reactors from thermochemical methods.

Another advantage of DBD reactors lies in their scalability and flexibility. They can be designed for a variety of operational setups, from small-scale laboratory experiments to modular systems capable of handling larger gas volumes [33]. Additionally, DBD reactors are highly adaptable to fluctuations in gas composition and energy input, making them ideal for coupling with renewable energy sources such as solar or wind power. This adaptability is particularly valuable for decentralised applications, where energy availability and gas streams may vary significantly. By leveraging these strengths, DBD reactors present a promising solution for sustainable CO<sub>2</sub> utilisation and reduction technologies.

## 2.4 Financial Analysis

### 2.4.1 Current Industrial Methods

Annually, 230 megatonnes [Mt] of CO<sub>2</sub> are utilised across industries [5], and the decomposition of CO<sub>2</sub> into valuable products has emerged as a vital strategy for mitigating climate change while generating economic benefits [17]. However, the financial viability of techniques varies significantly depending on their technological maturity, energy efficiency, scalability, and the market demand for their products [34]. Currently, the most commercially viable CO<sub>2</sub> decomposition methods consist of EOR, chemical conversion, biological conversion, and mineralisation. Full financial breakdowns of each method can be found in Appendix A.

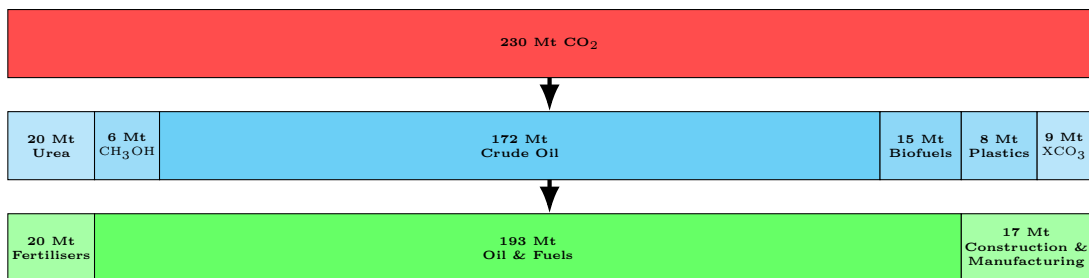


Figure 2.7: Annual CO<sub>2</sub> utilisation, products, and downstream applications [5]

#### 2.4.1.1 Enhanced Oil Recovery

EOR is currently the most widely employed method for CO<sub>2</sub> utilisation, accounting for approximately 70–80% of global CO<sub>2</sub> use, with 172 Mt being used for reservoir injection. The process involves pumping CO<sub>2</sub> into oil reservoirs to extract crude oil that would otherwise remain inaccessible. The operational costs arise primarily from the capture, transport, compression, and injection of CO<sub>2</sub>, which is typically estimated at £16.00 to £49.00 per tonne of CO<sub>2</sub> [35].

Despite these costs, the recovered crude oil provides significant economic returns. Assuming oil prices of £49.00 to £74.00 per barrel, the additional oil extracted frequently offsets the cost of CO<sub>2</sub> injection, making EOR highly profitable in regions with established oil infrastructure. However, its reliance on fossil fuel markets raises concerns about long-term sustainability,

---

particularly as economies transition towards decarbonisation [11]. Additionally, EOR is not inherently carbon-neutral, as the recovered oil contributes to emissions upon combustion and other downstream industrial processes.

#### **2.4.1.2 Chemical Conversion**

Chemical conversion processes, including urea, methanol, and polycarbonate production, account for 10–15% of global CO<sub>2</sub> utilisation, including 20 Mt for urea (NH<sub>2</sub>CONH<sub>2</sub>), essential in fertilisers, and 6 Mt for methanol (CH<sub>3</sub>OH), a feedstock for fuels and plastics. Urea production is relatively cost-effective, with CO<sub>2</sub> capture costs ranging from £13.00 to £35.00 per tonne due to its integration with ammonia production processes. Methanol production is significantly more energy-intensive, particularly when renewable energy is used, with costs ranging between £283.00 and £429.00 per tonne of carbon dioxide [36]. The production of polycarbonates is cost-competitive, but the market size is limited compared to that of urea or methanol.

In terms of revenue, urea commands prices of £230.00 to £277.00 per tonne, making it a profitable application of CO<sub>2</sub> conversion. Methanol, with market prices ranging from £450.00 to £580.00 per tonne, offers moderate profitability, although this heavily depends on access to low-cost hydrogen. Polycarbonates, while higher in value, cater to a niche market. Overall, chemical conversion is commercially viable for well-established products such as urea but faces financial challenges for energy-intensive processes like methanol production unless renewable energy costs decrease significantly.

#### **2.4.1.3 Biological Conversion**

Biological conversion methods, accounting for 15 Mt in total, utilise microorganisms or enzymes to convert CO<sub>2</sub> into biofuels, such as ethanol and biodiesel, as well as bioplastics. These processes generally have lower energy requirements but require careful management of biological systems. Costs for biological conversion range from £41.00 to £205.00 per tonne of CO<sub>2</sub>, depending on the specific process and scalability.

Ethanol typically fetches prices between £400.00 and £600.00 per tonne, while biodiesel is valued at approximately £600.00 to £800.00 per tonne [36]. Profitability in this sector is often enhanced by subsidies and government incentives for renewable fuels. Bioplastics, such as PLA and polyhydroxyalkanoates (PHAs), command significantly higher prices of £1,500.00 to £2,500.00 per tonne, making them highly profitable despite their niche market [37]. Biological conversion holds significant promise, particularly for high-value products such as bioplastics, but scalability remains a critical challenge [38].

#### **2.4.1.4 Mineralisation**

Mineralisation processes convert CO<sub>2</sub> into stable carbonates, such as calcium carbonate and magnesium carbonate, for use in construction materials. These processes are relatively simple and cost-effective, with costs ranging from £40.00 to £135.00 per tonne of CO<sub>2</sub>. The resulting

---

products, including aggregates and cement for construction, typically command prices of £16.00 to £182.00 per tonne [39].

Mineralisation offers a scalable and long-term solution for carbon storage due to the abundance of mineral feedstocks and the large market for construction materials, like stable carbonates ( $\text{XCO}_3$ ) such as calcium carbonate ( $\text{CaCO}_3$ ) or magnesium carbonate ( $\text{MgCO}_3$ ) [38]. However, its financial margins are relatively low compared to those of other methods because of the low market value of these materials.

#### 2.4.2 Challenges and Opportunities

Several challenges and opportunities exist for these techniques. Energy costs are a critical factor, particularly for energy-intensive processes such as methanol production, which rely heavily on renewable energy sources [36]. Market volatility also influences revenue potential, particularly for crude oil and fertilisers. Government incentives, including subsidies, carbon taxes, and credits, significantly enhance the profitability of  $\text{CO}_2$  conversion technologies, particularly for emerging methods such as biological conversion and mineralisation [40]. Finally, scalability is a key consideration. While EOR and chemical conversion are well-established at scale, biological and mineralisation processes require further investment to achieve widespread adoption.

Table 2.1: Financial summary of industrial  $\text{CO}_2$  decomposition techniques

Method	Cost (£/t $\text{CO}_2$ )	Revenue Potential (£)	Profitability
Enhanced Oil Recovery [35]	16–49	49–74/barrel	High
Chemical Conversion [36]	13–429	230–580/t	Moderate to High
Biological Conversion [37]	41–205	400–2,500/t	High
Mineralisation [39]	40–123	16–182/t	Low to Moderate

Currently, EOR and chemical conversion dominate the market for  $\text{CO}_2$  utilisation due to their established infrastructure and profitability [41]. Biological conversion and mineralisation hold immense potential but require further technological development and scaling to achieve broader adoption. The long-term financial success of all these methods will depend on reducing energy costs, leveraging government incentives, and expanding markets for sustainable products.

#### 2.4.3 Plasma-Based $\text{CO}_2$ Decomposition

Assessing the financial feasibility of a DBD reactor for  $\text{CO}_2$  decomposition involves analysing CAPEX and OPEX, which depend on reactor scale, energy efficiency, and component quality. While this project focuses on developing a computational model to simulate  $\text{CO}_2$  decomposition, understanding the associated costs is crucial for industrial scale-up [42]. Detailed cost analysis reveals economic challenges and opportunities, guiding optimisation of reactor design and operational parameters. By linking computational studies with financial considerations, the approach identifies key cost drivers, such as high-voltage power supplies and advanced gas monitoring systems [34], and underscores the need for energy efficiency improvements and renewable

---

energy integration. A financial perspective will ensure advances in computational modelling contribute to the economic viability of DBD plasma-based CO<sub>2</sub> decomposition at an industrial scale. The analysis centres around a pilot processing reactor unit, the properties of which are listed in Table 2.2.

#### 2.4.3.1 Capital Expenditures

The CAPEX for a DBD NTP reactor covers construction, power supply, and monitoring systems. The reactor requires high-quality dielectric materials, such as quartz or ceramic, costing £80.00–£300.00 per unit, and electrodes, stainless steel, aluminium, or copper, costing £150.00–£600.00 [42]. For larger systems, enclosures with gas flow and pressure control cost £8,000–£15,000 for laboratory setups, scaling significantly for industrial use.

A high-voltage power supply capable of generating alternating currents or pulsed DC is a major expense, priced at £15,000.00–£60,000.00, depending on specifications, while gas monitoring and analysis tools, such as gas chromatography or infrared spectrometry, add £3,000.00–6,000.00. For a pilot-scale reactor, CAPEX typically totals to £28,500.00–£90,000.00, rising to £0.7–£1.2 million for large-scale industrial reactor upgrading, throughput and instrumentation dependent.

#### 2.4.3.2 Operational Expenditures

Table 2.2: Financial summary of DBD plasma-based CO<sub>2</sub> decomposition

Processing Scale: ~ 1 t CO <sub>2</sub> /diem Flow Rate: ~ 40–50 kg CO <sub>2</sub> /hr		Power Consumption: ~ 20–50 kW Operating Conditions: Atmospheric	
CAPEX		OPEX	
Process	Cost (£)	Process	Cost (£)
Reactor Construction	8,000–15,000/unit	Electricity Consumption	10–40/t CO <sub>2</sub>
Dielectric Materials	80–300/unit	CO <sub>2</sub> Feedstock	20–40/t CO <sub>2</sub>
Electrodes	150–600/unit	Carrier Gases (optional)	60–120/t CO <sub>2</sub>
Power Supply	15,000–60,000/unit	Maintenance	5,000–10,000/annum
Gas Monitoring	3,000–6,000/unit	Product Separation	10–30/t CO <sub>2</sub>
Balance of Plant (BoP)	2,000–5,000/unit		
Industrial-scale Setup	0.7–1.2 million (amortisable)		

The largest operating cost is electricity. Sustaining plasma requires 10–50 kWh per tonne of CO<sub>2</sub>, costing £10.00–£40.00 per tonne at UK industrial rates, or £0.20–£4.00 per kWh. Feedstock CO<sub>2</sub>, sourced from flue gas or other emissions, costs £20.00–£40.00 per tonne, while optional carrier gases, such as Argon, add £60.00–£120.00 per tonne. In addition, small-scale power supplies cost approximately £5,000.00–£10,000.00, depending on the voltage range and power capacity, while industrial-grade units can reach up to £10,000.00 [34].

Regular maintenance includes £5,000.00–£10,000.00 annually for electrode cleaning, dielectric replacement every 1–3 years at £500.00–£1,000.00 per unit, and general repairs for gas handling and power systems at £2,000.00–£5,000.00 annually. Monitoring costs, including gas analysis

calibration, add £1,000.00–£2,000.00 annually. If product separation, such as isolating CO and O<sub>2</sub>, is required, gas separation technologies increase costs by £10.00–£30.00 per tonne of CO<sub>2</sub> processed.

#### 2.4.4 The Value of CO

Carbon monoxide is an essential feedstock in numerous industrial processes, including synthesising hydrocarbons via the Fischer-Tropsch process, producing methanol, and various metallurgical applications [43]. Its role in creating synthetic fuels and other chemicals positions it as a cornerstone of carbon recycling technologies. Additionally, CO's use in syngas, a mixture of CO and H<sub>2</sub>, production aligns with efforts to transition towards green hydrogen economies [44].

From an environmental perspective, plasma-based CO production offers the advantage of using CO<sub>2</sub> as a raw material, potentially contributing to CCUS strategies [11]. By converting CO<sub>2</sub> emissions into valuable products, this approach helps mitigate the environmental impact of industrial processes while creating economic value. Thus, while the energy costs of DBD plasma reactors remain a challenge, their potential to support sustainable industrial systems and reduce carbon footprints is undeniable [45].

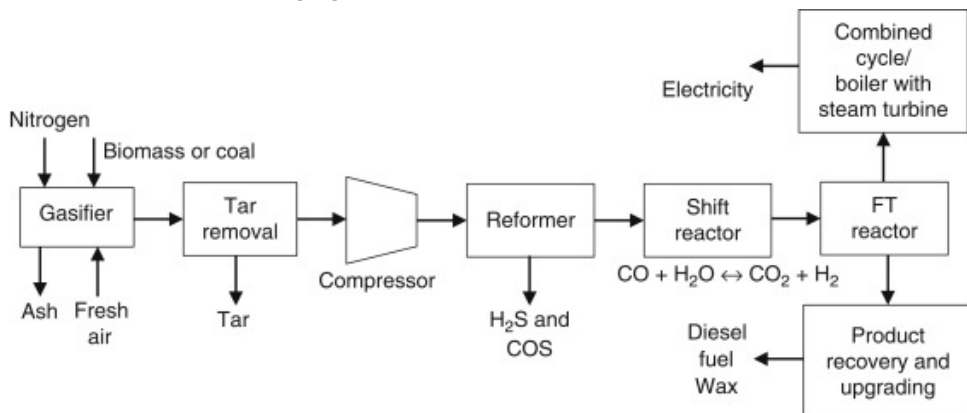


Figure 2.8: The Fischer-Tropsch process, from [46]

#### 2.4.5 Economic Viability & Future Directions

The viability of a DBD NTP reactor hinges on its efficiency, output value, and external incentives. CO<sub>2</sub> decomposition yields valuable products, most notably CO, valued at £300.00–£500.00 per tonne, and O<sub>2</sub>, but its high specific energy input (SEI) challenges scalability and makes it costlier than conventional methods like methane steam reforming, even with improved reactor geometries and catalysts [43]. Additionally, maintenance costs from dielectric degradation and electrode wear further elevate expenses. However, in contexts with abundant renewable energy or limited traditional feedstocks, government incentives such as carbon credits, valued at £50.00–£100.00 per tonne of CO<sub>2</sub> avoided, combined with CO revenues can significantly offset these costs, enhancing the technology's economic viability [34].

To enhance the viability of DBD plasma reactors for CO production, research is focusing on reactor optimisation, improved materials, and hybrid approaches that combine plasma with

---

catalysis. Integrating renewable energy sources to power these reactors is another promising avenue, potentially reducing costs and environmental impact. Advanced diagnostics such as optical emission spectroscopy (OES) are being employed to deepen understanding of plasma chemistry and fine-tune reactor conditions for optimal selectivity and efficiency.

Coupling DBD plasma reactors with advanced separation technologies, such as membrane separators or cryogenic systems, can significantly improve CO purity and overall process efficiency, streamlining downstream applications and enhancing economic appeal. Furthermore, exploring synergistic effects between plasma and photocatalysis or electrocatalysis may further reduce energy consumption and broaden feedstock flexibility. With continued multidisciplinary innovation, DBD plasma reactors could evolve into a cornerstone technology for carbon capture, utilisation, and sustainable industrial processes.

## 2.5 The Problem

NTP processes in DBD reactors offer a promising avenue for converting CO<sub>2</sub> into value-added chemicals, yet the underlying chemical and physical mechanisms remain profoundly complex [47]. In these systems, energetic electrons, accelerated by rapidly varying electric fields, induce a myriad of inelastic collisions, resulting in molecular dissociation, ionisation, and the formation of vibrationally and electronically excited species [48]. This non-equilibrium state drives reaction pathways that differ markedly from those observed under thermal conditions, making a detailed understanding of electron-impact processes and metastable species essential for optimising reaction efficiency and product selectivity [49].

Traditional models have often relied on simplified reaction networks, typically encompassing only a few bulk-gas reactions, which fall short in capturing the full complexity of excited-state chemistry and secondary processes such as recombination and ionisation [50]. Recent advances have led to more comprehensive frameworks that include many elementary reactions, thereby accounting for excited-state formation, de-excitation, and multiple competing pathways that significantly alter species concentration profiles [51]. Although these expanded models better reflect real plasma environments, their increased complexity poses substantial computational challenges, necessitating the use of advanced numerical techniques.

This project addresses these challenges by developing a comprehensive computational model that integrates plasma kinetics with non-thermal plasma physics [52]. By leveraging advanced computational methods and simulation tools, the code captures the essential transient and non-linear dynamics of dielectric barrier discharge reactors. It generalises the interaction between reactor electrodynamics and chemical kinetics, accounting for factors such as voltage division and the resulting effective electric field that governs electron-impact reactions and the formation of reactive species. Ultimately, this virtual laboratory aims to deepen theoretical understanding of plasma-assisted CO<sub>2</sub> conversion while guiding experimental design toward more sustainable and economically viable industrial applications.

---

### 3 Methodology

This project is entirely theoretical, with the majority of experimentation dedicated to ensuring that the model accurately reflects established knowledge in non-thermal plasma physics and dielectric barrier discharge chemistry [51]. Despite the robust theoretical foundations available, many relationships within this field, particularly those involving plasma-based decomposition, cannot be fully modelled through mathematical derivation or first-principle physics alone, thereby necessitating the incorporation of experimental input. Consequently, considerable care is taken in the development of a 0D model to ensure its fidelity to experimental trends.

To achieve this, the program incorporates several critical factors. These include the implementation of a reduced cross-section of reactions, the integration of a range of reaction mechanisms, and the comprehensive consideration of both electrodynamic and thermodynamic effects [53]. These elements are synthesised through advanced scientific computing and mathematical methods, ensuring a holistic and accurate representation of the complex interplay inherent in non-thermal plasma systems.

#### 3.1 Non-thermal Plasma Chemistry

The driving principles of this model are derived from existing understanding of non-thermal plasma physics and plasma chemistry. This requires careful attention to how the known derivations and formulae relate to the evolution of key metrics and measures. In the context of CO<sub>2</sub> decomposition in a DBD plasma reactor, the underlying complexity arises from a multitude of interacting processes, including electron-impact ionisation, excitation, recombination, and various radical-driven reactions [6]. These processes collectively govern the formation and consumption of reactive species and thereby dictate the overall efficiency of plasma-based CO<sub>2</sub> conversion.

##### 3.1.1 Reactions & Species

The vast majority of the species produced from the decomposition of pure CO<sub>2</sub>, as seen in Table 3.1, consist of carbon and oxygen in various forms. Key species include molecular intermediates such as CO, O<sub>2</sub>, and C<sub>2</sub>, along with their corresponding positive and negative ions, as well as atomic radicals and electrons. These species emerge from a range of fundamental processes that are crucial to the plasma chemistry of CO<sub>2</sub> decomposition.

As summarised in Table 3.2, the model includes both ‘Excited States’ pathways X1-X11 and ‘Bulk Gas’ reactions R1-R19. The Excited States pathways typically involve electron-driven events, such as dissociation, dissociative attachment, and ionisation, which can lead to the formation of radical species or the excitation of existing molecules [54]. These electron-impact processes are highly sensitive to the local electric field and electron energy distribution, both of which are strongly influenced by the dielectric barrier discharge conditions.

The bulk gas reactions encompass the subsequent chemical transformations of newly formed

species through pathways such as oxidation, partial oxidation, recombination, and charge transfer. These reactions illustrate the manifold routes by which  $\text{CO}_2$  is converted into other carbon and oxygen-containing products, depending on the local plasma conditions. The model is designed to capture the essential kinetics that govern the behaviour of both neutral and charged species in the plasma, thereby reflecting the complex interplay between chemical reactivity and energy transfer in non-thermal plasma environments [19].

Table 3.1: Species in the complex model

Species	Name
Key Species	
$\text{CO}_2$	Carbon Dioxide
$\text{CO}$	Carbon Monoxide
$\text{O}$	Atomic Oxygen
$\text{O}_2$	Oxygen
$\text{O}_3$	Ozone
Intermediate and Other Species	
$\text{CO}^+$	Carbon Monoxide Positive Ion
$\text{CO}_2^+$	Carbon Dioxide Positive Ion
$\text{O}^+$	Atomic Oxygen Positive Ion
$\text{O}_2^+$	Oxygen Positive Ion
$\text{O}_3^+$	Ozone Positive Ion
$\text{O}^-$	Atomic Oxygen Negative Ion
$\text{O}_2^-$	Oxygen Negative Ion
$\text{CO}_2^*$	Excited Carbon Dioxide
$\text{O}_2^*$	Excited Oxygen
$\text{C}$	Atomic Carbon
$\text{C}_2$	Diatomeric Carbon
$\text{O}_{\text{ad}}$	Surface Adsorbed Atomic Oxygen
$\text{M}$	Third-Body Specie
$\text{D}_{\text{surface}}$	Dielectric Surface
$e^-$	Electron

Table 3.2: Reaction profile of the complex model

Reaction	Process	Number
Excited States		
$e^- + \text{CO}_2 \rightleftharpoons \text{CO} + \text{O} + e^-$	Dissociation	X1
$e^- + \text{CO}_2 \rightleftharpoons \text{CO}_2^+ + 2e^-$	Ionisation	X2
$e^- + \text{CO}_2 \rightleftharpoons \text{CO}^+ + \text{O} + 2e^-$	Dissociative Ionisation	X3
$e^- + \text{CO}_2 \rightleftharpoons \text{CO}_2^* + e^-$	Excitation	X4
$e^- + \text{O}_2 \rightleftharpoons \text{O}_2^* + e^-$	Excitation	X5
$e^- + \text{O}_2 \rightleftharpoons \text{O}_2^+ + 2e^-$	Ionisation	X6
$e^- + \text{O}_2 \rightleftharpoons \text{O}_2^- + \text{O}$	Dissociative Attachment	X7
$e^- + \text{O} \rightleftharpoons \text{O}^- + e^-$	Attachment	X8
$e^- + \text{O} + \text{M} \rightleftharpoons \text{O}^- + \text{M}$	Three-Body Electron Attachment	X9
$\text{CO}_2^* \rightleftharpoons \text{CO} + \text{O}$	De-excitation Dissociation	X10
$\text{CO}_2^* + \text{CO}_2 \rightleftharpoons 2\text{CO} + \text{O}_2$	Energy Transfer	X11
Bulk Gas		
$\text{CO}_2 + \text{O} \rightleftharpoons \text{CO} + \text{O}_2$	Dissociation	R1
$\text{CO} + \text{O} \rightleftharpoons \text{C} + \text{O}_2$	Dissociation	R2
$\text{O} + \text{O}_2 + \text{M} \rightleftharpoons \text{O}_3 + \text{M}$	Recombination	R3
$2\text{O} + \text{M} \rightleftharpoons \text{O}_2 + \text{M}$	Ozone Formation	R4
$2\text{CO}_2 \rightleftharpoons 2\text{CO} + \text{O}_2$	Dissociation	R5
$\text{CO} + \text{O}_3 \rightleftharpoons \text{CO}_2 + \text{O}_2$	Ozone Decomposition	R6
$\text{O}_3 + \text{O} \rightleftharpoons 2\text{O}_2$	Ozone Decomposition	R7
$\text{CO}_2^+ + \text{CO}_2 \rightleftharpoons \text{CO}_2 + \text{CO} + \text{O}^+$	Dissociative Charge Transfer	R8
$\text{CO}_2^+ + \text{O}_2 \rightleftharpoons \text{O}_2^+ + \text{CO}_2$	Charge Transfer	R9
$\text{O}_2^+ + \text{O}_2 \rightleftharpoons \text{O}_3^+ + \text{O}$	Charge Transfer	R10
$\text{O}_2^- + \text{O}_2^+ \rightleftharpoons \text{O}_2 + \text{O}$	Ion Recombination	R11
$\text{CO}_2^+ + \text{O}^- \rightleftharpoons \text{CO}_2 + \text{O}$	Ion Recombination	R12
$\text{O} + \text{D}_{\text{surface}} \rightleftharpoons \text{O}_{\text{ad}}$	Surface Adsorption	R13
$2\text{O}_{\text{ad}} \rightleftharpoons \text{O}_2$	Surface Adsorption	R14
$\text{O}_3 + \text{D}_{\text{surface}} \rightleftharpoons \text{O}_2 + \text{O}_{\text{ad}}$	Surface Adsorption	R15
$\text{C} + \text{O} \rightleftharpoons \text{CO}$	Association	R16
$2\text{C} \rightleftharpoons \text{C}_2$	Dimerisation	R17
$\text{CO} + \text{C} \rightleftharpoons \text{C}_2 + \text{O}$	Displacement	R18
$\text{C}_2 + \text{O}_2 \rightleftharpoons 2\text{CO}$	Partial Oxidation	R19

The inclusion of positive and negative ions highlights the importance of ion-neutral and ion-ion interactions, which significantly affect electron density, discharge stability, and reaction efficiency. Metastable species also play a crucial role, as their long lifetimes enable energetically inaccessible reactions. By integrating these multiple pathways into a coherent 0D model and employing a reduced reaction cross-section focused on dominant processes under typical DBD conditions, the approach maintains close alignment with experimental observations and facilitates robust predictions of conversion efficiency and selectivity.

### 3.1.2 Reversibility and Equilibrium Considerations

In plasma reactors, the equilibrium of each reaction is governed by the SEI and electron density, with the DBD plasma environment generally favouring forward reactions that produce  $\text{CO}$ ,  $\text{O}$ , and  $\text{O}_2$ . Forward rates exceed reverse rates, limiting recombination and enhancing product formation. The Fortran model updates rate constants based on temperature and energy con-

---

ditions, simulating partial equilibrium, some reactions stabilise while others continue to favour dissociation [54]. For example, although O atoms recombine to form O<sub>2</sub>, this occurs more slowly than CO<sub>2</sub> dissociation, making CO and O<sub>2</sub> the dominant products, which is crucial for reactor efficiency.

## 3.2 Mathematical Modelling

The development of a rigorous mathematical model is essential for understanding the complex processes involved in CO<sub>2</sub> decomposition in DBD plasma reactors [55]. Coupled with scientific computing, mathematical modelling provides a systematic framework to quantify the interplay between plasma physics and chemical kinetics. By utilising numerical methods and simulations, this approach captures transient behaviours, evaluates non-linear dynamics, and predicts reaction outcomes under various operating conditions. In projects where experimental observation is limited by the extreme conditions of plasma environments, robust mathematical models act as a virtual laboratory, guiding future experimental design and fostering innovation in optimising conversion strategies.

### 3.2.1 Numerical Methods

Numerical methods are vital for linking theory to the complex, non-linear dynamics of plasma-chemical processes. Techniques such as Runge-Kutta and Euler integration enable precise simulation of transient behaviours in DBD CO<sub>2</sub> decomposition, offering a virtual laboratory to validate predictions and optimise reactor performance [56].

Euler integration is a basic numerical method for solving ordinary differential equations, prized for its simplicity. In plasma reactors, where species concentrations vary rapidly due to electron-driven processes and more slowly via neutral reactions, it offers a straightforward means to capture temporal evolution. Although only first-order accurate and prone to stability issues with larger time steps, its computational efficiency makes it useful for preliminary simulations and systems where extreme precision is unnecessary [57]. Despite its limitations compared to higher-order methods, Euler integration remains vital in modelling the dynamic behaviour of non-thermal plasmas and enhancing understanding of reaction kinetics and energy transfer in CO<sub>2</sub> conversion [47].

The fourth-order Runge-Kutta (RK4) method effectively solves the ordinary differential equations that describe species concentration evolution in plasma reactors, where reactions occur on vastly different timescales owing to rapid electron interactions and slower neutral processes [56]. RK4 delivers enhanced numerical stability and accuracy, making it well suited for stiff systems and the simulation of kinetics, including critical vibrational-translational (VT) and vibrational-vibrational (VV) relaxation processes essential for CO<sub>2</sub> dissociation [24]. Its implementation in Fortran, which benefits from robust array-handling, enables efficient modelling of large reaction networks and complex species interactions, capturing the dynamic behaviour of plasma systems while ensuring computational feasibility.

### 3.2.2 Reaction Kinetics

Table 3.3: List of key constants, parameters, and variables

Symbol	Name	Value	Units
<b>Constants - hardcoded to the model</b>			
Physical			
$k_B$	Boltzmann constant	$1.381 \times 10^{-23}$	$\text{JK}^{-1}$
$R$	universal gas constant	8.134	$\text{Jmol}^{-1}\text{K}^{-1}$
$p_{\text{atm}}$	atmospheric pressure	101325	Pa
$T_0$	room temperature	298.15	K
$\epsilon_0$	permittivity of free space	$8.854 \times 10^{-12}$	$\text{Fm}^{-1}$
$\epsilon_{\text{dielectric}}$	permittivity of dielectric material	$4.427 \times 10^{-11}$	$\text{Fm}^{-1}$
$\rho$	$\text{CO}_2$ gas density	1.799	$\text{kgm}^{-3}$
$k$	$\text{CO}_2$ thermal conductivity	0.0168	$\text{Wm}^{-1}\text{K}^{-1}$
$\mu$	$\text{CO}_2$ dynamic viscosity	$1.48 \times 10^{-5}$	Pas
$\bar{h}$	$\text{CO}_2$ heat transfer coefficient	0.658	$\text{Wm}^{-2}\text{K}^{-1}$
$E_{\text{vib}}$	$\text{CO}_2$ vibrational energy quantum	$4.662 \times 10^{-20}$	J
$e$	elementary charge	$1.602 \times 10^{-19}$	C
Geometric			
$d_{\text{dielectric}}$	dielectric width	0.2	m
$d_{\text{reactor}}$	reactor diameter	$23 \times 10^{-3}$	m
$A_{\text{ground}}$	ground electrode surface area	$4.155 \times 10^{-4}$	$\text{m}^2$
$A$	total reactor surface area	$7.080 \times 10^{-4}$	$\text{m}^2$
Process			
$\eta_{\text{discharge}}$	discharge efficiency	0.2	
$V_{\text{discharge}}$	discharge threshold voltage	5200	V
$C_{\text{dielectric}}$	dielectric capacitance	$1.623 \times 10^{-10}$	F
<b>Parameters - key parameters of the model</b>			
Physical			
$c_p$	specific heat capacity at constant pressure	[844.9, 946.5]	$\text{Jkg}^{-1}\text{K}^{-1}$
$\epsilon_{\text{gap}}$	permittivity of gas mixture	$[8.850, 8.852] \times 10^{-12}$	$\text{Fm}^{-1}$
Process			
$t_{\text{discharge}}$	time of initial discharge	$2.170 \times 10^{-6}$	s
$C_{\text{gap}}$	effective gas mixture capacitance	$[1.4709, 1.4712] \times 10^{-11}$	F
$C_{\text{input}}$	effective input capacitance	$[1.34867, 1.34892] \times 10^{-11}$	F
$V_{\text{gap}}$	gas mixture voltage	$\{V_{\text{gap}} \in \mathbb{R}\}$	V
$V_{\text{input}}$	input voltage	$\{V_{\text{input}} \in \mathbb{R}\}$	V
$I_{\text{input}}$	input current	$\{I_{\text{input}} \in \mathbb{R} \mid I_{\text{input}} > 0\}$	A
$P_{\text{plasma}}$	plasma power	$\{P_{\text{plasma}} \in \mathbb{R} \mid P_{\text{plasma}} > 0\}$	W
SEI	specific energy input	$\{\text{SEI} \in \mathbb{R} \mid \text{SEI} > 0\}$	$\text{Jkg}^{-1}$
<b>Variables - variable experimental input values</b>			
Physical			
$p$	reactor pressure	[0.9, 1.1]	atm
Geometric			
$d_{\text{gap}}$	electrode gap	$[0.125, 0.375] \times 10^{-3}$	m
Process			
$V_{\text{AC}}$	AC supply voltage	[5850, 7150]	V
$f_{\text{AC}}$	AC supply frequency	[61200, 74800]	Hz
$\dot{V}$	volumetric flow rate	[15, 25]	$\text{mLmin}^{-1}$

Reaction kinetics are central to understanding the mechanisms driving  $\text{CO}_2$  decomposition in DBD reactors. By modelling individual pathways using Arrhenius expressions and electron impact processes, the dynamic interplay between energy input and chemical transformation is captured [58]. This approach enables the prediction of transient species concentrations under non-equilibrium conditions to validate against experimental data, providing insights for reactor performance and conversion efficiency. Any relevant values may be found in Table 3.3

### 3.2.2.1 Electrodynamics

The first task is determining the voltages across the reactor, which is derived from the applied AC voltage,  $V_{AC}$ , and the capacitive division between the electrode gap and the dielectric barrier [23]. The instantaneous input voltage  $V_{input}$  is defined in Equation 3.1, while the voltage across the electrode gap  $V_{gap}$  is defined in Equation 3.2.

$$V_{input} = \frac{V_{AC}}{2} \sin(2\pi f_{AC}t) \quad (3.1)$$

$$V_{gap} = \frac{V_{AC}C_{dielectric}}{2(C_{gap} + C_{dielectric})} \sin(2\pi f_{AC}(t - t_{discharge})) \quad (3.2)$$

$$C_{gap} = \frac{\epsilon_{gap}A_{plate}}{d_{gap}} \quad \text{derived fully in Appendix B.2} \quad (3.3)$$

$C_{dielectric}$  and  $C_{gap}$  are the effective capacitances of the dielectric barrier and the gas mixture within the gap respectively, where  $C_{dielectric} \approx 1.623 \times 10^{-10}$  F but  $C_{gap}$  changes based on the gas composition. This voltage partitioning is fundamental in non-thermal plasma physics, as  $V_{gap}$  directly determines the  $\frac{E}{N}$  within the gap that accelerates electrons to energies necessary for initiating chemical reactions.  $\frac{E}{N}$  is normalised by the number of reactant gas molecules within the reactor  $N_{gas}$ .

$$\frac{E}{N} = \frac{|V_{gap}|}{N_{gas}d_{gap}} \cdot 10^{21} \quad | \quad N_{gas} = \frac{p_{atm}}{k_B T_{gas}} \quad (3.4)$$

$N_{gas}$  = gas number density [ $\text{m}^{-3}$ ]

$T_{gas}$  = bulk gas temperature [K]

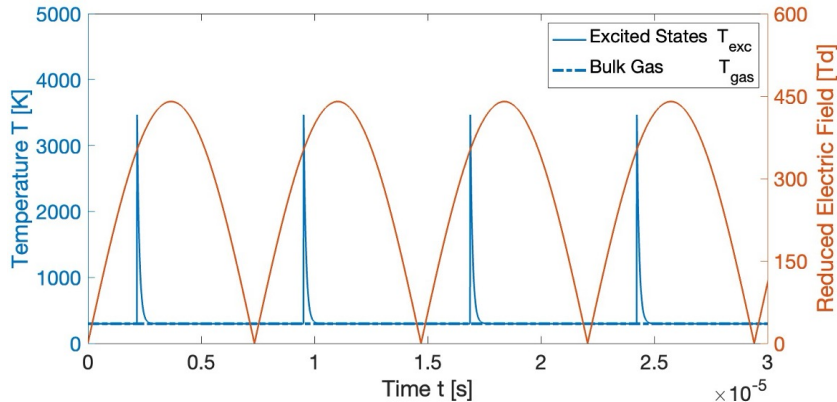


Figure 3.1: Evolution of the  $\frac{E}{N}$  and temperatures, with spikes of  $T_{exc}$  at DBDs

When the magnitude of the input voltage  $V_{input}$  exceeds a certain threshold, typically about half of the discharge threshold  $V_{discharge}$ , a discharge is initiated. At this juncture, a pulse current is induced across the gap. The current is calculated using the effective input capacitance  $C_{input}$ , derived in Appendix B.3, according to Equation 3.5, where  $\frac{dV_{input}}{dt}$  is derived in Appendix B.1.

$$I_{input} = \begin{cases} C_{input} \frac{dV_{input}}{dt}, & \text{if } |V_{input}| > \frac{V_{discharge}}{2} \\ 0, & \text{if } |V_{input}| \leq \frac{V_{discharge}}{2} \end{cases} \quad (3.5)$$

$C_{\text{input}}$  = effective input capacitance [F]

$V_{\text{input}}$  = input voltage [V]

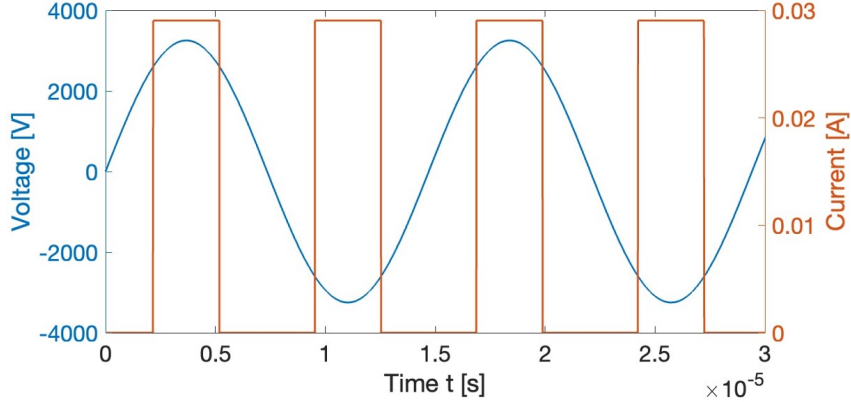


Figure 3.2: Evolution of  $V_{\text{input}}$  and  $I_{\text{input}}$

This relation utilises the fundamental capacitor law  $I = C \frac{dV}{dt}$ , and underscores how the dynamics of the applied voltage translate into the current that drives the plasma. Consequently, the power input to the plasma  $P_{\text{plasma}}$  is calculated using the relation in 3.6 and fully derived in Appendix B.4, where it is damped using an efficiency factor  $\eta_{\text{discharge}}$  of 0.2 derived from literature [22], and therefore the specific energy input per mole of CO<sub>2</sub>, seen in Equation 3.8.

$$P_{\text{input}} = \frac{C_{\text{input}} f_{\text{AC}} V_{\text{AC}}^2}{8} | \sin^2(2\pi f_{\text{AC}} t) | \quad (3.6)$$

$$P_{\text{plasma}} = 0.2 P_{\text{input}} \quad (3.7)$$

$$\text{SEI} = \frac{P_{\text{plasma}}}{\dot{n}_{\text{CO}_2}} \quad (3.8)$$

$\dot{n}_{\text{CO}_2}$  = molar flow rate of CO<sub>2</sub> [mols<sup>-1</sup>]

This sequence of equations, from  $V_{\text{input}}$  to  $V_{\text{gap}}$ , through the  $\frac{E}{N}$  and finally to the induced current and plasma power, captures the interplay between the electrical characteristics and the underlying non-thermal plasma processes. It provides a comprehensive framework that links the applied voltage to the local electric field conditions, the subsequent acceleration of electrons, and ultimately the energy available to drive the chemical reactions essential for CO<sub>2</sub> decomposition.

### 3.2.2.2 Thermal-Energy Balance

Modelling the gas temperature,  $T_{\text{gas}}$ , is vital as it directly influences reaction rates, species concentrations, and overall reactor performance [59]. Accurate predictions are essential for optimising energy efficiency and plasma-chemical processes, incorporating power input, reactor geometry, and environmental conditions to reflect real-world operations [60]. The uncoupled temperature dynamics of the DBD reactor are governed by the mass-energy balance equation in Equation 3.9 [57], from the First Law of Thermodynamics and Newton's Law of Cooling.

---


$$\dot{m}c_p \frac{dT_{\text{gas}}}{dt} = Q - hA(T_{\text{gas}} - T_0) \quad (3.9)$$

$\dot{m}$  = gas mass flow rate [kgs<sup>-1</sup>]

$Q$  = system heat generated [W]

$h$  = heat transfer coefficient [Wm<sup>-2</sup>K<sup>-1</sup>] *derived fully in Appendix B.6*

At steady state, the transient energy term vanishes,  $\frac{dT}{dt} = 0$ , so the plasma energy is entirely used entirely to heat the gas to the inlet gas temperature  $T_{\text{in}}$  and accounts only for environmental losses  $\dot{Q}_{\text{loss}}$ , shown in Equation 3.10.

$$\dot{Q}_{\text{loss}} = hA(T_{\text{ex}} - T_0) \quad (3.10)$$

For a flowing gas,  $\dot{m} \neq 0$ , the inlet temperature  $T_{\text{in}}$ , expected to equal  $T_0$ , relates  $T_{\text{ex}}$  to bond energisation in the gas in Equation 3.11.

$$\begin{aligned} \dot{Q} &= \dot{m}c_p \frac{dT_{\text{gas}}}{dt} \\ Q_{\text{gas}} &= \dot{m}c_p(T_{\text{ex}} - T_{\text{in}}) \end{aligned} \quad (3.11)$$

Thus, the mass-energy balance relation becomes Equation 3.12 at a steady-state and the energy the plasma  $Q$  provides is partitioned into energising the flowing gas and compensating for losses.

$$Q = Q_{\text{gas}} + \dot{Q}_{\text{loss}} = \dot{m}c_p(T_{\text{ex}} - T_{\text{in}}) + hA(T_{\text{ex}} - T_0) \quad (3.12)$$

Assuming a discharge efficiency  $\eta_{\text{discharge}}$  of 0.2, 80% of the plasma input power  $P_{\text{plasma}}$  is transferred to the surrounding environment as heat, establishing a relationship that can be used to find the exit temperature  $T_{\text{ex}}$  in Equation 3.13, which in turn gives the average reactor internal temperature  $T_{\text{avg}}$  in Equation 3.14.

$$\begin{aligned} Q &= (1 - \eta_{\text{discharge}})P_{\text{plasma}} \\ &\approx 0.8P_{\text{plasma}} \\ 0.8P_{\text{plasma}} &\approx \dot{m}c_p(T_{\text{ex}} - T_{\text{in}}) + hA(T_{\text{ex}} - T_0) \\ T_{\text{ex}} &\approx \frac{0.8P_{\text{plasma}} + \dot{m}c_pT_{\text{in}} + hAT_0}{\dot{m}c_p + hA} \\ T_{\text{ex}} &\approx \frac{0.8P_{\text{plasma}} + (\dot{m}c_p + hA)T_0}{\dot{m}c_p + hA} \quad | \quad T_{\text{in}} = T_0 \end{aligned} \quad (3.13)$$

$$T_{\text{avg}} = \frac{T_{\text{ex}} + T_{\text{in}}}{2} \quad (3.14)$$

$T_{\text{avg}}$  is the temperature at which the lumped specific heat  $c_p$  of the gas mixture within the reactor is found as a weighted average of the mixed species  $i$  by molar fraction  $y_i$ , shown in Equation 3.15. A simplified cross-section of CO<sub>2</sub>, O<sub>2</sub>, CO, and O is taken to do this, with

---

individual  $c_{p,i}$  values taken from NASA's tables [61] being 844.9, 910.7, 1049.0, and 1369.5 respectively, although there is also a derivation in Appendix B.8 using Statistical Mechanics.

$$\begin{aligned} c_p &= \sum_i y_i c_{p,i} \\ c_p &= y_{\text{CO}_2} c_{p,\text{CO}_2}(T_{\text{avg}}) + y_{\text{CO}} c_{p,\text{CO}}(T_{\text{avg}}) + y_{\text{O}_2} c_{p,\text{O}_2}(T_{\text{avg}}) + y_{\text{O}} c_{p,\text{O}}(T_{\text{avg}}) \\ c_p &\in [844.9, 946.5] \text{ Jkg}^{-1}\text{K}^{-1} \end{aligned} \quad (3.15)$$

It can be seen later in Figure 4.1, that the fractions of these species remain in the ranges [0.375, 1], [0, 0.235], [0, 0.22], and [0, 0.135] respectively with the assumption that, as seen in Figure 3.1, the bulk gas temperature doesn't show enough of a measurable change from  $T_0$ .

The gas temperature is influenced by external energy input, heat loss to the environment, and the intrinsic thermal properties of the system. The rate of temperature change is proportional to the net heat flux  $\dot{Q}$ , the sum of  $Q$  and  $\dot{Q}_{\text{loss}}$ , as expressed in Equation 3.16.

$$\frac{dT_{\text{gas}}}{dt} = \frac{\dot{Q}}{\dot{m}c_p} \quad | \quad \dot{Q} = Q - \dot{Q}_{\text{loss}} \quad (3.16)$$

The gas temperature can be updated iteratively, with a concise derivation in Appendix B.9 through numerical integration, such as via the Euler integration method.

$$T_{\text{gas}}(t + dt) = T_{\text{gas}}(t) + \frac{\dot{Q}}{\dot{m}c_p} \cdot dt \quad (3.17)$$

Equally important is the vibrational excitation temperature,  $T_{\text{exc}}$ , which characterises the energy distribution among molecular vibrational states and underpins reaction mechanisms in non-thermal plasmas [62]. High-energy electrons excite vibrational modes via inelastic collisions, while vibrational-translational relaxation drives  $T_{\text{exc}}$  toward  $T_{\text{gas}}$ , seen in Equation 3.18. Together, accurate predictions of  $T_{\text{gas}}$  and  $T_{\text{exc}}$  provide valuable insights for enhancing reactor design and operation.

$$\dot{E}_{\text{loss}} = \frac{T_{\text{exc}}(t) - T_{\text{gas}}(t)}{\tau_{\text{vt}}} \quad (3.18)$$

$\tau_{\text{vt}}$  = relaxation time constant [s]

Energy gain,  $\dot{E}_{\text{gain}}$ , arises from electron-molecule collisions that elevate the vibrational energy levels of the molecules. Equation 3.19 governs this process.

$$\dot{E}_{\text{gain}} = \frac{k_{\text{exc}} n_e E_e E_{\text{vib}}}{k_B} \quad (3.19)$$

$k_{\text{exc}}$  = excitation rate coefficient [ $\text{m}^3\text{s}^{-1}$ ]

$n_e$  = electron density [ $\text{m}^{-3}$ ] *derived fully in Appendix B.5*

$E_e$  = average electron energy [J] *extracted from BOLSIG+ [53]*

$T_{\text{exc}}$  can then be updated iteratively like the  $T_{\text{gas}}$ , shown in Equation 3.20.

---


$$T_{\text{exc}}(t + dt) = T_{\text{exc}}(t) + (\dot{E}_{\text{gain}} - \dot{E}_{\text{loss}}) \cdot dt \quad (3.20)$$

To ensure physical consistency, a constraint is imposed to prevent  $T_{\text{exc}}$  from falling below  $T_{\text{gas}}$  [63], reflecting the principle that vibrational states cannot equilibrate at temperatures lower than the ambient gas. Accurate modelling of  $T_{\text{exc}}$  is pivotal because enhanced vibrational excitation lowers energy barriers for key pathways such as dissociation and ionisation [64]. This approach reveals how energy is partitioned within the plasma, thereby optimising reaction efficiencies and yields and advancing plasma-assisted chemical technologies [63].

### 3.2.2.3 Reaction Rates

Accurate reaction rate determination is essential for modelling plasma-based processes, such as CO<sub>2</sub> decomposition [49]. Reaction rates quantify how quickly species transform under given conditions, and they depend on factors like temperature, activation energy, and the energy transfer mechanisms within the plasma. For thermally driven reactions, the Arrhenius equation provides the reaction rate coefficient.

$$k = A e^{-\frac{E_a}{RT_{\text{gas}}}} \quad (3.21)$$

$A$  = pre-exponential factor [m<sup>3</sup>s<sup>-1</sup>]

$E_a$  = activation energy [Jmol<sup>-1</sup>]

Computational tools like BOLSIG+ are widely used to calculate the EEDF and derive reaction rate coefficients for electron-impact processes. These rate coefficients  $k$  are crucial for plasma kinetic models and directly influence predictions of conversion efficiency and energy balance in plasma reactors [52].

$$k = \int_0^{\infty} \sigma(\epsilon)v(\epsilon)f(\epsilon)d\epsilon \quad (3.22)$$

$\epsilon$  = electron energy [eV]

$\sigma(\epsilon)$  = cross-section [m<sup>2</sup>]

$v(\epsilon)$  = electron velocity [ms<sup>-1</sup>]

$f(\epsilon)$  = EEDF [eV<sup>-1</sup>]

BOLSIG+ solves the Boltzmann equation, Equation 3.23, for electrons in an electric field, using cross-sectional data to calculate rate coefficients for ionisation, excitation, and dissociation processes based on the EEDF. In NTPs, energy transfer to vibrational excitation is critical for efficient dissociation [49]. These computed reaction rates are integrated into chemical kinetic models to simulate plasma dynamics and assess how external parameters, such as electric field strength or gas composition, influence performance [64].

---


$$\frac{\partial f}{\partial t} + \mathbf{v} \cdot \nabla_{\mathbf{x}} f + \frac{\mathbf{F}}{m} \cdot \nabla_{\mathbf{v}} f = \left( \frac{\partial f}{\partial t} \right)_{\text{coll}} \quad (3.23)$$

The evolution of species concentrations in a plasma-chemical reactor is governed by first-order ODEs based on the law of mass action. These equations capture both forward and backward reactions involving key species by incorporating rate constants that characterise dissociation, recombination, and ionisation pathways [19]. For example, the dissociation of carbon dioxide into carbon monoxide and atomic oxygen is expressed mathematically by 3.24.



This illustrates the competition between forward dissociation and the recombination of CO and atomic oxygen to regenerate  $\text{CO}_2$  [64]. At the same time, species kinetics are similarly affected by the formation of  $\text{O}_2$  via atomic oxygen recombination and  $\text{O}_3$  production from oxygen interactions. The model incorporates quadratic and higher-order terms, such as  $[\text{O}]^2$  in  $\text{O}_2$  formation and  $[\text{O}_2][\text{O}]$  in  $\text{O}_3$  production, to capture non-linear dependencies on parameters like temperature and electron energy [19]. To solve these coupled equations, the fourth-order RK4 method is employed, reducing numerical error and permitting longer time steps without loss of precision. This high-fidelity approach is essential for analysing reaction efficiencies, energy transfer, and byproduct formation, thereby advancing the optimisation of plasma reactors [48].

### 3.3 Computational Implementation

There are several computational tools and methodologies employed in the development of the simulation model for the  $\text{CO}_2$  decomposition process in a DBD reactor. A combination of specialised software tools was utilised to simulate plasma reactions, solve complex systems of coupled differential equations, and visualise the results in a manner that facilitates deeper understanding and informed analysis [62]. Each tool was chosen for its unique capabilities and its ability to complement the other components of the computational framework.

#### 3.3.1 Program Design

##### 3.3.1.1 BOLSIG+

BOLSIG+ is a specialised software tool widely used in plasma physics to compute electron transport properties and rate coefficients for non-thermal plasmas. This tool was integral in generating the EEDFs, which describe the energy states of electrons within the plasma, and rate coefficients for electron-induced reactions [53]. These parameters are critical for accurately modelling the plasma's microscopic behaviour, ensuring that the physical properties and chemical dynamics of the system are well-represented. By enabling the calculation of these fundamental

quantities, BOLSIG+ provided a reliable foundation for incorporating plasma-specific characteristics into the broader simulation framework. This ensured that the reactor model could accurately reflect the complex and dynamic nature of the plasma environment.

### 3.3.1.2 Fortran Programming

Fortran, renowned for its numerical efficiency, was chosen as the backbone of the simulation model due to its aptitude for solving the coupled and decoupled systems of ODEs and PDEs governing reaction kinetics and plasma conditions in the DBD reactor [65]. The model incorporates adaptive time-stepping, robust error control, and accurate boundary and initial conditions to reflect the system's physical constraints. Its modular structure not only facilitates iterative improvements and debugging but also ensures scalability for future enhancements, such as integrating more complex reaction networks or extending the model to other plasma-assisted processes. By leveraging Fortran's computational speed and precision, the simulation achieves both accuracy and efficiency, making it a powerful tool for optimising reactor performance.

### 3.3.1.3 Plotting

MATLAB played a central role in post-processing and visualising simulation results from the Fortran program, although its .dat outputs are also easily interpreted by alternatives such as Python or Origin. MATLAB's advanced plotting capabilities enabled detailed visualisations, time-dependent profiles of reactant conversion rates, energy efficiency trends, and temperature distributions, while its numerical and statistical tools facilitated further insights, including optimal reactor configurations and correlations between operating conditions and performance. This approach provided a robust platform for presenting findings and supporting informed decision-making in the field.

## 3.3.2 Simplified Model

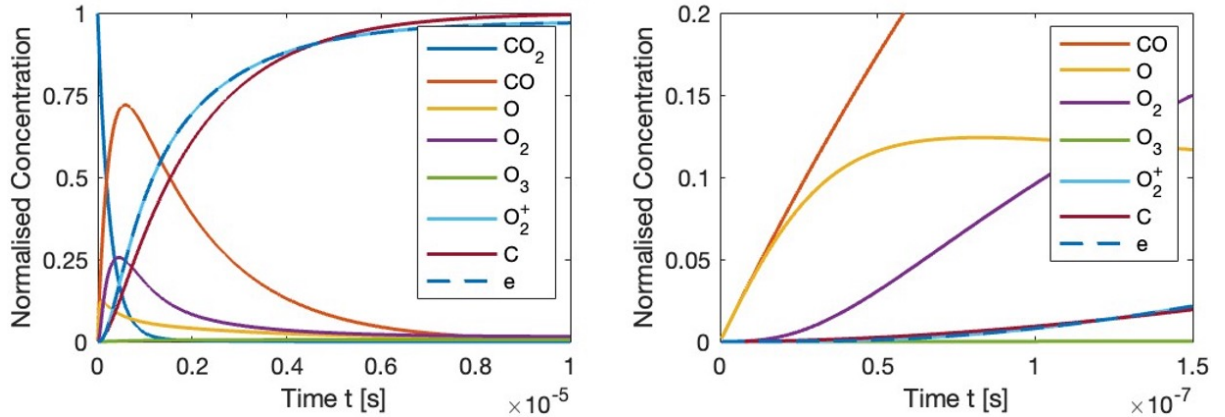


Figure 3.3: Normalised species concentration evolution for a simplified model

Figure 3.3 illustrates the time evolution of the key species in a simplified model of  $\text{CO}_2$  decomposition, governed by the reactions listed in Table 3.5. Although these five reactions represent a

---

highly idealised picture of plasma chemistry, they help to clarify the essential pathways leading to the observed shifts in species concentrations.  $\text{CO}_2$  is almost entirely consumed by about 1  $\mu\text{s}$ , dropping from a normalised concentration close to 1 at  $t=0$  to nearly 0 thereafter. CO becomes the predominant product during this window, rising to a peak of around 0.8 before gradually declining. Both atomic O and  $\text{O}_2$  show significant increases followed by downturns, highlighting their roles as reactive intermediates driving further transformations.

Table 3.4: Species in a simplified model

Species	Name
Key Species	
$\text{CO}_2$	Carbon Dioxide
CO	Carbon Monoxide
O	Atomic Oxygen
$\text{O}_2$	Oxygen
$\text{O}_3$	Ozone
Other Species	
$\text{O}_2^+$	Oxygen Positive Ion
C	Atomic Carbon
$e^-$	Electron

Table 3.5: Reaction profile of a simplified model

Reaction	Number
$\text{CO}_2 \rightleftharpoons \text{CO} + \text{O}$	S1
$\text{O} + \text{O} \rightleftharpoons \text{O}_2$	S2
$\text{O}_2 \rightleftharpoons \text{O}_2^+ + e^-$	S3
$\text{CO} \rightleftharpoons \text{C} + \text{O}$	S4
$\text{O}_2 + \text{O} \rightleftharpoons \text{O}_3$	S5

Later in the simulation window, the electron density and  $\text{O}_2^+$  both increase from negligible levels to more noticeable values. This late-stage rise indicates that once enough radicals and excited states accumulate, ionisation pathways become more prominent. Atomic C also appears as the reactions proceed, although it does not reach the same magnitudes as CO, suggesting further bond-breaking and recombination routes producing free carbon atoms. By contrast,  $\text{O}_3$  remains at a very low level throughout, implying that either it is not strongly formed under these conditions or it is quickly consumed by other reactions.

At discharge, CO and O exhibit the steepest gradients of formation in Figure 3.3, reflecting their status as direct dissociation products of  $\text{CO}_2$ . In the very first fraction of a microsecond,  $\text{CO}_2$  cleavage releases both CO and O almost immediately, driving a rapid increase in these two species. By contrast, the gradient for  $\text{O}_2$  growth is less steep, because it requires two free O atoms to combine. As a result,  $\text{O}_2$  rises more slowly at first, though its concentration eventually begins to climb once enough O has been produced. This difference in the initial slopes of the concentration curves directly mirrors the reaction pathways, CO and O come from the first bond break in  $\text{CO}_2$ , whereas  $\text{O}_2$  must form secondarily through O–O recombination.

---

## 4 Results & Analysis

To test the model's efficacy and present a comprehensive overview of the numerical and experimental findings for CO<sub>2</sub> decomposition in a non-thermal plasma, the data is plotted and analysed in MATLAB. Under the initial baseline conditions, shown in Table 4.1 in a standard pressure and temperature environment, key parameters such as discharge characteristics, plasma composition, and resulting conversion efficiencies are predicted. The model contextualises the plasma composition by normalising species concentrations within the reactor concerning the initial mass of CO<sub>2</sub> present within the chamber.

Table 4.1: Initial baseline conditions for model testing

Variable	Units	Value
Pressure	[Pa]	101325
Electrode Gap	[mm]	0.25
Volumetric Flow Rate	[mLmin <sup>-1</sup> ]	20
AC Supply Voltage	[V peak-to-peak]	6500
AC Supply Frequency	[Hz]	68000

These conditions serve as a reference point throughout the discussion and are systematically varied in the parametric studies to assess their impact on both the extent of conversion and the energy efficiency of the process. While the model presented here is still in its preliminary stages, it represents a promising start to understanding the system under investigation. The results, although not entirely comprehensive, offer valuable insights that highlight both the model's strengths and its current limitations. The aim is that by showcasing both the accuracies and pitfalls, readers can appreciate the progress made thus far while recognising the areas that require further refinement and development.

### 4.1 Plasma Composition

While the previous simplified scheme featured only five primarily bulk-gas reactions, the current framework expands to 30 elementary reactions, in Table 3.2, incorporating excited-state formation, de-excitation, and ionisation processes. This expansion reflects the complexity of real plasma environments, where metastable species, vibrational excitations, and multiple recombination pathways significantly alter concentration profiles. Figure 4.1 illustrates the time evolution of key species in this comprehensive model of CO<sub>2</sub> decomposition.

Notably, there is a more rapid initial decline in CO<sub>2</sub> due to multiple competing decomposition pathways, including both direct dissociation X1 and alternative bond-cleavage routes via metastable carbon dioxide (CO<sub>2</sub><sup>\*</sup>). Consequently, CO and O<sub>2</sub> appear earlier, with O<sub>2</sub> accumulating faster owing to abundant O atoms and direct channels. Additionally, the rise of metastable oxygen (O<sub>2</sub><sup>\*</sup>), although not shown explicitly, facilitates alternate routes to CO, O, and C, contributing to a richer diversity of plasma species.

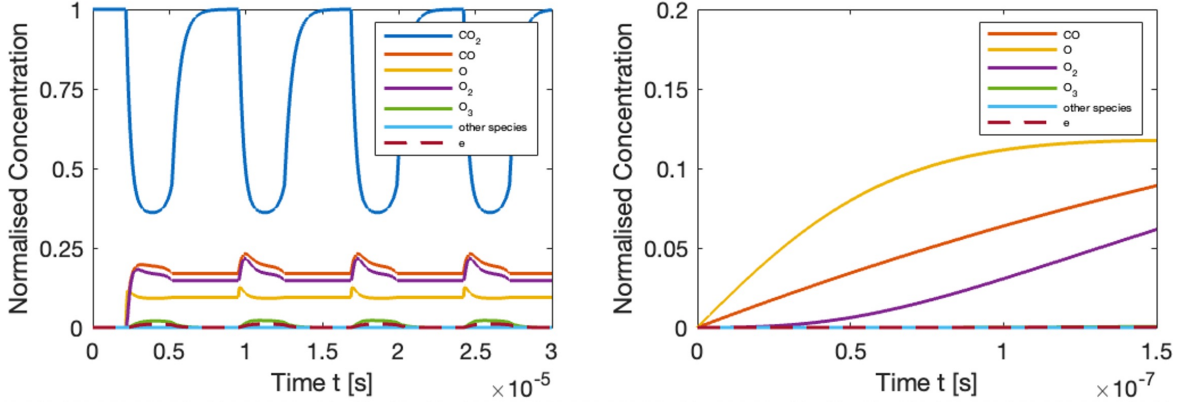


Figure 4.1: Normalised species concentration evolution for a complex model

Later in the simulation, as excited and ionised species accumulate, carbon becomes more available via CO splitting and direct  $O_2^*$  channels, though its concentration remains lower than that of the main products. Meanwhile,  $O_3$  may remain low if rapidly consumed or under unfavourable conditions, yet higher  $O_2$  partial pressures or longer reaction times can lead to increased ozone levels compared to a minimal five-reaction model. These observations show that incorporating excited-state chemistry opens additional pathways for decomposition, recombination, and ionisation, resulting in faster  $CO_2$  depletion and earlier by-product formation. Consequently, the plasma exhibits richer dynamics than the simpler model, underscoring the critical role of excited states and secondary collisions in determining overall composition and reaction rates.

## 4.2 Parametric Studies

Parametric studies are vital for validating the robustness and predictive power of any modelling framework, especially for complex plasma processes. By systematically varying parameters like pressure, electrode gap, volumetric flow rate, AC supply voltage, and frequency, one can assess model sensitivity and verify that predicted trends match physical and experimental expectations. These studies reveal weaknesses in reaction pathways, rate constants, and boundary conditions, while distinguishing dominant mechanisms from secondary effects, ultimately enabling model refinement, system optimisation, and reliable predictions across diverse regimes.

### 4.2.1 Pressure Variation

The computational model suggests that adjusting the pressure in a DBD plasma significantly influences the formation of  $O_2$  from  $CO_2$ . At lower pressures, the extended electron mean free path allows electrons to gain higher energies before colliding with  $CO_2$  molecules, leading to enhanced dissociation into O, which recombines to form  $O_2$ , seen in Figure 4.2. The cyclical peaks in both concentration and production rate reflect the pulsed nature of the plasma and underscore the importance of energetic electron impacts in driving these reactions.

Simultaneously, the model predicts that CO, a highly desired product, also benefits from slightly reduced pressures, as shown in Figure 4.3. With fewer collisional losses, a greater proportion

of electrons can exceed the threshold energy needed to cleave  $\text{CO}_2$  into  $\text{CO}$  and  $\text{O}$ , boosting  $\text{CO}$  production during the plasma pulses. From a plasma chemistry standpoint, the shift in the electron energy distribution under lower pressure appears to favour the dissociation pathways leading to  $\text{CO}$  formation.

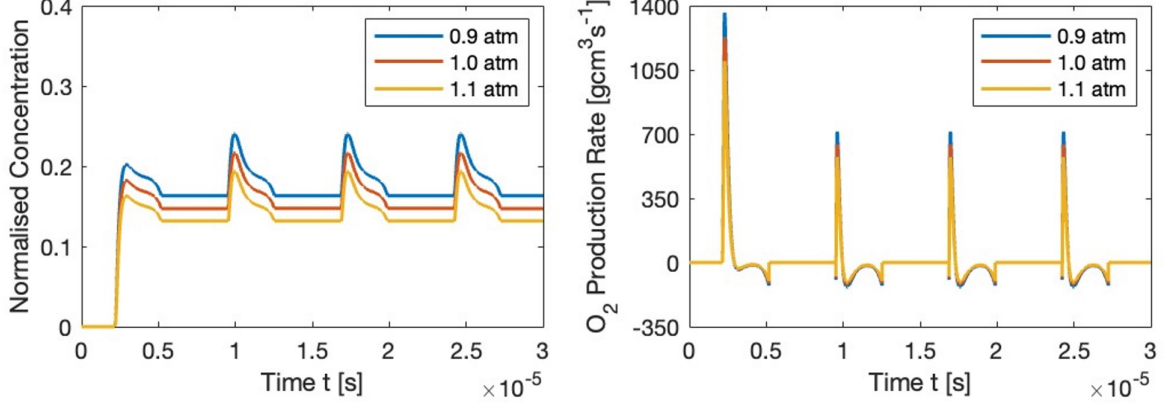


Figure 4.2: Effects of pressure change on the formation of  $\text{O}_2$  from  $\text{CO}_2$

However, at higher pressures, the model indicates that both  $\text{O}_2$  and  $\text{CO}$  production rates diminish. This indicates increased collisional quenching, which restricts electron energy gains, and from competition for  $\text{O}$  once  $\text{O}_2$  formation is underway. Overall, these findings emphasise that optimising the operating pressure, alongside other parameters such as voltage amplitude and pulse frequency, is key to steering the plasma chemistry more selectively towards  $\text{CO}$ .

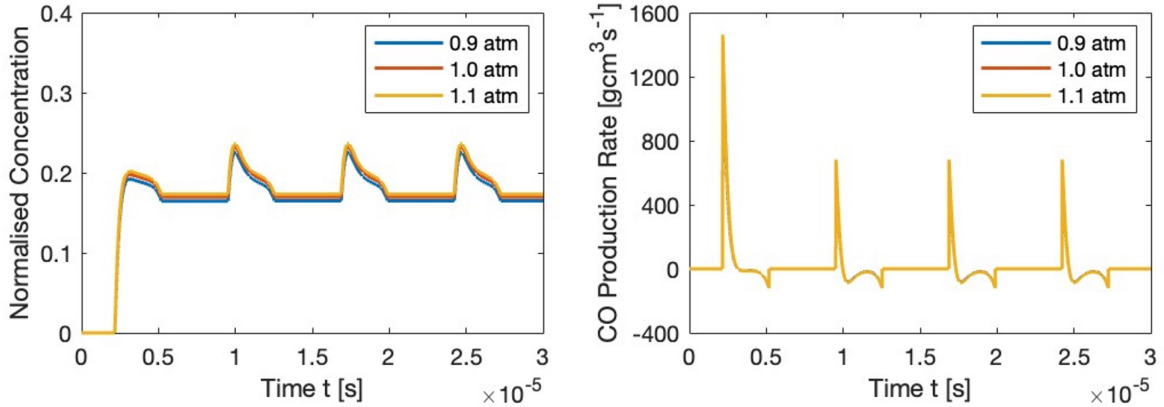


Figure 4.3: Effects of pressure change on the formation of  $\text{CO}$  from  $\text{CO}_2$

#### 4.2.2 Electrode Gap Variation

A key factor in the effect of electrode gap changes on  $\text{CO}_2$  decomposition is the reduced electric field  $\frac{E}{N}$ , which describes the electric field strength per unit density of neutral gas. When the gap between electrodes is reduced with constant voltage, the local electric field intensifies, raising  $\frac{E}{N}$  so electrons in the discharge can gain more energy before colliding with gas molecules, driving higher rates of  $\text{CO}_2$  dissociation. Conversely, at wider gaps, the electric field becomes more diffuse, lowering  $\frac{E}{N}$  and reducing the average electron energy available for breaking  $\text{CO}_2$  bonds.

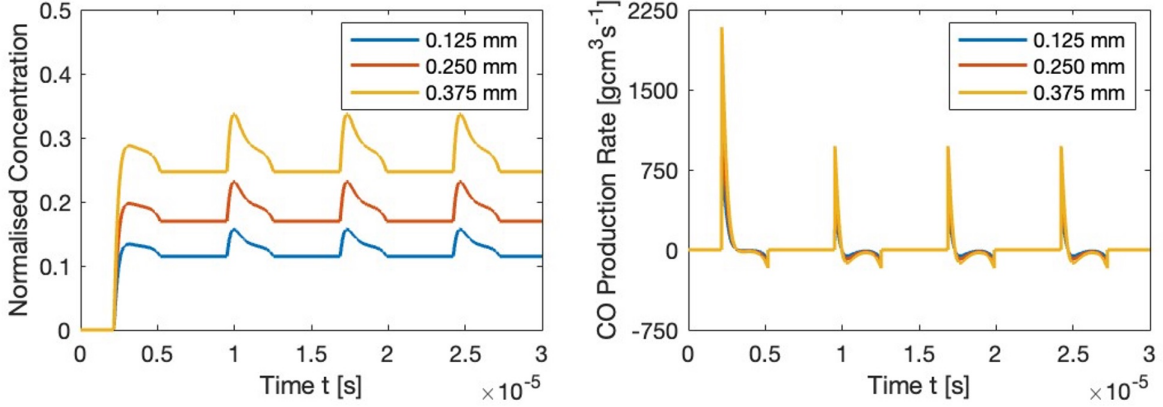


Figure 4.4: Effects of electrode gap change on the formation of CO from  $\text{CO}_2$

Such variations in the reduced electric field have a direct bearing on plasma chemistry, as electron impact processes dominate the initial steps of  $\text{CO}_2$  splitting. When  $\frac{E}{N}$  is sufficiently high, electrons surpass the energy thresholds for exciting and ionising  $\text{CO}_2$ , leading to increased formation of reactive species, particularly CO and O. The resulting reactive species can recombine or further react in a variety of pathways, but high electron energies generally promote the dissociation route towards CO, seen in Figure 4.4.

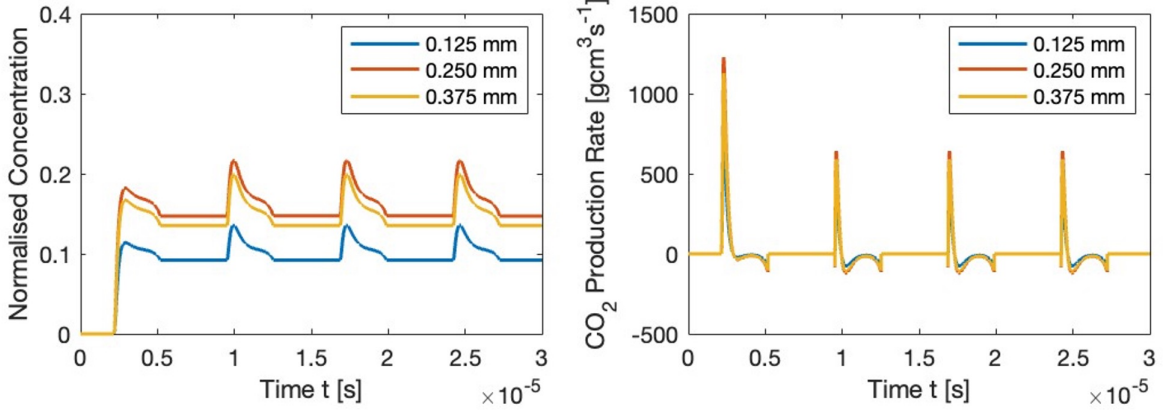


Figure 4.5: Effects of electrode gap change on the formation of  $\text{O}_2$  from  $\text{CO}_2$

By contrast, at lower  $\frac{E}{N}$  conditions associated with larger electrode gaps, electron collisions are more frequent yet less energetic. This favours pathways that allow oxygen atoms to find each other and form  $\text{O}_2$ , shown in Figure 4.5, and overall limits the production of CO. Hence, optimising the electrode gap, and thus the reduced electric field, is crucial for steering the plasma reactions toward the desired product, be it CO or  $\text{O}_2$ , depending on process requirements.

#### 4.2.3 Volumetric Flow Rate Variation

The model also reveals that the volumetric flow rate  $\dot{V}$  strongly influences the decomposition of  $\text{CO}_2$  into CO in a DBD reactor. When  $\dot{V}$  is low, the residence time of  $\text{CO}_2$  within the plasma region increases, allowing more extensive interaction with energetic electrons. As a result, CO formation is enhanced, as reflected in higher normalised CO concentration and production

rates. By contrast, raising  $\dot{V}$  reduces the time available for electron-molecule collisions, leading to lower overall CO conversion, as evidenced by Figure 4.6.

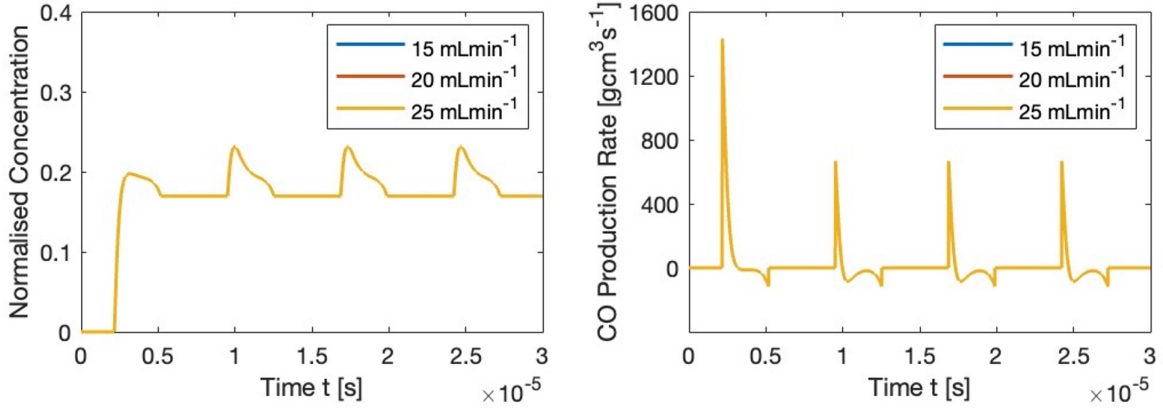


Figure 4.6: Effects of volumetric  $\dot{V}$  on the formation of CO from  $\text{CO}_2$

These findings correlate with shifts in the  $\frac{E}{N}$ . At lower flow rates, the model predicts a more pronounced electric field, enabling electrons to reach higher energies and thus more readily dissociate  $\text{CO}_2$  into CO and O. Conversely, as  $\dot{V}$  increases,  $\frac{E}{N}$  decreases, curtailing the average electron energy and diminishing the effectiveness of electron impact reactions. This reduction in electron energy also alters the pathways of plasma chemistry, subtly affecting the formation of other species, including  $\text{O}_2$ .

In parallel, the SEI reflects the energy expended per unit volume of  $\text{CO}_2$  flow. Holding the discharge power constant means that lowering  $\dot{V}$  concentrates more electrical energy per molecule of  $\text{CO}_2$ , boosting CO production. However, excessively low flow rates may compromise throughput, making the process less practical at scale. Hence, there is an optimal flow regime where residence time, reduced electric field, and SEI are balanced to maximise CO yield while retaining acceptable process efficiency.

#### 4.2.4 AC Voltage Variation

Increasing the AC supply voltage in the model seems to enhance the decomposition of  $\text{CO}_2$  into CO. Higher voltages yield stronger electric fields, shown in Figure 4.7, which in turn produce more energetic electrons and promote the electron impact reactions necessary to cleave  $\text{CO}_2$ . This effect is evident in both the normalised CO concentration and the peak CO production rates, which rise with increasing voltage and follow the pulsed nature of the discharge.

From a plasma chemistry perspective, the heightened electric field can be quantified through the  $\frac{E}{N}$ , which scales with supply voltage, as in Equation 3.4. As  $\frac{E}{N}$  grows, more electrons acquire energies above the dissociation threshold of  $\text{CO}_2$ , boosting the generation of CO and O. The increased electron impact frequency also influences secondary reactions, including vibrational and ionisation processes, which help sustain the plasma and reinforce the pathways leading to CO formation.

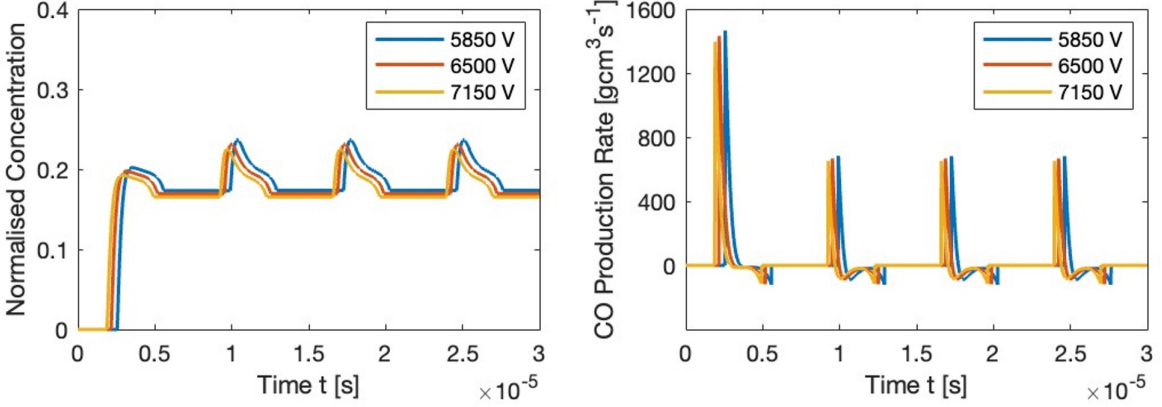


Figure 4.7: Effects of AC supply voltage change on the formation of CO from  $\text{CO}_2$

However, raising the supply voltage also elevates the SEI, meaning more electrical energy is expended per unit amount of  $\text{CO}_2$  treated. While this can improve conversion efficiency up to a point, excessive voltages may reduce overall energy efficiency by introducing competing side reactions and greater heat losses. Consequently, optimising the AC supply voltage involves balancing the benefit of higher CO yields against the associated rise in SEI, ensuring a favourable trade-off between conversion and energy consumption.

#### 4.2.5 AC Frequency Variation

Finally, the model indicates that increasing the AC supply frequency in a DBD reactor can enhance  $\text{CO}_2$  decomposition into CO, seen in Figure 4.8, primarily because more plasma pulses occur within a given timeframe. Each pulse delivers a surge of energetic electrons capable of dissociating  $\text{CO}_2$ , so increasing the pulse repetition rate increases the overall number of electron–molecule collisions. This leads to a noticeable rise in both the normalised CO concentration and the CO production rate, although the extent of improvement can be more subtle than that observed with voltage changes. In particular, higher frequencies may mean shorter pulse durations, which can limit the maximum electron density and energy per pulse, introducing a delicate balance in the plasma chemistry.

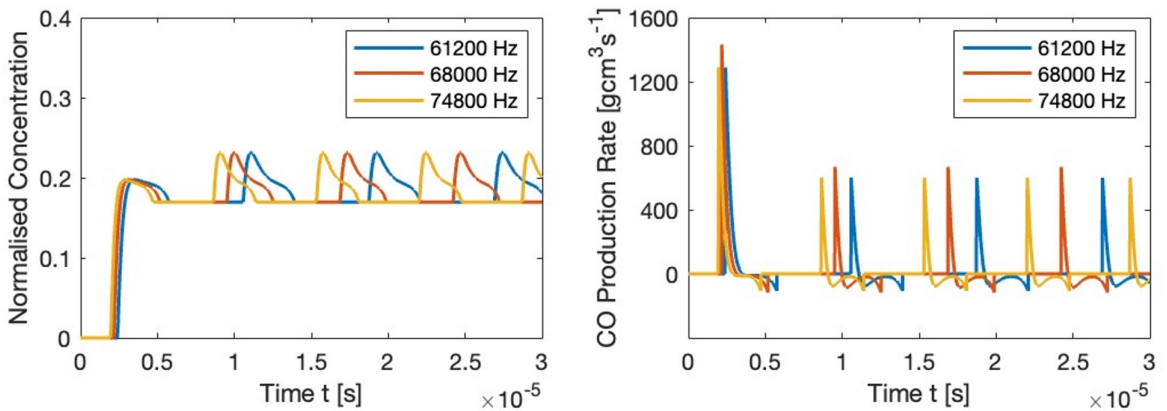


Figure 4.8: Effects of AC supply frequency change on the formation of CO from  $\text{CO}_2$

From a plasma chemistry perspective, raising the frequency also alters the temporal dynamics of the discharge. At higher repetition rates, the plasma may not fully extinguish between pulses, allowing excited states to persist from one pulse to the next. These long-lived intermediates play a critical role in enhancing CO formation, as they can participate in secondary reactions that bypass the need for additional high-energy electron impacts. Moreover, the EEDF shifts with changing pulse structure as frequent and shorter pulses can maintain a higher fraction of moderately energetic electrons, which in turn favours pathways leading to CO and O rather than complete quenching or recombination.

However, increasing the supply frequency also raises the SEI, because more pulses per second translates to higher power consumption. While this can boost CO yields by sustaining a more active plasma, it may also exacerbate side reactions, thermal losses, and electrode heating. As a result, finding the optimal frequency involves balancing the enhanced reaction kinetics, driven by persistent excited species and more frequent electron collisions, against the rising energy costs. By tuning frequency to maintain an advantageous EEDF and minimise parasitic processes, operators can maximise CO production efficiency for a given energy expenditure.

### 4.3 Production Rates and Energy Efficiency

The computational code model simulating a pulsed DBD reactor reveals transient chemical dynamics that underpin plasma-assisted CO<sub>2</sub> conversion. According to the model, within each plasma pulse, the strong electric field accelerates electrons to energies capable of dissociating CO<sub>2</sub>. For instance, around 20  $\mu$ s into a pulse, the CO production rate peaks at approximately 1450 gcm<sup>3</sup>s<sup>-1</sup>, indicating highly energetic, non-thermal processes. Simultaneously, reactive oxygen species produced by these electron-impact events recombine with O<sub>2</sub> to form O<sub>3</sub>, which reaches a peak production rate of about 50 gcm<sup>3</sup>s<sup>-1</sup>. Figure 4.9 illustrates the dual role of energetic electrons: they drive the desired CO<sub>2</sub> dissociation yet also promote competing reactions leading to by-products like O<sub>3</sub>.

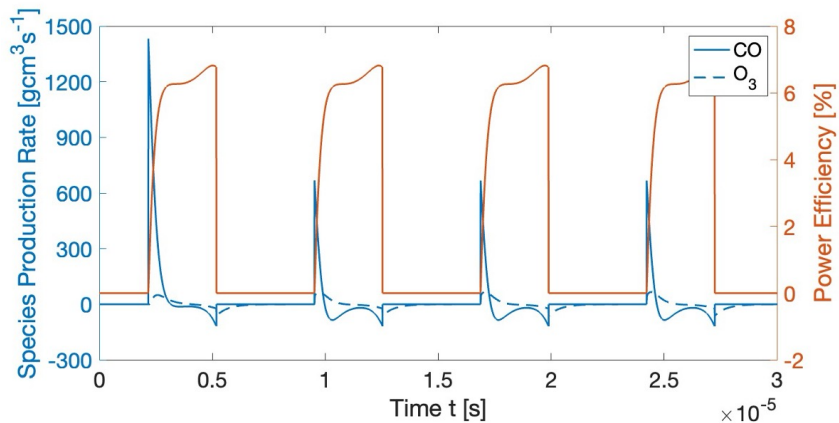


Figure 4.9: Production rates for species of interest compared to power input efficiency

From a plasma physics standpoint, the model captures key aspects such as the  $\frac{E}{N}$  and its effect

---

on the EEDF. Under high  $\frac{E}{N}$  conditions, electrons attain energies exceeding the dissociation threshold of CO<sub>2</sub>, thereby initiating a cascade of reactions that generate CO and O. The subsequent recombination of O with molecular oxygen underscores ozone formation. Moreover, the overall power input efficiency, measured at roughly 7% during peak discharge, highlights the inherent energy losses in non-thermal plasmas, only a fraction of the supplied energy is effectively utilised for chemical conversion.

The model reveals an inverse relationship between power efficiency and production rate, a major barrier in industrial applications, where conditions that enhance CO production often lead to increased energy consumption and reduced efficiency due to heightened side reactions. This virtual laboratory approach enables the optimisation of key operational parameters, ultimately paving the way for more energy-efficient plasma-assisted CO<sub>2</sub> conversion strategies that address the critical challenge of balancing high production rates with acceptable power efficiency.

#### 4.4 Technical Analysis

This model demonstrates notable strengths by integrating detailed plasma kinetics with non-thermal plasma physics, effectively capturing the transient dynamics and electron-impact reactions within a dielectric barrier discharge reactor. It successfully elucidates the competing pathways to CO production and by-product formation, such as O<sub>3</sub>, while accounting for key processes like vibrational CO<sub>2</sub> excitation and the generation of reactive radicals that lower activation barriers. This virtual framework enables systematic exploration of critical operational parameters, such as applied voltage and pulse frequency, in plasma-assisted CO<sub>2</sub> conversion.

From a scientific computing perspective, several improvements are required. The absence of a fluid mechanics module limits the model's ability to accurately simulate gas flow and mass transport, both essential for representing the spatial distribution of reactive species and energy within the reactor. The current electrodynamics treatment also relies on oversimplified approximations, failing to capture phenomena such as capacitive voltage division and the non-uniform electric fields that critically shape the EEDF. Since the EEDF directly influences the reaction rate coefficients for electron impact processes, a more rigorous electrodynamics model is vital.

From a plasma chemistry standpoint, the reaction profile and kinetic data need further refinement and validation to capture the complex interplay between plasma physics and chemical kinetics under varying conditions. The current reaction mechanisms are overly simplified, omitting detailed processes such as vibrational ladder climbing, metastable state formation, and the subsequent secondary reactions that affect CO production. A more comprehensive kinetics framework should include multiple reaction channels, such as vibrational-vibrational and vibrational-translational transfer processes, and accurately model the formation and quenching of reactive intermediates. Addressing these deficiencies through enhanced fluid mechanics, rigorous electrodynamics, and an updated reaction kinetics framework is essential for advancing the model toward a robust, industrially applicable platform for plasma-assisted CO<sub>2</sub> conversion.

---

## 5 Conclusion

This study has demonstrated that a global computational model is a highly effective tool to simulate the complex kinetics and dynamic behaviours inherent in dielectric barrier discharge plasma reactors used for CO<sub>2</sub> decomposition. The program, through its robust implementation of numerical methods, has successfully captured the transient evolution of reactive species alongside the nuanced interplay between electrodynamic forces and chemical reaction pathways. Its capacity to model both the rapid electron-driven processes and the more gradual thermal and vibrational phenomena has provided invaluable insight into optimising reactor performance.

The exploration of DBD technology for mass production appears promising, showing that the DBD reactor, operating under mild conditions and capable of utilising intermittent renewable energy sources, presents a compelling alternative to energy-intensive methods of CO<sub>2</sub> conversion. Although challenges remain, such as enhancing energy efficiency, ensuring material durability, and scaling the reactor design, the financial analyses suggest that, with further refinement, DBD reactors could be well-positioned within the industrial market. The objectives to demonstrate the viability of DBD technology are being met, although there is room for further optimisation.

The study has reaffirmed the pivotal role of scientific computing methods in advancing the field of plasma-assisted CO<sub>2</sub> decomposition. High-fidelity computational models have deepened understanding of the decomposition process and significantly reduced the reliance on expensive and time-consuming experimental trials. As the field progresses, the ability to simulate complex, multiphysical phenomena will be indispensable for optimising reactor design and process control, thereby expediting the transition from laboratory prototypes to industrial-scale applications. In this regard, the objective of advancing both scientific and practical understanding through computational modelling has been successfully realised.

Future improvements should focus on several key areas. Firstly, enhancing the model's resolution by incorporating multidimensional effects and real-time diagnostic feedback could provide a more comprehensive depiction of plasma behaviour. Considering quantum and statistical mechanics of the gas molecules and charged particles would also contribute to both increased accuracy and a more dynamic model. Secondly, further research into advanced materials for reactor components and electrodes is essential to mitigate issues related to wear and dielectric degradation. Lastly, closer integration of experimental data with computational predictions will be vital in refining the model's accuracy and predictive power.

Overall, this report highlights a transformative synergy between scientific computing and plasma-based CO<sub>2</sub> conversion technologies. By continuing to innovate and refine both the computational models and the physical reactor designs, the prospect of deploying DBD reactors at a commercial scale becomes increasingly tangible, promising a sustainable pathway for carbon management in the quest for a low-carbon future.

## References

- [1] C. D. Keeling *et al.*, *Atmospheric CO<sub>2</sub> and <sup>13</sup>CO<sub>2</sub> exchange with the terrestrial biosphere and oceans from 1978 to 2000: observations and carbon cycle implications*. Springer Verlag, 2005, pp. 83–113.
- [2] P. Smith *et al.*, “Biophysical and economic limits to negative CO<sub>2</sub> emissions,” pp. 42–50, 1 2016.
- [3] Department for Energy Security and Net Zero, “Net Zero Government Initiative: UK roadmap to net zero government emissions,” HM Government, Tech. Rep., 2023.
- [4] S&P Global, “Fact Sheet: Carbon Capture Utilization and Storage (CCUS),” 2023, [Accessed: Oct. 17, 2024]. [Online]. Available: [www.spglobal.com/commodityinsights](http://www.spglobal.com/commodityinsights).
- [5] International Energy Agency, “Electricity 2024 - Analysis and forecast to 2026,” 1 2024, [Accessed: Nov. 12, 2024]. [Online]. Available: [www.iea.org](http://www.iea.org)
- [6] T. Kozák and A. Bogaerts, “Splitting of CO<sub>2</sub> by vibrational excitation in non-equilibrium plasmas: A reaction kinetics model,” *Plasma Sources Science and Technology*, vol. 23, 2014.
- [7] D. W. Keith *et al.*, “A Process for Capturing CO<sub>2</sub> from the Atmosphere,” *Joule*, vol. 2, pp. 1573–1594, 8 2018.
- [8] C. Beuttler, L. Charles, and J. Wurzbacher, “The Role of Direct Air Capture in Mitigation of Anthropogenic Greenhouse Gas Emissions,” *Frontiers in Climate*, vol. 1, 11 2019.
- [9] World Bank Group, “State and Trends of Carbon Pricing Dashboard,” 12 2024, [Accessed: Nov. 03, 2024]. [Online]. Available: <https://carbonpricingdashboard.worldbank.org/compliance/price>
- [10] P. Gladysz *et al.*, “Merging Climate Action with Energy Security through CCS-A Multi-Disciplinary Framework for Assessment,” *Energies*, vol. 16, 1 2023.
- [11] Intergovernmental Panel on Climate Change, *Technical Summary*. Cambridge University Press, 6 2023, pp. 35–144.
- [12] R. Agarwal and D. Liu, “Direct air CO<sub>2</sub> capture and storage (DACCs),” *Introduction to Modeling, Simulation and Optimization of CO<sub>2</sub> Sequestration in Various Types of Reservoirs*, pp. 363–379, 1 2025, [Accessed: Oct. 21, 2024]. [Online]. Available: <https://linkinghub.elsevier.com/retrieve/pii/B9780443153310000113>
- [13] H. Pilorgé *et al.*, “Cost Analysis of Carbon Capture and Sequestration of Process Emissions from the U.S. Industrial Sector,” *Environmental Science and Technology*, vol. 54, pp. 7524–7532, 6 2020.
- [14] S. He *et al.*, “Thermodynamic evaluation of a Ca-Cu looping post-combustion CO<sub>2</sub> capture system integrated with thermochemical recuperation based on steam methane reforming,” *Case Studies in Thermal Engineering*, vol. 63, p. 105327, 11 2024.
- [15] Z. Li *et al.*, “Photochemical reduction of CO<sub>2</sub> into CO coupling with triethanolamine decomposition,” *RSC Advances*, vol. 13, pp. 31 616–31 621, 10 2023, [Accessed: Oct. 09, 2024]. [Online]. Available: <https://pubs.rsc.org/en/content/articlehtml/2023/ra/d3ra06585ehttps://pubs.rsc.org/en/content/articlelanding/2023/ra/d3ra06585e>
- [16] X. Li *et al.*, “Electrochemical CO<sub>2</sub> reduction to liquid fuels: Mechanistic pathways and surface/interface engineering of catalysts and electrolytes,” *The Innovation*, p. 100807, 1 2025, [Accessed: Oct. 11, 2024]. [Online]. Available: <https://linkinghub.elsevier.com/retrieve/pii/S2666675825000104>
- [17] Z. Li *et al.*, “Efficient CO<sub>2</sub> capture from flue gases achieving by an electrochemical reactor with porous solid-state electrolyte,” *Chemical Engineering Journal*, vol. 505, p. 159468, 2 2025.
- [18] W. Xie *et al.*, “Metal-Organic Frameworks for Electrocatalytic CO<sub>2</sub> Reduction into Formic Acid,” *Catalysts*, 2023, [Accessed: Dec. 06, 2024]. [Online]. Available: <https://doi.org/10.3390/catal13071109>
- [19] K. Zhang and A. P. Harvey, “CO<sub>2</sub> decomposition to CO in the presence of up to 50% O<sub>2</sub> using a non-thermal plasma at atmospheric temperature and pressure,” *Chemical Engineering Journal*, vol. 405, p. 126625, 2 2021.
- [20] Y. Miao *et al.*, “Application-oriented non-thermal plasma in chemical reaction engineering: A review,” *Green Energy and Resources*, vol. 1, p. 100004, 3 2023.
- [21] J. Osorio-Tejada *et al.*, “CO<sub>2</sub> conversion to CO via plasma and electrolysis: a techno-economic and energy cost analysis,” *Energy & Environmental Science*, vol. 17, p. 5833, 5 2024, [Accessed: Nov. 06, 2024]. [Online]. Available: <https://pmc.ncbi.nlm.nih.gov/articles/PMC11320396>
- [22] D. Khunda *et al.*, “Scaling Down the Great Egypt Pyramids to Enhance CO<sub>2</sub>

- Splitting in a Micro DBD Reactor," *Plasma Chemistry and Plasma Processing*, vol. 43, pp. 2017–2034, 11 2023.
- [23] N. Pourali *et al.*, "Nonoxidative methane coupling in a micro-DBD with enhanced secondary electron emission," *Plasma Processes and Polymers*, vol. 20, 11 2023.
- [24] D. Khunda *et al.*, "Effect of temperature on the CO<sub>2</sub> splitting rate in a DBD microreactor," *Reaction Chemistry and Engineering*, vol. 8, pp. 2223–2233, 5 2023.
- [25] P. Lamichhane *et al.*, "Energy Intensified Nitrogen Fixation Through Fast Modulated Gas Discharge from Pyramid-shaped Micro-electrode," *Plasma Chemistry and Plasma Processing*, vol. 44, pp. 1369–1392, 5 2024.
- [26] N. Pourali *et al.*, "Development of a microkinetic model for non-oxidative coupling of methane over a Cu catalyst in a non-thermal plasma reactor," *Journal of Physics D: Applied Physics*, vol. 55, 9 2022.
- [27] H. Lamberts-Van Assche, G. Thomassen, and T. Compernolle, "The early-stage design of plasma for the conversion of CO<sub>2</sub> to chemicals: A prospective techno-economic assessment," *Journal of CO<sub>2</sub> Utilization*, 2022, [Accessed: Nov. 14, 2024]. [Online]. Available: <https://doi.org/10.1016/J.JCOU.2022.102156>
- [28] H. Hatami *et al.*, "CO<sub>2</sub> conversion in a dielectric barrier discharge plasma by argon dilution over MgO/HKUST-1 catalyst using response surface methodology," *Heliyon*, vol. 10, p. e26280, 2 2024, [Accessed: Dec. 28, 2024]. [Online]. Available: <https://pmc.ncbi.nlm.nih.gov/articles/PMC10878997/>
- [29] A. Bogaerts *et al.*, "CO<sub>2</sub> conversion by plasma technology: Insights from modeling the plasma chemistry and plasma reactor design," *Plasma Sources Science and Technology*, vol. 26, 5 2017.
- [30] A. M. Banerjee *et al.*, "Conversion of CO<sub>2</sub> in a packed-bed dielectric barrier discharge reactor," *Journal of Vacuum Science & Technology A: Vacuum, Surfaces, and Films*, vol. 36, 7 2018.
- [31] E. Rebrov and S. Li, "Plasma Chemistry in Microflow - Basics of plasma chemistry and applications," September 2024.
- [32] Y. Uytdenhouwen *et al.*, "A packed-bed DBD micro plasma reactor for CO<sub>2</sub> dissociation: Does size matter?" *Chemical Engineering Journal*, vol. 348, pp. 557–568, 9 2018.
- [33] N. Pourali *et al.*, "Study of plasma parameters and gas heating in the voltage range of nondischarge to full-discharge in a methane-fed dielectric barrier discharge," *Plasma Processes and Polymers*, vol. 20, 1 2023.
- [34] M. Bui *et al.*, "Carbon capture and storage (CCS): the way forward," *Energy & Environmental Science*, vol. 11, pp. 1062–1176, 5 2018, [Accessed: Dec. 01, 2024]. [Online]. Available: <https://pubs.rsc.org/en/content/articlehtml/2018/ee/c7ee02342ahttps://pubs.rsc.org/en/content/articlelanding/2018/ee/c7ee02342a>
- [35] R. C. Ferguson *et al.*, "Storing CO<sub>2</sub> with Enhanced Oil Recovery," in *Energy Procedia*, vol. 1, 2 2009, pp. 1989–1996.
- [36] Y. Zheng *et al.*, *Economic Analysis of CO<sub>2</sub> Conversion to Useful Fuels/Chemicals*. CRC Press, 7 2019, pp. 287–296.
- [37] L. Hu *et al.*, "Chemico-biological conversion of carbon dioxide," *Journal of Energy Chemistry*, vol. 89, pp. 371–387, 2 2024.
- [38] P. Xu *et al.*, "Recent advances in CO<sub>2</sub> fixation by microalgae and its potential contribution to carbon neutrality," 4 2023.
- [39] H. Ostovari *et al.*, "Towards a European supply chain for CO<sub>2</sub> capture, utilization, and storage by mineralization: Insights from cost-optimal design," *Journal of CO<sub>2</sub> Utilization*, vol. 72, 6 2023.
- [40] M. Hanifa *et al.*, "A review on CO<sub>2</sub> capture and sequestration in the construction industry: Emerging approaches and commercialised technologies," 1 2023.
- [41] P. Roefs *et al.*, "CO<sub>2</sub>-enhanced oil recovery and CO<sub>2</sub> capture and storage: An environmental economic trade-off analysis," *Journal of Environmental Management*, vol. 239, pp. 167–177, 6 2019.
- [42] J. Lindorfer, L. Zeilerbauer, and J. Kepler, "Technical, Economic and Environmental (TEE) Assessment of Integrated Biorefineries Gasification based biorefinery case studies," 2022.
- [43] C. De Bie, J. Van Dijk, and A. Bogaerts, "CO<sub>2</sub> Hydrogenation in a Dielectric Barrier Discharge Plasma Revealed," *Journal of Physical Chemistry C*, vol. 120, pp. 25 210–25 224, 11 2016, [Accessed: Oct. 29, 2024]. [Online]. Available: <https://pubs.acs.org/doi/full/10.1021/acs.jpcc.6b07639>
- [44] R. B.-R. others, "Tandem catalytic approaches for CO<sub>2</sub> enriched Fischer-Tropsch synthesis," *Progress in Energy and Combustion Science*, vol. 103, p. 101159, 7 2024.
- [45] A. George *et al.*, "A Review of Non-

- Thermal Plasma Technology: A novel solution for CO<sub>2</sub> conversion and utilization,” 1 2021.
- [46] M. Ozturk and I. Dincer, “Integrated Gasification Combined Cycles,” *Comprehensive Energy Systems: Volumes 1-5*, vol. 4, pp. 364–473, 1 2018.
- [47] A. Berthelot and A. Bogaerts, “Modeling of CO<sub>2</sub> plasma: Effect of uncertainties in the plasma chemistry,” *Plasma Sources Science and Technology*, vol. 26, 10 2017.
- [48] P. Koelman, “Chemical aspects of CO<sub>2</sub> plasma modelling,” *Applied Physics and Science Education*, 4 2019, [Accessed: Nov. 16, 2024]. [Online]. Available: [www.tue.nl/taverne](http://www.tue.nl/taverne)
- [49] R. Aerts, W. Somers, and A. Bogaerts, “Carbon Dioxide Splitting in a Dielectric Barrier Discharge Plasma: A Combined Experimental and Computational Study,” *ChemSusChem*, vol. 8, pp. 702–716, 2 2015.
- [50] S. Maerivoet *et al.*, “Coupled multi-dimensional modelling of warm plasmas: Application and validation for an atmospheric pressure glow discharge in CO<sub>2</sub>/CH<sub>4</sub>/O<sub>2</sub>,” *Chemical Engineering Journal*, vol. 492, 7 2024.
- [51] P. Koelman *et al.*, “A Comprehensive Chemical Model for the Splitting of CO<sub>2</sub> in Non-Equilibrium Plasmas,” *Plasma Processes and Polymers*, vol. 14, 4 2017.
- [52] A. Berthelot and A. Bogaerts, “Modeling of plasma-based CO<sub>2</sub> conversion: Lumping of the vibrational levels,” 7 2016.
- [53] G. J. M. Hagelaar, “Brief documentation of BOLSIG+ version 07/2024,” 2024, [Accessed: Oct. 16, 2024]. [Online]. Available: [www.bolsig.laplace.univ-tlse.fr](http://www.bolsig.laplace.univ-tlse.fr)
- [54] A. Bogaerts *et al.*, “Modeling plasma-based CO<sub>2</sub> conversion: Crucial role of the dissociation cross section,” *Plasma Sources Science and Technology*, vol. 25, 8 2016.
- [55] H. Cheng, X. Lei, and X. Lu, “The CO<sub>2</sub> Conversion in a DBD Plasma: A 1D Synergistic Catalysis Model,” *Modern Low Temperature Plasma*, 12 2023, [Accessed: Nov. 22, 2024]. [Online]. Available: <https://www.innovationforever.com/article.MLTP20230134>
- [56] M. Calvo, S. G. Pinto, and J. Montijano, “Runge-Kutta Methods for the Numerical Solution of Stiff Semilinear Systems,” *BIT*, vol. 40, pp. 611–639, 12 2000.
- [57] S. Cowley *et al.*, *Plasma Physics via Computer Simulation*. CRC Press, 10 2018, [Accessed: Jan. 17, 2025]. [Online]. Available: <https://www.taylorfrancis.com/books/mono/10.1201/9781315275048/plasma-physics-via-computer-simulation-birdsall-langdon>
- [58] E. Rebrov and S. Li, “Microplasma In Flow - Introduction of plasma,” September 2024.
- [59] N. Mou *et al.*, “Numerical study and experimental validation of heat transfer capacity of flat-type divertor for fusion reactor,” *Nuclear Materials and Energy*, vol. 40, p. 101716, 9 2024.
- [60] M. Elshafie, S. Kambara, and Y. Hayakawa, “Study of the reactor temperature effect on H<sub>2</sub> production from steam decomposition using DBD plasma,” *Energy Reports*, 11 2019, [Accessed: Jan. 21, 2025]. [Online]. Available: [https://www.academia.edu/96435206/Study\\_of\\_the\\_reactor\\_temperature\\_effect\\_on\\_H2\\_production\\_from\\_steam\\_decomposition\\_using\\_DBD\\_plasma](https://www.academia.edu/96435206/Study_of_the_reactor_temperature_effect_on_H2_production_from_steam_decomposition_using_DBD_plasma)
- [61] B. J. McBride, M. J. Zehe, and S. Gordon, “NASA Glenn Coefficients for Calculating Thermodynamic Properties of Individual Species,” NASA, Tech. Rep., 9 2002, [Accessed: Jan. 20, 2025]. [Online]. Available: <http://www.sti.nasa.gov>
- [62] A. Fridman, *Plasma Chemistry*. Cambridge University Press, 1 2008, vol. 9780521847353, [Accessed: Jan. 16, 2025]. [Online]. Available: <https://www.cambridge.org/core/books/plasma-chemistry/842EA140F5D8C59F15AB82544A3E44CC>
- [63] K. H. R. Rouwenhorst, H. H. Kim, and L. Lefferts, “Vibrationally Excited Activation of N<sub>2</sub> in Plasma-Enhanced Catalytic Ammonia Synthesis: A Kinetic Analysis,” *ACS Sustainable Chemistry and Engineering*, vol. 7, pp. 17515–17522, 10 2019, [Accessed: Jan. 18, 2025]. [Online]. Available: <https://pubs.acs.org/doi/full/10.1021/acssuschemeng.9b04997>
- [64] M. Capitelli *et al.*, “Non-equilibrium plasma kinetics: a state-to-state approach,” *Plasma Sources Science and Technology*, vol. 16, p. S30, 1 2007, [Accessed: Jan. 20, 2025]. [Online]. Available: <https://iopscience.iop.org/article/10.1088/0963-0252/16/1/S03>
- [65] S. J. Chapman, *Fortran for Scientists and Engineers 4<sup>th</sup> Ed.* McGraw-Hill, 2017, p. 1049.

## Appendices

### A Financial

*All financial and market analysis is given as total value per annum, with total amortised values for larger infrastructural investments such as industrial-scale reactors and plants.*

Table A.1: Financial summary of EOR

CAPEX	Cost (£)	OPEX	Cost (£)
CO <sub>2</sub> capture facilities	100–500	Energy consumption	10–40
Pipeline infrastructure	1–5 million/km	Maintenance	5–15
Injection wells	2–10 million (amortisable)	Monitoring	0.35–0.75

Table A.2: Financial summary of chemical conversion

CAPEX	Cost (£)	OPEX	Cost (£)
Chemical plants	50–500 million (amortisable)	Urea production	10–20
Electrochemical systems	500–1,000/kW	Methanol production	300–800
Catalyst purchase		Catalyst maintenance	300–400
Urea production	300–500		
Methanol synthesis	1,600–2,400		
Polycarbonate production	10,000–20,000		

Table A.3: Financial summary of biological conversion

CAPEX	Cost (£)	OPEX	Cost (£)
Bioreactors	5–50 million (amortisable)	CO <sub>2</sub> feedstock	20–50
Support infrastructure		Energy requirements	60–225
CO <sub>2</sub> Capture and supply	100–500	Micro-organism replacement	120–250
Nutrient delivery	0.5–5 million		
Reactor support	1–10 million		
Waste treatment and disposal	0.5–3 million		
Storage and handling	1–5 million		
Monitoring and control	0.5–2 million		

Table A.4: Financial summary of mineralisation

CAPEX	Cost (£)	OPEX	Cost (£)
Processing plant	10–50 million (amortisable)	Mineral feedstock processing	5–20
Feedstock acquisition		Energy requirements	10–30
Mining	5–15	Logistics	5–20
Transport	5–20		
Processing	10–30		

---

## B Derivations

Any relevant values may be found in Table 3.3

### B.1 Electrodynamics

#### Voltage

$$\begin{aligned}\frac{dV_{\text{input}}}{dt} &= \frac{d}{dt} \left( \frac{V_{\text{AC}}}{2} \sin(2\pi f_{\text{AC}} t) \right) \\ &= 2\pi \frac{V_{\text{AC}}^2}{2} f_{\text{AC}} \cos(2\pi f_{\text{AC}} t) \\ &= V_{\text{AC}} f_{\text{AC}} \pi \cos(2\pi f_{\text{AC}} t)\end{aligned}\tag{B.1}$$

#### Capacitance

#### Gas Mixture

Let us assume a reduced gas cross-section of CO<sub>2</sub>, O<sub>2</sub>, CO, and O. This allows us to find  $\varepsilon_{\text{gap}}$  via the individual species fractions  $y_i$  and species polarisability  $\alpha_i$  [Fm<sup>2</sup>]. A full derivation would need to consider Quantum Mechanics.

let

$$\begin{aligned}y &= \{y_{\text{CO}_2}, y_{\text{O}_2}, y_{\text{CO}}, y_{\text{O}}\} \\ &\approx \{[0.375, 1], [0, 0.235], [0, 0.22], [0, 0.135]\} \\ \alpha &= \{\alpha_{\text{CO}_2}, \alpha_{\text{O}_2}, \alpha_{\text{CO}}, \alpha_{\text{O}}\} \\ &\approx \{2.9, 1.6, 2.0, 0.8\} \times 10^{-40}\end{aligned}$$

$$\begin{aligned}\alpha_{\text{gap}} &= \sum_i y_i \alpha_i \\ &= y_{\text{CO}_2} \alpha_{\text{CO}_2} + y_{\text{O}_2} \alpha_{\text{O}_2} + y_{\text{CO}} \alpha_{\text{CO}} + y_{\text{O}} \alpha_{\text{O}} \\ &\in [2.0, 2.9] \times 10^{-40} \text{ Fm}^2\end{aligned}$$

Apply the Clausius-Mossotti relation relating macroscopic material properties to the microscopic polarisability.

$$\frac{\varepsilon_{r,\text{gap}} - 1}{\varepsilon_{r,\text{gap}} + 2} = \frac{N \alpha_{\text{gap}}}{3 \varepsilon_0} \quad | \quad N = \frac{P}{k_B T_{\text{gas}}}$$

$$\begin{aligned}\varepsilon_{r,\text{gap}} &= \frac{1 + \frac{2N\alpha_{\text{gap}}}{3\varepsilon_0}}{1 - \frac{N\alpha_{\text{gap}}}{3\varepsilon_0}} \\ &= \frac{3\varepsilon_0 + 2N\alpha_{\text{gap}}}{3\varepsilon_0 - N\alpha_{\text{gap}}}\end{aligned}$$

$$\begin{aligned}\varepsilon_{\text{gap}} &= \varepsilon_0 \varepsilon_{r,\text{gap}} \\ &= \frac{3\varepsilon_0^2 + 2N\varepsilon_0\alpha_{\text{gap}}}{3\varepsilon_0 - N\alpha_{\text{gap}}}\end{aligned}$$

---

assume that  $T_{\text{gas}} = T_0 = 298.15$  throughout the reactor operation and pressure stays atmospheric  $\Rightarrow N \approx 2.461 \times 10^{25} [\text{m}^{-3}]$

$$\begin{aligned}\varepsilon_{\text{gap}} &= \frac{3\varepsilon_0^2 + 2N\varepsilon_0\alpha_{\text{gap}}}{3\varepsilon_0 - N\alpha_{\text{gap}}} \\ &\in [8.850, 8.852] \times 10^{-12} \text{ Fm}^{-1}\end{aligned}$$

assume that  $d_{\text{gap}} = 0.25$  mm for this approximation

$$\begin{aligned}C_{\text{gap}} &= \frac{\varepsilon_{\text{gap}} A_{\text{ground}}}{d_{\text{gap}}} \\ &\in [1.4709, 1.4712] \times 10^{-11} \text{ F}\end{aligned}\tag{B.2}$$

### Input

The circuit including the reactor is modelled as a circuit in series.

$$\begin{aligned}\frac{1}{C_{\text{input}}} &= \frac{1}{C_{\text{gap}}} + \frac{1}{C_{\text{dielectric}}} \\ C_{\text{input}} &= \frac{C_{\text{gap}} C_{\text{dielectric}}}{C_{\text{gap}} + C_{\text{dielectric}}} \\ &\in [1.34867, 1.34892] \times 10^{-11} \text{ F}\end{aligned}\tag{B.3}$$

### Power

#### Input

$$\begin{aligned}P_{\text{input}} &= f_{\text{AC}} \int_0^t V_{\text{input}}(t) I_{\text{input}}(t) dt \\ &= f_{\text{AC}} \int_0^t \frac{C_{\text{input}} f_{\text{AC}} V_{\text{AC}}^2 \pi}{2} \sin(2\pi f_{\text{AC}} t) \cos(2\pi f_{\text{AC}} t) dt \\ &= \frac{C_{\text{input}} f_{\text{AC}}^2 V_{\text{AC}}^2 \pi}{2} \int_0^t \sin(2\pi f_{\text{AC}} t) \cos(2\pi f_{\text{AC}} t) dt \\ &= \frac{C_{\text{input}} f_{\text{AC}}^2 V_{\text{AC}}^2 \pi}{2} \left[ \frac{\sin^2(2\pi f_{\text{AC}} t)}{4\pi f_{\text{AC}}} \right]_0^t \\ &= \frac{C_{\text{input}} f_{\text{AC}} V_{\text{AC}}^2}{8} |\sin^2(2\pi f_{\text{AC}} t)|\end{aligned}\tag{B.4}$$

### Electron Density

The electron drift velocity is dependent on the reduced electric field  $\frac{E}{N}$ , a relationship that is simulated in BOLSIG+.

$$n_e = \frac{I_{\text{input}}}{e A_{\text{ground}} v_d} \tag{B.5}$$

$v_d$  = electron drift velocity [ $\text{ms}^{-1}$ ]

---

## B.2 Thermal-Energy Balance

### Heat Transfer Coefficient and Rate

Let us assume that there is laminar flow of CO<sub>2</sub> across to the mica layer upon the ground electrode, which is modelled as a flat plate. (geometry shown in Figures 2.6 and 2.5)

assume uniform flow

$$U_{\infty} = \frac{\dot{V}}{A_{\text{ground}}} \\ \approx 8.023 \times 10^{-4} \text{ ms}^{-1}$$

let  $L = d_{\text{reactor}} = 23 \times 10^{-3} \text{ m}$

$$\text{Re}_L = \frac{\rho U_{\infty} L}{\mu} \\ \approx 2.243$$

The Reynolds number is very low and so the correlation should be viewed as an approximate order-of-magnitude estimate.

assume pure CO<sub>2</sub> flow  $\Rightarrow c_p = 844.9 \text{ J kg}^{-1} \text{ K}^{-1}$

$$\text{Pr} = \frac{\mu c_p}{k} \\ \approx 0.744$$

via average laminar correlation  $\in [0, L]$

$$\overline{\text{Nu}}_L = 0.664(\text{Re}_L)^{\frac{1}{2}}(\text{Pr})^{\frac{1}{3}} \\ \approx 0.901$$

using the values found above, average heat transfer coefficient  $\bar{h}$

$$\bar{h} = \frac{\overline{\text{Nu}}_L k}{L} \\ \approx 0.658 \text{ W m}^{-2} \text{ K}^{-1} \quad (\text{B.6})$$

Assuming that the dielectric layer experiences heating to  $T_s$  and that free stream temperature  $T_{\infty}$  returns to ambient temperature  $T_0$ , the heat transfer rate  $Q$  can be found.

$$Q = \bar{h} A_{\text{ground}} |T_{\infty} - T_s| \quad (\text{B.7})$$

let  $T_s = 323.15 \text{ K}$  and  $T_{\infty} = T_0 = 298.15 \text{ K}$

$$Q = \bar{h} A_{\text{ground}} |T_{\infty} - T_s| \\ \approx 6.835 \times 10^{-3} \text{ W}$$

---

## Specific Heat Capacity

For a system in thermal equilibrium at temperature  $T$ , the canonical partition function is defined as  $Z$  for a system of  $i$  states. This partition function accounts for several energetic contributions, translational, rotational, vibrational, and electronic.

$$Z = \sum_i e^{-\frac{E_i}{k_B T}}$$

$$Z = Z_{\text{trans}} Z_{\text{rot}} Z_{\text{vib}} Z_{\text{elec}}$$

$$\ln Z = \ln Z_{\text{trans}} + \ln Z_{\text{rot}} + \ln Z_{\text{vib}} + \ln Z_{\text{elec}}$$

The average internal energy  $U$  per mole of gas, defined using the partition function  $Z$ , can then be used to find the specific heat at constant volume  $c_v$ , which has contributions of all the kinds contained in  $Z$ .

$$\begin{aligned} U &= -\frac{\partial \ln Z}{\partial \beta} \quad | \quad \beta = \frac{1}{k_B T} & c_v &= \left( \frac{\partial U}{\partial T} \right)_V \\ &= RT^2 \frac{\partial \ln Z}{\partial T} & &= R \frac{\partial}{\partial T} \left( T^2 \frac{\partial \ln Z}{\partial T} \right) \end{aligned}$$

Now each specific heat contribution can be found for an ideal gas in three dimensions, using standard statistical physical laws and with the derived relationship between the internal energy  $U$  and the partition function  $Z$ .

$\lambda$ = de Broglie wavelength	$\theta_{\text{rot}}$ = rot. temperature	$E_n$ = energy level $n$
$\hbar$ = Planck's constant	$I$ = moment of inertia	$n$ = quantum number
$R$ = universal gas constant	$\sigma$ = symmetry number	$\theta_{\text{vib}}$ = vib. temperature
$m$ = mass of a particle		$\nu$ = vib. frequency

### Translational

$$\begin{aligned} \text{for } \lambda &= \sqrt{\frac{\hbar^2}{2\pi m k_B T}} \\ Z_{\text{trans}} &= \frac{V}{\lambda^3} \\ &= \frac{V}{\left(\frac{\hbar^2}{2\pi m k_B T}\right)^{\frac{3}{2}}} \\ &= \frac{V(2\pi m k_B T)^{\frac{3}{2}}}{(\hbar^3)} \\ Z_{\text{trans}} &\propto T^{\frac{3}{2}} \\ \ln Z_{\text{trans}} &\propto \frac{3}{2} \ln T \\ c_{v,\text{trans}} &= \frac{3}{2} R \end{aligned}$$

### Rotational

$$\begin{aligned} \text{for } \theta_{\text{rot}} &= \frac{\hbar^2}{2\pi I k_B} \\ Z_{\text{rot}} &= \frac{T}{\sigma \theta_{\text{rot}}} \\ Z_{\text{rot}} &\propto T \\ \ln Z_{\text{rot}} &\propto \ln T \\ c_{v,\text{rot}} &= R \end{aligned}$$

### Vibrational

$$\begin{aligned} \text{for } \theta_{\text{vib}} &= \frac{\hbar \nu}{k_B} \\ E_n &= k_B \theta_{\text{vib}} \left( n + \frac{1}{2} \right) \\ Z_{\text{vib}} &= \frac{e^{-\frac{\theta_{\text{vib}}}{2T}}}{1 - e^{-\frac{\theta_{\text{vib}}}{T}}} \\ \ln Z_{\text{vib}} &= -\frac{\theta_{\text{vib}}}{2T} - \ln \left( 1 - e^{-\frac{\theta_{\text{vib}}}{T}} \right) \\ U_{\text{vib}} &= R \theta_{\text{vib}} \left( \frac{1}{2} + \frac{1}{e^{\frac{\theta_{\text{vib}}}{T}} - 1} \right) \\ c_{v,\text{vib}} &= R \left( \frac{\theta_{\text{vib}}}{T} \right)^2 \frac{e^{\frac{\theta_{\text{vib}}}{T}}}{\left( e^{\frac{\theta_{\text{vib}}}{T}} - 1 \right)^2} \end{aligned}$$

---

Note that at low  $T$ ,  $T \ll \theta_{\text{vib}}$ , the vibrational contribution is nearly zero, while at high  $T$ ,  $T \gg \theta_{\text{vib}}$ , it approaches the classical limit  $R$ , and that at the current working temperature range  $c_{v,\text{elec}} \approx 0$ , giving no electronic contribution.

$$\begin{aligned} c_v(T) &= c_{v,\text{trans}} + c_{v,\text{rot}} + c_{v,\text{vib}}(T) + c_{v,\text{elec}} \\ &= \frac{3}{2}R + R + R \left( \frac{\theta_{\text{vib}}}{T} \right)^2 \frac{e^{\frac{\theta_{\text{vib}}}{T}}}{\left( e^{\frac{\theta_{\text{vib}}}{T}} - 1 \right)^2} \\ &= \frac{5}{2}R + R \left( \frac{\theta_{\text{vib}}}{T} \right)^2 \frac{e^{\frac{\theta_{\text{vib}}}{T}}}{\left( e^{\frac{\theta_{\text{vib}}}{T}} - 1 \right)^2} \end{aligned}$$

The total molar specific heat at constant volume is the sum of the contributions is given above. For an ideal gas, the specific heat at constant pressure is related to  $c_v$  via  $R$ .

$$\begin{aligned} c_p(T) &= c_v(T) + R \\ &= \frac{7}{2}R + R \left( \frac{\theta_{\text{vib}}}{T} \right)^2 \frac{e^{\frac{\theta_{\text{vib}}}{T}}}{\left( e^{\frac{\theta_{\text{vib}}}{T}} - 1 \right)^2} \end{aligned} \quad (\text{B.8})$$

### Bulk Gas Temperature

$$\begin{aligned} \dot{m}c_p \frac{dT_{\text{gas}}}{dt} &= Q - hA(T_{\text{gas}} - T_0) \\ \frac{dT_{\text{gas}}}{dt} &= \frac{Q - hA(T_{\text{gas}} - T_0)}{\dot{m}c_p} \end{aligned}$$

using the Euler integration method

$$\begin{aligned} T_{\text{gas}}(t+1) &= T_{\text{gas}}(t) + \frac{dT_{\text{gas}}(t)}{dt} dt \quad | \quad dt \rightarrow 0 \\ T_{\text{gas}}(t+1) &= T_{\text{gas}}(t) + dt \frac{Q(t) - hA(T_{\text{gas}}(t) - T_0)}{\dot{m}c_p} \end{aligned} \quad (\text{B.9})$$

## C Supplementary Results

### C.1 Reduced Electric Field and SEI

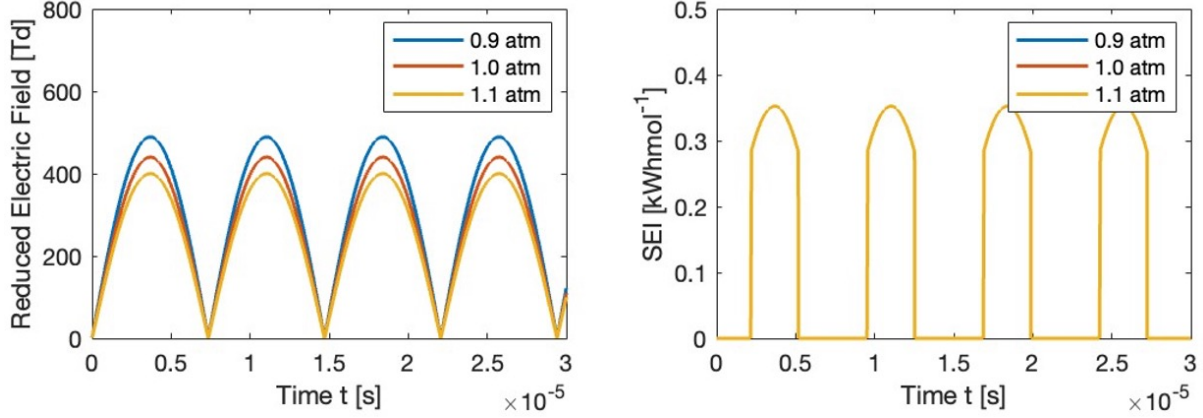


Figure C.1: Effects of electrode gap change on the reduced electric field  $\frac{E}{N}$  and SEI

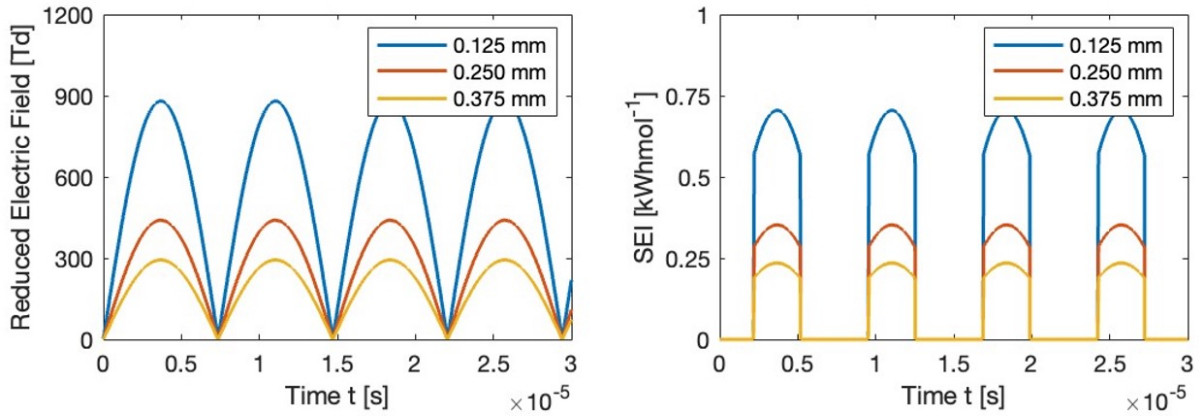


Figure C.2: Effects of electrode gap change on the reduced electric field  $\frac{E}{N}$  and SEI

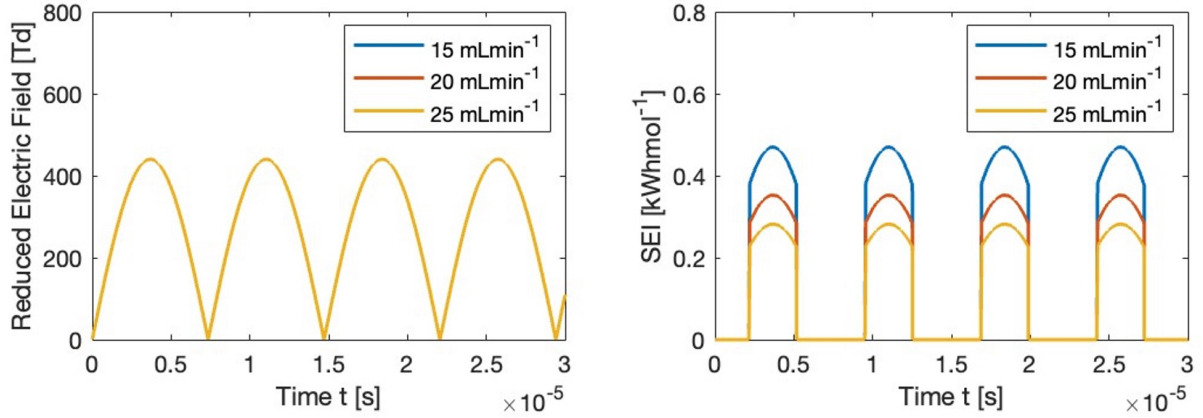


Figure C.3: Effects of volumetric  $\dot{V}$  change on specific energy input SEI

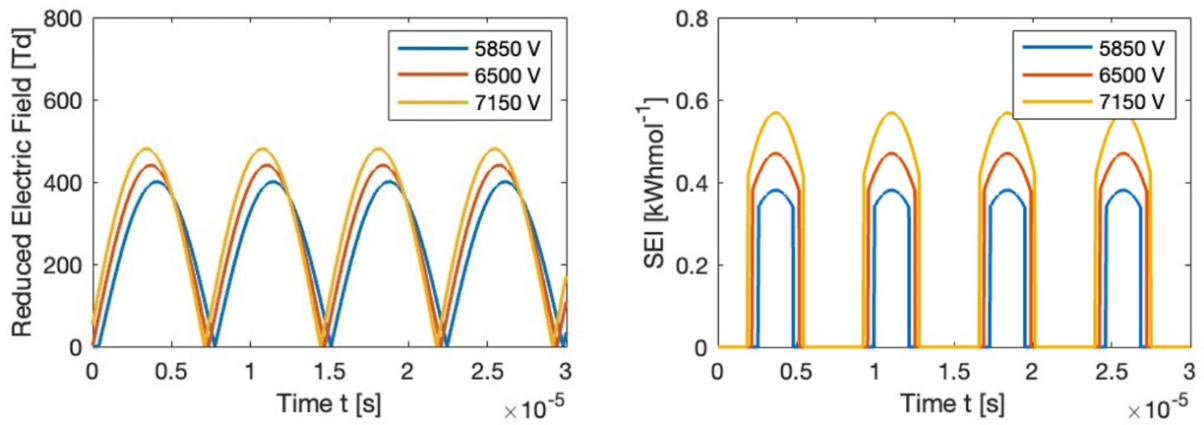


Figure C.4: Effects of AC supply voltage change on the reduced electric field  $\frac{E}{N}$  and SEI

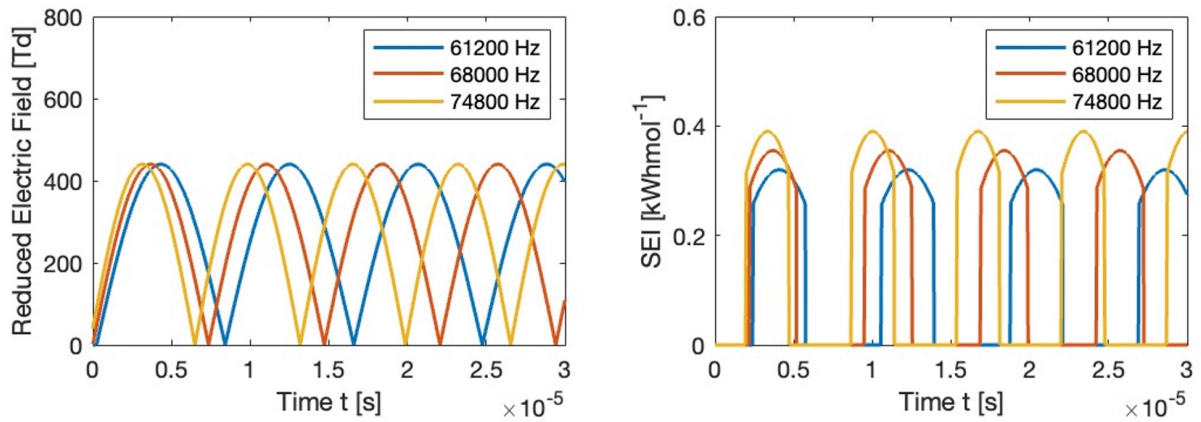


Figure C.5: Effects of AC supply frequency change on the reduced electric field  $\frac{E}{N}$  and SEI

## D Code

### D.1 Diagram

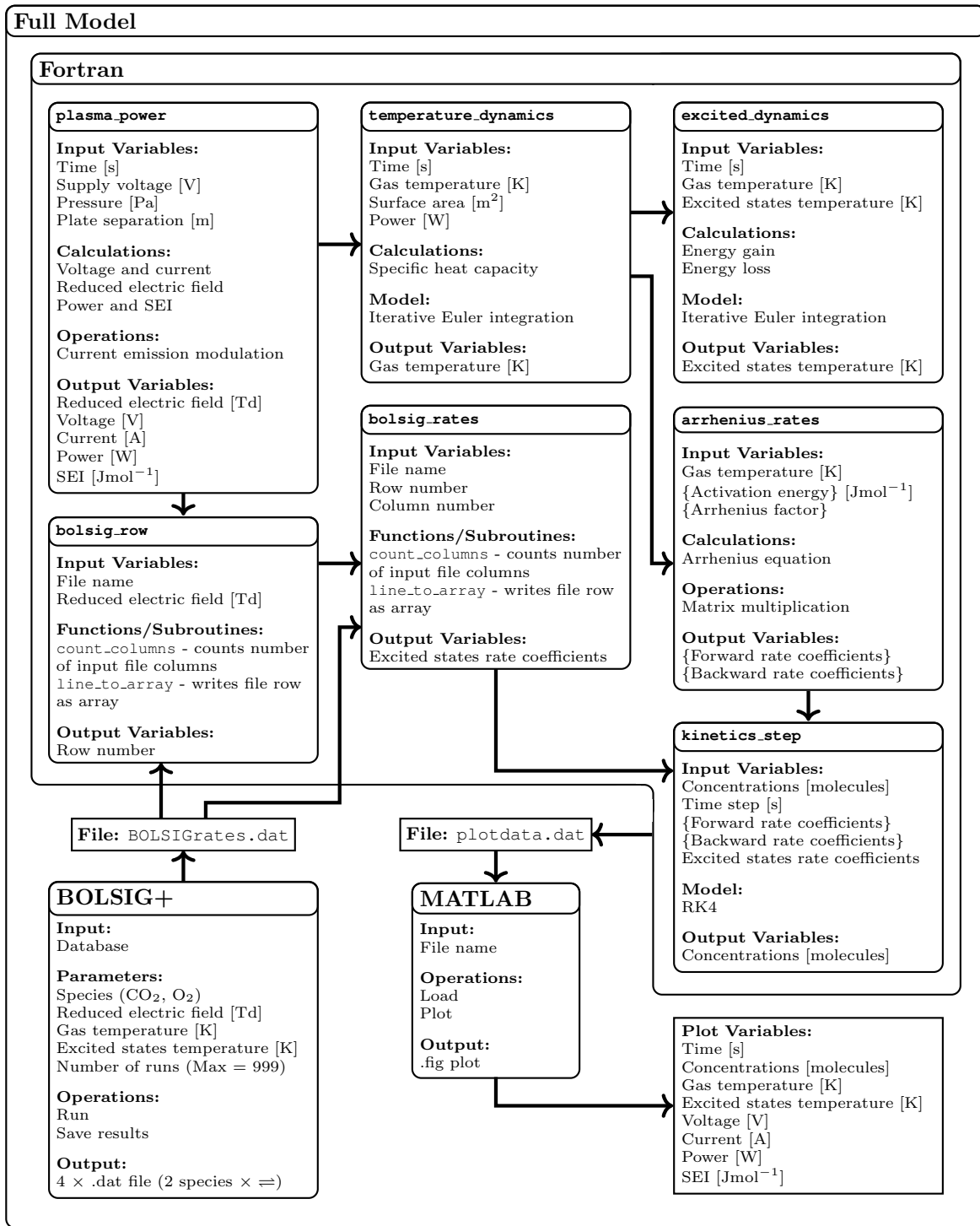


Figure D.1: Flow diagram showing the program structure

---

## D.2 Listings

```
1 program CO2modelling
2     implicit none
3
4     real(8), parameter :: R = 8.31446261815324
5     real(8), parameter :: epsilon_0 = 8.85418782E-12
6     real(8), parameter :: kB = 1.380649E-23
7     real(8), parameter :: pi = acos(-1.0)
8     real(8), parameter :: n_AV = 6.02214076E23
9     real(8), parameter :: Evib = 0.291 * 1.60218E-19
10    real(8), parameter :: Ee_avg = 5.09003 * 1.60218E-19
11
12    real(8), parameter :: dt = 1E-9
13    integer, parameter :: n = 5E4
14
15    real(8), parameter :: diam_reac = 23E-3
16    real(8), parameter :: b_pyr = 1E-3
17    real(8), parameter :: h_pyr = 1E-3
18    integer, parameter :: n_pyr = 160
19
20    real(8), parameter :: m_mol = 4.4009E-2
21    real(8), parameter :: V_mol = 2.24E-2
22
23    real(8), parameter :: c_pCO2 = 844.9
24    real(8), parameter :: c_pO2 = 910.7
25    real(8), parameter :: c_pCO = 1049.0
26    real(8), parameter :: c_pO = 1369.5
27
28    real(8), parameter :: h = 0.658
29    real(8), parameter :: epsilon_gap = 1.000984 * 8.85418782E-12
30
31    real(8), parameter :: v_discharge = 5.2E3
32    real(8), parameter :: eff_discharge = 0.2
33    real(8), parameter :: tau_vt = 1E-7
34    real(8), parameter :: T0 = 298.15
35
36    real(8), parameter :: d_dielectric = 200E-6
37    real(8), parameter :: epsilon_dielectric = 5 * 8.85418782E-12
38
39    integer, parameter :: reactions = 30
40    real(8), dimension(reactions) :: A_f(reactions), A_b(reactions), Ea_f(reactions),
41        Ea_b(reactions), k_f(reactions), k_b(reactions)
42
43    integer :: i, j
44
45    real(8) :: t
46    real(8) :: Patm, v_AC, f_AC
47    real(8) :: d_gap, V, A
48    real(8) :: Q, n_dot, n_mol, n_CO2, m_kg, N_gas, m_dot
49    real(8) :: Tgas, Texc
50    real(8) :: ne, kexc
51    real(8) :: CO2, CO, C, C2, O, O2, O3, CO2_plus, CO_plus, O3_plus, O2_plus, O_minus,
52        O2_minus, CO2_exc, O2_exc, O_ad, M, S, e
53    real(8) :: P_plasma, E_N, v_input, i_input, SEI, dv_input, t_discharge
54    real(8) :: k
55    character(len=20) :: input_str
56    integer :: choice1, choice2, status, istat
57    logical :: is_valid
58
59    character(len=20) :: filename
60    integer :: target_row, target_column
61
62    real(8), parameter :: alpha = 1.8E3
63    real(8), parameter :: beta = 0
64
65    Tgas = 298.15
66    Texc = 298.15
67
68    CO2 = n_CO2
69    CO = 0
70    C = 0
71    C2 = 0
```

---

```

70      O = 0
71      O2 = 0
72      O3 = 0
73      CO2_plus = 0
74      CO_plus = 0
75      O3_plus = 0
76      O2_plus = 0
77      O_plus = 0
78      O2_minus = 0
79      O_minus = 0
80      CO2_exc = 0
81      O2_exc = 0
82      O_ad = 0
83      M = 0
84      S = 0
85      e = 0
86
87      A_f = (/ 0.0, 0.0, 0.0, 0.0, 0.0, 0.0, 0.0, 0.0, 1.0E12, 1.0E11, 1.0E8, 1.0E8,
88      1.0E12, 1.0E9, 1.0E10, 1.0E11, 1.0E10, 1.0E10, 1.0E11, 1.0E11, 0.0, 0.0, 0.0, 0.0, 1.0E11
89      , 1.0E10, 1.0E10, 1.0E11, 0.0, 0.0 /)
90      A_b = (/ 0.0, 0.0, 0.0, 0.0, 0.0, 0.0, 0.0, 0.0, 1.0E9, 1.0E10, 1.0E12, 1.0E9,
91      1.0E12, 1.0E10, 1.0E10, 1.0E11, 1.0E10, 1.0E10, 1.0E10, 1.0E11, 0.0, 0.0, 0.0, 0.0, 1.0
92      E11, 1.0E10, 1.0E10, 1.0E11, 0.0, 0.0 /)
93      Ea_f = 1E3 * (/ 0, 0, 0, 0, 0, 0, 0, 0, 275, 225, 5, 5, 325, 125, 30, 75, 40, 30,
94      5, 5, 0, 0, 75, 125, 175, 225, 0, 0 /)
95      Ea_b = 1E3 * (/ 0, 0, 0, 0, 0, 0, 0, 0, 75, 325, 450, 125, 325, 150, 150, 75, 40,
96      75, 125, 175, 0, 0, 325, 150, 200, 250, 0, 0 /)
97
98      filename = 'CO2ratesF.dat'
99
100     print *, "
101     =====
102     "
103
104     print *, "
105     =====
106     "
107     print *, "
108     =====
109     "
110     print *, "
111     =====
112     "
113     print *, "
114     =====
115     "
116     print *, "
117     =====
118     "
119     print *, "
120     =====
121     "
122     print *, "
123     =====
124     "

```

---

```

125         if (choice1 == 1) then
126             exit
127         else if (choice1 == 4) then
128             stop
129         else
130             print *, "Invalid choice. Please try again."
131             print *, "
132         end if
133     end do
134
135     print *, "
136     print *, "
137     print *, "                                     Input Parameters"
138     print *, "
139     print *, " 1. Optimised Parameters"
140     print *, " 2. Custom Parameters"
141     print *, " 3. Exit"
142     print *, "
143
144     do
145         do
146             is_valid = .true.
147             print *, "Enter your choice: "
148             read(*, '(A)') input_str
149             do i = 1, len_trim(input_str)
150                 if (input_str(i:i) < '0' .or. input_str(i:i) > '9') then
151                     is_valid = .false.
152                     exit
153                 end if
154             end do
155             if (is_valid) then
156                 read(input_str, '(I10)', IOSTAT=status) choice2
157                 if (status == 0 .and. choice2 > 0) then
158                     exit
159                 end if
160             end if
161             print *, "Invalid choice. Please enter a natural number (1, 2, 3, ...).
162             Please try again."
163             print *, "
164         end do
165         if (choice2 == 1) then
166             Patm = 101325
167             v_AC = 6500
168             f_AC = 68000
169             Q = 20
170             d_gap = 0.25
171             exit
172         else if (choice2 == 2) then
173             exit
174         else if (choice2 == 3) then
175             stop
176         else
177             print *, "Invalid choice. Please try again."
178             print *, "
179         end if
180         print *, "
181     end do
182     if (choice2 == 2) then
183         do
184             print *, "Enter reactor chamber pressure [atm]:"
185             read(*,* ,iostat=istat) Patm

```

---

```

186     if (istat == 0 .and. Patm >= 0.5 .and. Patm <= 1.5) then
187         exit
188     else
189         print *, "Invalid input. Input must be a real number in the range [0.5,
1.5]. Please try again."
190         end if
191     end do
192
193     do
194         print *, "Enter AC input voltage [V]:"
195         read(*,* ,iostat=istat) v_AC
196
197         if (istat == 0 .and. v_AC >= 0 .and. v_AC <= 10000) then
198             exit
199         else
200             print *, "Invalid input. Input must be a real number in the range [0,
10,000]. Please try again."
201             end if
202         end do
203
204     do
205         print *, "Enter AC input frequency [Hz]:"
206         read(*,* ,iostat=istat) f_AC
207
208         if (istat == 0 .and. f_AC >= 0 .and. f_AC <= 100000) then
209             exit
210         else
211             print *, "Invalid input. Input must be a real number in the range [0,
100,000]. Please try again."
212             end if
213         end do
214
215     do
216         print *, "Enter volumetric flow rate [mL/min]:"
217         read(*,* ,iostat=istat) Q
218
219         if (istat == 0 .and. Q >= 0 .and. Q <= 1000) then
220             exit
221         else
222             print *, "Invalid input. Input must be a real number in the range [0,
1,000]. Please try again."
223             end if
224         end do
225
226     do
227         print *, "Enter electrode gap [mm]:"
228         read(*,* ,iostat=istat) d_gap
229
230         if (istat == 0 .and. d_gap >= 0 .and. d_gap <= 1) then
231             exit
232         else
233             print *, "Invalid input. Input must be a real number in the range [0,
1]. Please try again."
234             end if
235         end do
236     end if
237     Patm = Patm * 101325
238
239     Q = Q * (1E-6 / 60)
240     n_dot = Q / V_mol
241     m_dot = n_dot * m_mol
242
243     d_gap = d_gap * 1E-3
244     V = pi * (diam_reac/2)**2 * (d_gap + h_pyr) - n_pyr * ((b_pyr**2 * h_pyr) / 3)
245     A = pi * (diam_reac/2)**2 + n_pyr * (4 * (0.5 * ((b_pyr**2 + h_pyr**2)**0.5) * b_pyr
246 ) - b_pyr**2)
247     m_kg = (Patm * V * m_mol) / (R * Tgas)
248     n_mol = V / V_mol
249     n_CO2 = n_mol * n_AV
250
251     N_gas = Patm / (kB * Tgas)
252     ne = Patm / (kB * Texc)

```

---

```

253     kexc = 0.426196E-15
254
255     print *, "
256         "
256     print *, "
257 ====="
257     print *, "                               Simulation running...
258
259     open(10, file='plotdata.dat')
260         do i = 1, n
261             t = i * dt
262
263             C02 = n_C02
264             C0 = 0
265             C = 0
266             C2 = 0
267             O = 0
268             O2 = 0
269             O3 = 0
270             C02_plus = 0
271             C0_plus = 0
272             O3_plus = 0
273             O2_plus = 0
274             O_plus = 0
275             O2_minus = 0
276             O_minus = 0
277             C02_exc = 0
278             O2_exc = 0
279             O_ad = 0
280             M = 0
281             S = 0
282             e = 0
283
284             call plasma_power(v_AC, v_discharge, f_AC, d_gap, epsilon_0,
284 epsilon_dielectric, epsilon_gap, A, t, eff_discharge, E_N, P_plasma, pi, v_input,
285 i_input, dv_input, SEI, n_dot, N_gas, t_discharge)
285                 call temperature_dynamics(Tgas, dt, A, P_plasma, c_pC02, c_pC0, c_pO2,
285 c_pO, h, C02, C0, O2, O, n_C02, m_dot, T0)
286                 call excited_dynamics(Texc, dt, ne, Evib, Ee_avg, Tgas, kexc, tau_vt, kB
286 )
287                 call arrhenius_rates(R, Tgas, A_f, A_b, Ea_f, Ea_b, k_f, k_b, j,
287 reactions)
288                 call bolsig_row(filename, E_N, target_row)
289
290             filename = 'C02ratesF.dat'
291             target_column = 4
292             call bolsig_rates(filename, target_row, target_column, k)
293             k_f(1) = k
294             target_column = 16
295             call bolsig_rates(filename, target_row, target_column, k)
296             k_f(2) = k
297             target_column = 4
298             call bolsig_rates(filename, target_row, target_column, k)
299             k_f(3) = k
300             target_column = 12
301             call bolsig_rates(filename, target_row, target_column, k)
302             k_f(4) = k
303             target_column = 4
304             call bolsig_rates(filename, target_row, target_column, k)
305             k_f(29) = k
306             target_column = 4
307             call bolsig_rates(filename, target_row, target_column, k)
308             k_f(30) = k
309             filename = 'O2ratesF.dat'
310             target_column = 16
311             call bolsig_rates(filename, target_row, target_column, k)
312             k_f(5) = k
313             target_column = 20
314             call bolsig_rates(filename, target_row, target_column, k)
315             k_f(6) = k
316             target_column = 5

```

---

```

317   call bolsig_rates(filename, target_row, target_column, k)
318   k_f(7) = k
319   target_column = 20
320   call bolsig_rates(filename, target_row, target_column, k)
321   k_f(8) = k
322   target_column = 4
323   call bolsig_rates(filename, target_row, target_column, k)
324   k_f(9) = k
325   k_b(1) = 0
326   k_b(2) = 0
327   k_b(3) = 0
328   k_b(6) = 0
329   k_b(7) = 0
330   k_b(8) = 0
331   k_b(9) = 0
332   k_b(29) = 0
333   k_b(30) = 0
334   filename = 'CO2ratesB.dat'
335   target_column = 13
336   call bolsig_rates(filename, target_row, target_column, k)
337   k_b(4) = k
338   filename = 'O2ratesB.dat'
339   target_column = 16
340   call bolsig_rates(filename, target_row, target_column, k)
341   k_b(5) = k
342
343   k_f = alpha * k_f
344   k_b = beta * k_b
345
346   if (v_input > 0) then
347     if (abs(v_input) > ((0.5 * v_discharge) - 0.5)) then
348       if (abs(v_input) < ((0.5 * v_discharge) + 0.5)) then
349         if (dv_input > 0) then
350           Tgas = 298.15
351           Texc = 3500
352
353           CO2 = n_CO2
354
355           call kinetics_step(CO2, C0, C, C2, O, O2, O3,
356           CO2_plus, C0_plus, O3_plus, O2_plus, O_plus, O2_minus, O_minus, CO2_exc, O2_exc,
357           O_ad, M, S, e, k_f, k_b, t, t_discharge, dt, reactions, n_CO2)
358             end if
359           end if
360         end if
361       else if (v_input < 0) then
362         if (abs(v_input) > ((0.5 * v_discharge) - 0.5)) then
363           if (abs(v_input) < ((0.5 * v_discharge) + 0.5)) then
364             if (dv_input < 0) then
365               Tgas = 298.15
366               Texc = 3500
367
368               CO2 = n_CO2
369
370               call kinetics_step(CO2, C0, C, C2, O, O2, O3,
371               CO2_plus, C0_plus, O3_plus, O2_plus, O_plus, O2_minus, O_minus, CO2_exc, O2_exc,
372               O_ad, M, S, e, k_f, k_b, t, t_discharge, dt, reactions, n_CO2)
373             end if
374           end if
375         end if
376       call kinetics_step(CO2, C0, C, C2, O, O2, O3, CO2_plus, C0_plus, O3_plus
377       , O2_plus, O_plus, O2_minus, O_minus, CO2_exc, O2_exc, O_ad, M, S, e, k_f, k_b, t,
378       t_discharge, dt, reactions, n_CO2)
379
380       if (t <= t_discharge) then
381         CO2 = n_CO2
382         C0 = 0
383         C = 0
384         C2 = 0
385         O2 = 0
386         O3 = 0

```

---

```

384      C02_plus = 0
385      C0_plus = 0
386      O3_plus = 0
387      O2_plus = 0
388      O_plus = 0
389      O2_minus = 0
390      O_minus = 0
391      CO2_exc = 0
392      O2_exc = 0
393      O_ad = 0
394      M = 0
395      S = 0
396      e = 0
397
398      E_N = 0
399  end if
400
401      write(10,*) t, E_N, v_input, i_input, P_plasma, SEI, Tgas, Texc, CO2 / n_CO2
402 , CO / n_CO2, C / n_CO2, C2 / n_CO2, O / n_CO2, O2 / n_CO2, O3 / n_CO2, C02_plus /
403 n_CO2, CO_plus / n_CO2, O3_plus / n_CO2, O2_plus / n_CO2, O_plus / n_CO2, O2_minus /
404 n_CO2, O_minus / n_CO2, CO2_exc / n_CO2, O2_exc / n_CO2, O_ad / n_CO2, M / n_CO2, S
405 / n_CO2, e / n_CO2
406      end do
407  close(10)
408  print *, "                                     Simulation complete."
409  print *, "                                     Data saved to plotdata.dat."
410  print *, "-----"
411  print *, "-----"
412  print *, "-----"
413  print *, "-----"
414  print *, "-----"
415  print *, "-----"
416  print *, "-----"
417  print *, "-----"
418  print *, "-----"
419  print *, "-----"
420  print *, "-----"
421  print *, "-----"
422  print *, "-----"
423  print *, "-----"
424  print *, "-----"
425  print *, "-----"
426  print *, "-----"
427  print *, "-----"

```

---

```

428     print *, "
429         "
430     print *, "
431     ====="
432     print *, "
433         "
434     print *, "
435         "
436     print *, "
437
438 end program CO2modelling
439
440 subroutine plasma_power(v_AC, v_discharge, f_AC, d_gap, epsilon_0, epsilon_dielectric,
441 epsilon_gap, A, t, eff_discharge, E_N, P_plasma, pi, v_input, i_input, dv_input, SEI
442 , n_dot, N_gas, t_discharge)
443 implicit none
444
445 real(8), intent(in) :: t, pi, d_gap, A, N_gas, n_dot, v_AC, v_discharge,
446 eff_discharge, f_AC, epsilon_0, epsilon_dielectric, epsilon_gap
447 real(8), intent(out) :: E_N, v_input, i_input, P_plasma, SEI, dv_input, t_discharge
448 real(8) :: C_gap, C_dielectric, C_input, v_gap, v_dielectric
449
450 C_gap = (epsilon_0 * epsilon_gap * A)/ d_gap
451 C_dielectric = (epsilon_0 * epsilon_dielectric * A) / d_gap
452 C_input = (epsilon_0 * epsilon_dielectric * epsilon_gap * A) / (d_gap * (epsilon_gap
453 + epsilon_dielectric))
454
455 v_input = (v_AC / 2) * sin(2 * pi * f_AC * t)
456 dv_input = (v_AC / 2) * 2 * pi * f_AC * cos(2 * pi * f_AC * t)
457 t_discharge = (1 / (2 * pi * f_AC)) * asin(2 * ((v_discharge / 2) / v_AC))
458 v_gap = ((v_AC / 2) * sin((2 * pi * f_AC) * (t - t_discharge))) * (C_dielectric / (
459 C_gap + C_dielectric))
460 v_dielectric = v_input * (C_gap / (C_gap + C_dielectric))
461
462 E_N = abs(((v_gap / d_gap) / N_gas) * 1E21)
463
464 if (abs(v_input) > (0.5 * v_discharge)) then
465     i_input = C_input * v_AC * f_AC * pi
466 else
467     i_input = 0
468 end if
469
470 P_plasma = abs(v_input * i_input * eff_discharge)
471 SEI = P_plasma / n_dot
472 end subroutine plasma_power
473
474 subroutine temperature_dynamics(Tgas, dt, A, P_plasma, c_pCO2, c_pCO, c_pO2, c_p0, h,
475 CO2, CO, O2, 0, n_CO2, m_dot, T0)
476 implicit none
477
478 real(8), intent(inout) :: Tgas
479 real(8), intent(in) :: dt, A, P_plasma, c_pCO2, c_pCO, c_pO2, c_p0, h, CO2, CO, O2,
480 0, n_CO2, m_dot, T0
481 real(8) :: c_p
482
483 c_p = (CO2 / n_CO2) * (c_pCO2) + (CO / n_CO2) * (c_pCO) + (O2 / n_CO2) * (c_pO2) + (
484 0 / n_CO2) * (c_p0)
485 Tgas = Tgas + dt * ((P_plasma - (h * A) * (Tgas - T0)) / (m_dot * c_p))
486 end subroutine temperature_dynamics
487
488 subroutine excited_dynamics(Texc, dt, ne, Evib, Ee_avg, Tgas, kexc, tau_vt, kB)
489 implicit none
490
491
492
493
494
495
496
497
498
499
500
501
502
503
504
505
506
507
508
509
510
511
512
513
514
515
516
517
518
519
520
521
522
523
524
525
526
527
528
529
530
531
532
533
534
535
536
537
538
539
540
541
542
543
544
545
546
547
548
549
550
551
552
553
554
555
556
557
558
559
560
561
562
563
564
565
566
567
568
569
570
571
572
573
574
575
576
577
578
579
580
581
582
583
584
585
586
587
588
589
590
591
592
593
594
595
596
597
598
599
600
601
602
603
604
605
606
607
608
609
610
611
612
613
614
615
616
617
618
619
620
621
622
623
624
625
626
627
628
629
630
631
632
633
634
635
636
637
638
639
640
641
642
643
644
645
646
647
648
649
650
651
652
653
654
655
656
657
658
659
660
661
662
663
664
665
666
667
668
669
670
671
672
673
674
675
676
677
678
679
680
681
682
683
684
685
686
687
688
689
690
691
692
693
694
695
696
697
698
699
700
701
702
703
704
705
706
707
708
709
710
711
712
713
714
715
716
717
718
719
720
721
722
723
724
725
726
727
728
729
730
731
732
733
734
735
736
737
738
739
740
741
742
743
744
745
746
747
748
749
750
751
752
753
754
755
756
757
758
759
760
761
762
763
764
765
766
767
768
769
770
771
772
773
774
775
776
777
778
779
780
781
782
783
784
785
786
787
788
789
790
791
792
793
794
795
796
797
798
799
800
801
802
803
804
805
806
807
808
809
810
811
812
813
814
815
816
817
818
819
820
821
822
823
824
825
826
827
828
829
830
831
832
833
834
835
836
837
838
839
840
841
842
843
844
845
846
847
848
849
850
851
852
853
854
855
856
857
858
859
860
861
862
863
864
865
866
867
868
869
870
871
872
873
874
875
876
877
878
879
880
881
882
883
884
885
886
887
888
889
890
891
892
893
894
895
896
897
898
899
900
901
902
903
904
905
906
907
908
909
910
911
912
913
914
915
916
917
918
919
920
921
922
923
924
925
926
927
928
929
930
931
932
933
934
935
936
937
938
939
940
941
942
943
944
945
946
947
948
949
950
951
952
953
954
955
956
957
958
959
960
961
962
963
964
965
966
967
968
969
970
971
972
973
974
975
976
977
978
979
980
981
982
983
984
985
986
987
988
989
990
991
992
993
994
995
996
997
998
999
999

```

---

```

483   real(8), intent(inout) :: Texc
484   real(8), intent(in) :: dt, ne, Evib, Ee_avg, kexc, tau_vt, kB, Tgas
485   real(8) :: E_gain, E_loss
486
487   E_gain = kexc * ne * Ee_avg * Evib / kB
488   E_loss = (Texc - Tgas) / tau_vt
489
490   Texc = Texc + (E_gain - E_loss) * dt
491   if (Texc < Tgas) Texc = Tgas
492 end subroutine excited_dynamics
493
494 subroutine bolsig_row(filename, E_N, target_row)
495   implicit none
496
497   character(len=*), intent(in) :: filename
498   real(8), intent(in) :: E_N
499   integer, intent(out) :: target_row
500   character(len=300) :: line
501   integer :: iostat, current_row
502   real(8) :: current_value, target_EN, diff, min_diff
503   real(8), allocatable :: data_row(:)
504
505   target_EN = 0.0
506   min_diff = huge(0.0)
507   target_row = -1
508   current_row = 0
509
510   open(unit=20, file=filename, status="old", action="read")
511
512   do
513     read(20, '(A)', iostat=iostat) line
514     if (iostat /= 0) exit
515
516     current_row = current_row + 1
517
518     allocate(data_row(count_columns(line)))
519     call line_to_array(line, data_row)
520
521     if (size(data_row) >= 2) then
522       current_value = data_row(2)
523       diff = abs(current_value - E_N)
524
525       if (diff < min_diff) then
526         min_diff = diff
527         target_EN = current_value
528         target_row = current_row
529       end if
530     end if
531
532     deallocate(data_row)
533   end do
534
535   close(20)
536
537   if (target_row <= 0) then
538     print *, "Error: No valid data found in the file. Please try again"
539     stop
540   end if
541
542 contains
543
544   integer function count_columns(input_line)
545     character(len=*), intent(in) :: input_line
546     integer :: i, n
547     logical :: in_word
548
549     n = 0
550     in_word = .false.
551     do i = 1, len_trim(input_line)
552       if (input_line(i:i) /= ' ' .and. .not. in_word) then
553         n = n + 1
554         in_word = .true.
555       else if (input_line(i:i) == ' ') then

```

---

```

556         in_word = .false.
557     end if
558   end do
559   count_columns = n
560 end function count_columns
561
562 subroutine line_to_array(input_line, array)
563   character(len=*), intent(in) :: input_line
564   real(8), allocatable, intent(out) :: array(:)
565   integer :: i, local_n_columns
566
567   local_n_columns = count_columns(input_line)
568   allocate(array(local_n_columns))
569   read(input_line, *) (array(i), i = 1, local_n_columns)
570 end subroutine line_to_array
571 end subroutine bolsig_row
572
573 subroutine arrhenius_rates(R, Tgas, A_f, A_b, Ea_f, Ea_b, k_f, k_b, j, reactions)
574   implicit none
575
576   integer :: j, reactions
577   real(8), intent(in) :: R, Tgas
578   real(8), dimension(reactions), intent(in) :: A_f, A_b, Ea_f, Ea_b
579   real(8), dimension(reactions), intent(out) :: k_f, k_b
580   do j = 1, reactions
581     k_f(j) = A_f(j) * exp(-Ea_f(j) / (R * Tgas))
582     k_b(j) = A_b(j) * exp(-Ea_b(j) / (R * Tgas))
583   end do
584
585 end subroutine arrhenius_rates
586
587 subroutine bolsig_rates(filename, target_row, target_column, k)
588   implicit none
589
590   character(len=*), intent(in) :: filename
591   integer, intent(in) :: target_row, target_column
592   real(8), intent(out) :: k
593
594   integer :: iostat, current_row
595   character(len=300) :: line
596   real(8), allocatable :: data_row(:)
597   integer :: n_columns
598
599   current_row = 0
600   k = 0.0
601
602   open(unit=30, file=filename, status="old", action="read")
603
604   do
605     read(30, '(A)', iostat=iostat) line
606     if (iostat /= 0) exit
607
608     current_row = current_row + 1
609
610     if (current_row == target_row) then
611       n_columns = count_columns(line)
612       allocate(data_row(n_columns))
613       call line_to_array(line, data_row)
614
615       if (size(data_row) >= target_column) then
616         k = data_row(target_column)
617       else
618         print *, "Error: Target column out of range."
619       end if
620
621       deallocate(data_row)
622       exit
623     end if
624   end do
625
626   close(30)
627
628 contains

```

```

629
630     integer function count_columns(input_line)
631         character(len=*), intent(in) :: input_line
632         integer :: i, n
633         logical :: in_word
634
635         n = 0
636         in_word = .false.
637         do i = 1, len_trim(input_line)
638             if (input_line(i:i) /= ' ' .and. .not. in_word) then
639                 n = n + 1
640                 in_word = .true.
641             else if (input_line(i:i) == ' ') then
642                 in_word = .false.
643             end if
644         end do
645         count_columns = n
646     end function count_columns
647
648     subroutine line_to_array(input_line, array)
649         character(len=*), intent(in) :: input_line
650         real(8), allocatable, intent(out) :: array(:)
651         integer :: i, local_n_columns
652
653         local_n_columns = count_columns(input_line)
654         allocate(array(local_n_columns))
655         read(input_line, *) (array(i), i = 1, local_n_columns)
656     end subroutine line_to_array
657
658 end subroutine bolsig_rates
659
660 subroutine kinetics_step(CO2, CO, C, C2, O, O2, O3, CO2_plus, CO_plus, O3_plus, O2_plus,
661   O_plus, O2_minus, O_minus, CO2_exc, O2_exc, O_ad, M, S, e, k_f, k_b, t, t_discharge
662   , dt, reactions, n_CO2)
663     implicit none
664
665     real(8), intent(inout) :: CO2, CO, C, C2, O, O2, O3, CO2_plus, CO_plus, O3_plus,
666     O2_plus, O2_minus, O_plus, O_minus, CO2_exc, O2_exc, O_ad, M, S, e
667     real(8), intent(in) :: t, t_discharge, dt, n_CO2
668     integer, intent(in) :: reactions
669     real(8), dimension(reactions) :: k_f, k_b
670     real(8) :: dCO2_1, dC_1, dC2_1, dO_1, dO2_1, dO3_1, dCO2_plus_1, dCO_plus_1,
671     dO3_plus_1, dO2_plus_1, dO_plus_1, dO2_minus_1, dO_minus_1, dCO2_exc_1, dO2_exc_1,
672     dO_ad_1, dM_1, dS_1, de_1
673     real(8) :: dCO2_2, dCO_2, dC_2, dC2_2, dO_2, dO2_2, dO3_2, dCO2_plus_2, dCO_plus_2,
674     dO3_plus_2, dO2_plus_2, dO_plus_2, dO2_minus_2, dO_minus_2, dCO2_exc_2, dO2_exc_2,
675     dO_ad_2, dM_2, dS_2, de_2
676     real(8) :: dCO2_3, dCO_3, dC_3, dC2_3, dO_3, dO2_3, dO3_3, dCO2_plus_3, dCO_plus_3,
677     dO3_plus_3, dO2_plus_3, dO_plus_3, dO2_minus_3, dO_minus_3, dCO2_exc_3, dO2_exc_3,
678     dO_ad_3, dM_3, dS_3, de_3
679     real(8) :: dCO2_4, dCO_4, dC_4, dC2_4, dO_4, dO2_4, dO3_4, dCO2_plus_4, dCO_plus_4,
680     dO3_plus_4, dO2_plus_4, dO_plus_4, dO2_minus_4, dO_minus_4, dCO2_exc_4, dO2_exc_4,
681     dO_ad_4, dM_4, dS_4, de_4
682     real(8) :: CO2_temp, CO_temp, C_temp, C2_temp, O_temp, O2_temp, O3_temp,
683     CO2_plus_temp, CO_plus_temp, O3_plus_temp, O2_plus_temp, O2_minus_temp, O_plus_temp,
684     O_minus_temp, CO2_exc_temp, O2_exc_temp, O_ad_temp, M_temp, S_temp, e_temp
685     real(8) :: CO2_old, CO_old, C_old, C2_old, O_old, O2_old, O3_old, CO2_plus_old,
686     CO_plus_old, O3_plus_old, O2_plus_old, O2_minus_old, O_plus_old, O_minus_old,
687     CO2_exc_old, O2_exc_old, O_ad_old, M_old, S_old, e_old
688
689     CO2_old = CO2
690     CO_old = CO
691     C_old = C
692     C2_old = C2
693     O_old = O
694     O2_old = O2
695     O3_old = O3
696     CO2_plus_old = CO2_plus
697     CO_plus_old = CO_plus
698     O3_plus_old = O3_plus
699     O2_plus_old = O2_plus
700     O2_minus_old = O2_minus
701     O_plus_old = O_plus

```

```

687 O_minus_old = O_minus
688 C02_exc_old = C02_exc
689 O2_exc_old = O2_exc
690 O_ad_old = O_ad
691 M_old = M
692 S_old = S
693 e_old = e
694
695 dC02_1 = -2 * C02**2 * k_f(14) - C02 * C02_exc * k_f(30) - C02 * 02 * k_b(15) - C02
* 02_plus * k_b(18) - C02 * 0 * k_b(21) - C02 * 0 * k_f(10) - C02 * e * k_f(1) - C02
* e * k_f(2) - C02 * e * k_f(3) - C02 * e * k_f(4) + C02_exc * e * k_b(4) +
C02_plus * 02 * k_f(18) + C02_plus * O_minus * k_f(21) + C02_plus * e**2 * k_b(2) +
2 * C0**2 * 02 * k_b(14) + C0**2 * 02 * k_b(30) + C0 * 02 * k_b(10) + C0 * 0 * e *
k_b(1) + C0_plus * 0 * e**2 * k_b(3) + 03 * 0 * k_f(15)
696 dC0_1 = 2 * C2 * 02 * k_f(28) + C2 * 0 * k_b(27) + 2 * C02**2 * k_f(14) + 2 * C02 *
C02_exc * k_f(30) + C02 * C02_plus * k_f(17) - C02 * C0 * 0_plus * k_b(17) + C02 * 0
* k_f(10) + C02 * e * k_f(1) + C02_exc * k_f(29) - 2 * C0**2 * 02 * k_b(14) - 2 *
C0**2 * 02 * k_b(30) - 2 * C0**2 * k_b(28) - C0 * C * k_f(27) - C0 * 02 * k_b(10) -
C0 * 0 * e * k_b(1) - C0 * 0 * k_b(29) - C0 * 0 * k_f(11) - C0 * k_b(25) + C * 02 *
k_b(11) + C * 0 * k_f(25)
697 dC_1 = C2 * 0 * k_b(27) + 2 * C2 * k_b(26) - C0 * C * k_f(27) + C0 * 0 * k_f(11) +
C0 * k_b(25) - 2 * C**2 * k_f(26) - C * 02 * k_b(11) - C * 0 * k_f(25)
698 dC2_1 = -C2 * 02 * k_f(28) - C2 * 0 * k_b(27) - C2 * k_b(26) + C0**2 * k_b(28) + C0
* C * k_f(27) + C**2 * k_f(26)
699 d0_1 = -C2 * 0 * k_b(27) + C02 * 02 * k_b(15) - C02 * 0 * k_b(21) - C02 * 0 * k_f
(10) + C02 * e * k_f(1) + C02 * e * k_f(3) + C02_exc * k_f(29) + C02_plus * O_minus
* k_f(21) + C0 * C * k_f(27) + C0 * 02 * k_b(10) - C0 * 0 * e * k_b(1) - C0 * 0 *
k_b(29) - C0 * 0 * k_f(11) + C0 * k_b(25) - C0_plus * 0 * e**2 * k_b(3) + C * 02 *
k_b(11) - C * 0 * k_f(25) - M * 02 * 0 * k_f(13) + 2 * M * 02 * k_b(12) + M * 03 *
k_b(13) - 2 * M * 0**2 * k_f(12) - M * 0 * e * k_f(9) + M * O_minus * k_b(9) + 02**2
* k_b(16) + 02 * 02_plus * k_f(19) - 02 * 0 * k_b(20) + 02 * e * k_f(7) - 02_minus
* 0 * k_b(7) + 02_minus * O_plus * k_f(20) - 03 * 0 * k_f(15) - 03 * 0 * k_f(16) -
03_plus * 0 * k_b(19) - 0 * S * k_f(22) - 0 * e * k_f(8) + 0_ad * k_b(22) + O_minus
* e * k_b(8)
700 d02_1 = -C2 * 02 * k_f(28) + C02**2 * k_f(14) + C02 * C02_exc * k_f(30) - C02 * 02 *
k_b(15) + C02 * 02_plus * k_b(18) + C02 * 0 * k_f(10) - C02_plus * 02 * k_f(18) -
C0**2 * 02 * k_b(14) - C0**2 * 02 * k_b(30) + C0**2 * k_b(28) - C0 * 02 * k_b(10) +
C0 * 0 * k_f(11) - C * 02 * k_b(11) - M * 02 * 0 * k_f(13) - M * 02 * k_b(12) + M *
03 * k_b(13) + M * 0**2 * k_f(12) - 2 * 02**2 * k_b(16) - 02 * 02_plus * k_f(19) -
02 * 0 * k_b(20) - 02 * 0_ad * k_b(24) - 02 * e * k_f(5) - 02 * e * k_f(6) - 02 * e
* k_f(7) - 02 * k_b(23) + 02_exc * e * k_b(5) + 02_minus * 0 * k_b(7) + 02_minus *
0_plus * k_f(20) + 02_plus * e**2 * k_b(6) + 03 * 0 * k_f(15) + 2 * 03 * 0 * k_f(16)
+ 03 * S * k_f(24) + 03_plus * 0 * k_b(19) + 0_ad**2 * k_f(23)
701 d03_1 = C02 * 02 * k_b(15) + M * 02 * 0 * k_f(13) - M * 03 * k_b(13) + 02**2 * k_b
(16) + 02 * 0_ad * k_b(24) - 03 * 0 * k_f(15) - 03 * 0 * k_f(16) - 03 * S * k_f(24)
702 dC02_plus_1 = -C02 * C02_plus * k_f(17) + C02 * C0 * 0_plus * k_b(17) + C02 *
02_plus * k_b(18) + C02 * 0 * k_b(21) + C02 * e * k_f(2) - C02_plus * 02 * k_f(18) -
C02_plus * O_minus * k_f(21) - C02_plus * e**2 * k_b(2)
703 dC0_plus_1 = C02 * e * k_f(3) - C0_plus * 0 * e**2 * k_b(3)
704 d03_plus_1 = 02 * 02_plus * k_f(19) - 03_plus * 0 * k_b(19)
705 d02_plus_1 = -C02 * 02_plus * k_b(18) + C02_plus * 02 * k_f(18) - 02 * 02_plus * k_f
(19) + 02 * e * k_f(6) - 02_plus * e**2 * k_b(6) + 03_plus * 0 * k_b(19)
706 d0_plus_1 = C02 * C02_plus * k_f(17) - C02 * C0 * 0_plus * k_b(17) + 02 * 0 * k_b
(20) - 02_minus * 0_plus * k_f(20)
707 d02_minus_1 = 02 * 0 * k_b(20) - 02_minus * 0_plus * k_f(20) + 02 * e * k_f(7) + 02
* e * k_f(5)
708 d0_minus_1 = C02 * 0 * k_b(21) - C02_plus * O_minus * k_f(21) + M * 0 * e * e * k_f(9) -
M * O_minus * k_b(9) + 0 * e * k_f(8) - O_minus * e * k_b(8)
709 dC02_exc_1 = -C02 * C02_exc * k_f(30) + C02 * e * k_f(4) - C02_exc * e * k_b(4) -
C02_exc * k_f(29) + C0**2 * 02 * k_b(30) + C0 * 0 * k_b(29)
710 d02_exc_1 = 02 * e * k_f(5) - 02_exc * e * k_b(5)
711 d0_ad_1 = -02 * 0_ad * k_b(24) + 2 * 02 * k_b(23) + 03 * S * k_f(24) + 0 * S * k_f
(22) - 2 * 0_ad**2 * k_f(23) - 0_ad * k_b(22)
712 dM_1 = 0
713 dS_1 = 02 * 0_ad * k_b(24) - 03 * S * k_f(24) - 0 * S * k_f(22) + 0_ad * k_b(22)
714 de_1 = C02 * e * k_f(2) + C02 * e * k_f(3) - C02_plus * e**2 * k_b(2) - C0_plus * 0
* e**2 * k_b(3) - M * 0 * e * k_f(9) + M * O_minus * k_b(9) + 02 * e * k_f(6) - 02 *
e * k_f(7) + 02_minus * 0 * k_b(7) - 02_plus * e**2 * k_b(6)
715
716 C02_temp = C02 + 0.5 * dC02_1 * dt
717 C0_temp = C0 + 0.5 * dC0_1 * dt
718 C_temp = C + 0.5 * dC_1 * dt
719 C2_temp = C2 + 0.5 * dC2_1 * dt

```

```

720   O_temp = 0 + 0.5 * dO_1 * dt
721   O2_temp = O2 + 0.5 * dO2_1 * dt
722   O3_temp = O3 + 0.5 * dO3_1 * dt
723   CO2_plus_temp = CO2_plus + 0.5 * dCO2_plus_1 * dt
724   CO_plus_temp = CO_plus + 0.5 * dCO_plus_1 * dt
725   O3_plus_temp = O3_plus + 0.5 * dO3_plus_1 * dt
726   O2_plus_temp = O2_plus + 0.5 * dO2_plus_1 * dt
727   O_plus_temp = O_plus + 0.5 * dO_plus_1 * dt
728   O2_minus_temp = O2_minus + 0.5 * dO2_minus_1 * dt
729   O_minus_temp = O_minus + 0.5 * dO_minus_1 * dt
730   CO2_exc_temp = CO2_exc + 0.5 * dCO2_exc_1 * dt
731   O2_exc_temp = O2_exc + 0.5 * dO2_exc_1 * dt
732   O_ad_temp = O_ad + 0.5 * dO_ad_1 * dt
733   M_temp = M + 0.5 * dM_1 * dt
734   S_temp = S + 0.5 * dS_1 * dt
735   e_temp = e + 0.5 * de_1 * dt
736
737   dCO2_2 = -2 * CO2_temp**2 * k_f(14) - CO2_temp * CO2_exc_temp * k_f(30) - CO2_temp *
    O2_temp * k_b(15) - CO2_temp * O2_plus_temp * k_b(18) - CO2_temp * O_temp * k_b(21)
    - CO2_temp * O_temp * k_f(10) - CO2_temp * e_temp * k_f(1) - CO2_temp * e_temp *
    k_f(2) - CO2_temp * e_temp * k_f(3) - CO2_temp * e_temp * k_f(4) + CO2_exc_temp *
    e_temp * k_b(4) + CO2_plus_temp * O2_temp * k_f(18) + CO2_plus_temp * O_minus_temp *
    k_f(21) + CO2_plus_temp * e_temp**2 * k_b(2) + 2 * CO_temp**2 * O2_temp * k_b(14) +
    CO_temp**2 * O2_temp * k_b(30) + CO_temp * O2_temp * k_b(10) + CO_temp * O_temp *
    e_temp * k_b(1) + CO_plus_temp * O_temp * e_temp**2 * k_b(3) + O3_temp * O_temp *
    k_f(15)
738   dCO2_2 = 2 * C2_temp * O2_temp * k_f(28) + C2_temp * O_temp * k_b(27) + 2 * CO2_temp *
    **2 * k_f(14) + 2 * CO2_temp * CO2_exc_temp * k_f(30) + CO2_temp * CO2_plus_temp *
    k_f(17) - CO2_temp * CO_temp * O_plus_temp * k_b(17) + CO2_temp * O_temp * k_f(10) +
    CO2_temp * e_temp * k_f(1) + CO2_exc_temp * k_f(29) - 2 * CO_temp**2 * O2_temp *
    k_b(14) - 2 * CO_temp**2 * O2_temp * k_b(30) - 2 * CO_temp**2 * k_b(28) - CO_temp *
    C_temp * k_f(27) - CO_temp * O2_temp * k_b(10) - CO_temp * O_temp * e_temp * k_b(1)
    - CO_temp * O_temp * k_b(29) - CO_temp * O_temp * k_f(11) - CO_temp * k_b(25) +
    C_temp * O2_temp * k_b(11) + C_temp * O_temp * k_f(25)
739   dC_2 = C2_temp * O_temp * k_b(27) + 2 * C2_temp * k_b(26) - CO_temp * C_temp * k_f(
    27) + CO_temp * O_temp * k_f(11) + CO_temp * k_b(25) - 2 * C_temp**2 * k_f(26) -
    C_temp * O2_temp * k_b(11) - C_temp * O_temp * k_f(25)
740   dC2_2 = -C2_temp * O2_temp * k_f(28) - C2_temp * O_temp * k_b(27) - C2_temp * k_b(
    26) + CO_temp**2 * k_b(28) + CO_temp * C_temp * k_f(27) + C_temp**2 * k_f(26)
741   dO_2 = -C2_temp * O_temp * k_b(27) + CO2_temp * O2_temp * k_b(15) - CO2_temp *
    O_temp * k_b(21) - CO2_temp * O_temp * k_f(10) + CO2_temp * e_temp * k_f(1) +
    CO2_temp * e_temp * k_f(3) + CO2_exc_temp * k_f(29) + CO2_plus_temp * O_minus_temp *
    k_f(21) + CO_temp * C_temp * k_f(27) + CO_temp * O2_temp * k_b(10) - CO_temp *
    O_temp * e_temp * k_b(1) - CO_temp * O_temp * k_b(29) - CO_temp * O_temp * k_f(11) +
    CO_temp * k_b(25) - CO_plus_temp * O_temp * e_temp**2 * k_b(3) + C_temp * O2_temp *
    k_b(11) - C_temp * O_temp * k_f(25) - M_temp * O2_temp * O_temp * k_f(13) + 2 *
    M_temp * O2_temp * k_b(12) + M_temp * O3_temp * k_b(13) - 2 * M_temp * O_temp**2 *
    k_f(12) - M_temp * O_temp * e_temp * k_f(9) + M_temp * O_minus_temp * k_b(9) +
    O2_temp**2 * k_b(16) + O2_temp * O2_plus_temp * k_f(19) - O2_temp * O_temp * k_b(20)
    + O2_temp * e_temp * k_f(7) - O2_minus_temp * O_temp * k_b(7) + O2_minus_temp *
    O_plus_temp * k_f(20) - O3_temp * O_temp * k_f(15) - O3_temp * O_temp * k_f(16) -
    O3_plus_temp * O_temp * k_b(19) - O_temp * S_temp * k_f(22) - O_temp * e_temp * k_f(
    8) + O_ad_temp * k_b(22) + O_minus_temp * e_temp * k_b(8)
742   dO2_2 = -C2_temp * O2_temp * k_f(28) + CO2_temp**2 * k_f(14) + CO2_temp *
    CO2_exc_temp * k_f(30) - CO2_temp * O2_temp * k_b(15) + CO2_temp * O2_plus_temp *
    k_b(18) + CO2_temp * O_temp * k_f(10) - CO2_plus_temp * O2_temp * k_f(18) - CO_temp *
    **2 * O2_temp * k_b(14) - CO_temp**2 * O2_temp * k_b(30) + CO_temp**2 * k_b(28) -
    CO_temp * O2_temp * k_b(10) + CO_temp * O_temp * k_f(11) - C_temp * O2_temp * k_b(
    11) - M_temp * O2_temp * O_temp * k_f(13) - M_temp * O2_temp * k_b(12) + M_temp *
    O3_temp * k_b(13) + M_temp * O_temp**2 * k_f(12) - 2 * O2_temp**2 * k_b(16) -
    O2_temp * O2_plus_temp * k_f(19) - O2_temp * O_temp * k_b(20) - O2_temp * O_ad_temp *
    k_b(24) - O2_temp * e_temp * k_f(5) - O2_temp * e_temp * k_f(6) - O2_temp * e_temp *
    k_f(7) - O2_temp * k_b(23) + O2_exc_temp * e_temp * k_b(5) + O2_minus_temp *
    O_temp * k_b(7) + O2_minus_temp * O_plus_temp * k_f(20) + O2_plus_temp * e_temp**2 *
    k_b(6) + O3_temp * O_temp * k_f(15) + 2 * O3_temp * O_temp * k_f(16) + O3_temp *
    S_temp * k_f(24) + O3_plus_temp * O_temp * k_b(19) + O_ad_temp**2 * k_f(23)
743   dO3_2 = CO2_temp * O2_temp * k_b(15) + M_temp * O2_temp * O_temp * k_f(13) - M_temp *
    O3_temp * k_b(13) + O2_temp**2 * k_b(16) + O2_temp * O_ad_temp * k_b(24) - O3_temp *
    * O_temp * k_f(15) - O3_temp * O_temp * k_f(16) - O3_temp * S_temp * k_f(24)
744   dCO2_plus_2 = -CO2_temp * CO2_plus_temp * k_f(17) + CO2_temp * CO_temp * O_plus_temp *
    * k_b(17) + CO2_temp * O2_plus_temp * k_b(18) + CO2_temp * O_temp * k_b(21) +
    CO2_temp * e_temp * k_f(2) - CO2_plus_temp * O2_temp * k_f(18) - CO2_plus_temp *
    O_minus_temp * k_f(21) - CO2_plus_temp * e_temp**2 * k_b(2)

```

---

```

745 dC0_plus_2 = C02_temp * e_temp * k_f(3) - C0_plus_temp * 0_temp * e_temp**2 * k_b(3)
746 d03_plus_2 = O2_temp * O2_plus_temp * k_f(19) - O3_plus_temp * 0_temp * k_b(19)
747 d02_plus_2 = -C02_temp * O2_plus_temp * k_b(18) + C02_plus_temp * O2_temp * k_f(18)
748 - O2_temp * O2_plus_temp * k_f(19) + O2_temp * e_temp * k_f(6) - O2_plus_temp *
e_temp**2 * k_b(6) + O3_plus_temp * 0_temp * k_b(19)
749 d0_plus_2 = C02_temp * C02_plus_temp * k_f(17) - C02_temp * C0_temp * 0_plus_temp *
k_b(17) + O2_temp * 0_temp * k_b(20) - O2_minus_temp * 0_plus_temp * k_f(20)
750 d02_minus_2 = O2_temp * 0_temp * k_b(20) - O2_minus_temp * 0_plus_temp * k_f(20) +
O2_temp * e_temp * k_f(7) + O2_temp * e_temp * k_f(5)
751 d0_minus_2 = C02_temp * 0_temp * k_b(21) - C02_plus_temp * 0_minus_temp * k_f(21) +
M_temp * 0_temp * e_temp * k_f(9) - M_temp * 0_minus_temp * k_b(9) + 0_temp * e_temp
* k_f(8) - 0_minus_temp * e_temp * k_b(8)
752 dC02_exc_2 = -C02_temp * C02_exc_temp * k_f(30) + C02_temp * e_temp * k_f(4) -
C02_exc_temp * e_temp * k_b(4) - C02_exc_temp * k_f(29) + C0_temp**2 * O2_temp * k_b
(30) + C0_temp * 0_temp * k_b(29)
753 d02_exc_2 = O2_temp * e_temp * k_f(5) - O2_exc_temp * e_temp * k_b(5)
754 d0_ad_2 = -O2_temp * 0_ad_temp * k_b(24) + 2 * O2_temp * k_b(23) + O3_temp * S_temp
* k_f(24) + 0_temp * S_temp * k_f(22) - 2 * 0_ad_temp**2 * k_f(23) - 0_ad_temp * k_b
(22)
755 dM_2 = 0
756 dS_2 = O2_temp * 0_ad_temp * k_b(24) - O3_temp * S_temp * k_f(24) - 0_temp * S_temp
* k_f(22) + 0_ad_temp * k_b(22)
757 de_2 = C02_temp * e_temp * k_f(2) + C02_temp * e_temp * k_f(3) - C02_plus_temp *
e_temp**2 * k_b(2) - C0_plus_temp * 0_temp * e_temp**2 * k_b(3) - M_temp * 0_temp *
e_temp * k_f(9) + M_temp * 0_minus_temp * k_b(9) + O2_temp * e_temp * k_f(6) -
O2_temp * e_temp * k_f(7) + O2_minus_temp * 0_temp * k_b(7) - O2_plus_temp * e_temp
**2 * k_b(6)
758 C02_temp = C02 + 0.5 * dC02_2 * dt
759 C0_temp = C0 + 0.5 * dC0_2 * dt
760 C_temp = C + 0.5 * dC_2 * dt
761 C2_temp = C2 + 0.5 * dC2_2 * dt
762 O_temp = O + 0.5 * dO_2 * dt
763 O2_temp = O2 + 0.5 * dO2_2 * dt
764 O3_temp = O3 + 0.5 * dO3_2 * dt
765 C02_plus_temp = C02_plus + 0.5 * dC02_plus_2 * dt
766 C0_plus_temp = C0_plus + 0.5 * dC0_plus_2 * dt
767 O3_plus_temp = O3_plus + 0.5 * dO3_plus_2 * dt
768 O2_plus_temp = O2_plus + 0.5 * dO2_plus_2 * dt
769 O_plus_temp = O_plus + 0.5 * dO_plus_2 * dt
770 O2_minus_temp = O2_minus + 0.5 * dO2_minus_2 * dt
771 O_minus_temp = O_minus + 0.5 * dO_minus_2 * dt
772 C02_exc_temp = C02_exc + 0.5 * dC02_exc_2 * dt
773 O2_exc_temp = O2_exc + 0.5 * dO2_exc_2 * dt
774 O_ad_temp = O_ad + 0.5 * dO_ad_2 * dt
775 M_temp = M + 0.5 * dM_2 * dt
776 S_temp = S + 0.5 * dS_2 * dt
777 e_temp = e + 0.5 * de_2 * dt
778
779 dC02_3 = -2 * C02_temp**2 * k_f(14) - C02_temp * C02_exc_temp * k_f(30) - C02_temp *
O2_temp * k_b(15) - C02_temp * O2_plus_temp * k_b(18) - C02_temp * 0_temp * k_b(21)
- C02_temp * 0_temp * k_f(10) - C02_temp * e_temp * k_f(1) - C02_temp * e_temp *
k_f(2) - C02_temp * e_temp * k_f(3) - C02_temp * e_temp * k_f(4) + C02_exc_temp *
e_temp * k_b(4) + C02_plus_temp * O2_temp * k_f(18) + C02_plus_temp * 0_minus_temp *
k_f(21) + C02_plus_temp * e_temp**2 * k_b(2) + 2 * C0_temp**2 * O2_temp * k_b(14) +
C0_temp**2 * O2_temp * k_b(30) + C0_temp * O2_temp * k_b(10) + C0_temp * 0_temp *
e_temp * k_b(1) + C0_plus_temp * 0_temp * e_temp**2 * k_b(3) + O3_temp * 0_temp *
k_f(15)
780 dC0_3 = 2 * C2_temp * O2_temp * k_f(28) + C2_temp * 0_temp * k_b(27) + 2 * C02_temp
**2 * k_f(14) + 2 * C02_temp * C02_exc_temp * k_f(30) + C02_temp * C02_plus_temp *
k_f(17) - C02_temp * C0_temp * 0_plus_temp * k_b(17) + C02_temp * 0_temp * k_f(10) +
C02_temp * e_temp * k_f(1) + C02_exc_temp * k_f(29) - 2 * C0_temp**2 * O2_temp *
k_b(14) - 2 * C0_temp**2 * O2_temp * k_b(30) - 2 * C0_temp**2 * k_b(28) - C0_temp *
C_temp * k_f(27) - C0_temp * O2_temp * k_b(10) - C0_temp * 0_temp * e_temp * k_b(1)
- C0_temp * 0_temp * k_b(29) - C0_temp * 0_temp * k_f(11) - C0_temp * k_b(25) +
C_temp * O2_temp * k_b(11) + C_temp * 0_temp * k_f(25)
781 dC_3 = C2_temp * 0_temp * k_b(27) + 2 * C2_temp * k_b(26) - C0_temp * C_temp * k_f
(27) + C0_temp * 0_temp * k_f(11) + C0_temp * k_b(25) - 2 * C_temp**2 * k_f(26) -
C_temp * O2_temp * k_b(11) - C_temp * 0_temp * k_f(25)
782 dC2_3 = -C2_temp * O2_temp * k_f(28) - C2_temp * 0_temp * k_b(27) - C2_temp * k_b
(26) + C0_temp**2 * k_b(28) + C0_temp * C_temp * k_f(27) + C_temp**2 * k_f(26)
783 dO_3 = -C2_temp * 0_temp * k_b(27) + C02_temp * O2_temp * k_b(15) - C02_temp *
0_temp * k_b(21) - C02_temp * 0_temp * k_f(10) + C02_temp * e_temp * k_f(1) +

```

---

```

C02_temp * e_temp * k_f(3) + C02_exc_temp * k_f(29) + C02_plus_temp * 0_minus_temp *
k_f(21) + C0_temp * C_temp * k_f(27) + C0_temp * 02_temp * k_b(10) - C0_temp *
0_temp * e_temp * k_b(1) - C0_temp * 0_temp * k_b(29) - C0_temp * 0_temp * k_f(11) +
C0_temp * k_b(25) - C0_plus_temp * 0_temp * e_temp**2 * k_b(3) + C_temp * 02_temp *
k_b(11) - C_temp * 0_temp * k_f(25) - M_temp * 02_temp * 0_temp * k_f(13) + 2 *
M_temp * 02_temp * k_b(12) + M_temp * 03_temp * k_b(13) - 2 * M_temp * 0_temp**2 *
k_f(12) - M_temp * 0_temp * e_temp * k_f(9) + M_temp * 0_minus_temp * k_b(9) +
02_temp**2 * k_b(16) + 02_temp * 02_plus_temp * k_f(19) - 02_temp * 0_temp * k_b(20)
+ 02_temp * e_temp * k_f(7) - 02_minus_temp * 0_temp * k_b(7) + 02_minus_temp *
0_plus_temp * k_f(20) - 03_temp * 0_temp * k_f(15) - 03_temp * 0_temp * k_f(16) -
03_plus_temp * 0_temp * k_b(19) - 0_temp * S_temp * k_f(22) - 0_temp * e_temp * k_f
(8) + 0_ad_temp * k_b(22) + 0_minus_temp * e_temp * k_b(8)

784 d02_3 = -C2_temp * 02_temp * k_f(28) + C02_temp**2 * k_f(14) + C02_temp *
C02_exc_temp * k_f(30) - C02_temp * 02_temp * k_b(15) + C02_temp * 02_plus_temp *
k_b(18) + C02_temp * 0_temp * k_f(10) - C02_plus_temp * 02_temp * k_f(18) - C0_temp
**2 * 02_temp * k_b(14) - C0_temp**2 * 02_temp * k_b(30) + C0_temp**2 * k_b(28) -
C0_temp * 02_temp * k_b(10) + C0_temp * 0_temp * k_f(11) - C_temp * 02_temp * k_b
(11) - M_temp * 02_temp * 0_temp * k_f(13) - M_temp * 02_temp * k_b(12) + M_temp *
03_temp * k_b(13) + M_temp * 0_temp**2 * k_f(12) - 2 * 02_temp**2 * k_b(16) -
02_temp * 02_plus_temp * k_f(19) - 02_temp * 0_temp * k_b(20) - 02_temp * 0_ad_temp
* k_b(24) - 02_temp * e_temp * k_f(5) - 02_temp * e_temp * k_f(6) - 02_temp * e_temp
* k_f(7) - 02_temp * k_b(23) + 02_exc_temp * e_temp * k_b(5) + 02_minus_temp *
0_temp * k_b(7) + 02_minus_temp * 0_plus_temp * k_f(20) + 02_plus_temp * e_temp**2 *
k_b(6) + 03_temp * 0_temp * k_f(15) + 2 * 03_temp * 0_temp * k_f(16) + 03_temp *
S_temp * k_f(24) + 03_plus_temp * 0_temp * k_b(19) + 0_ad_temp**2 * k_f(23)

785 d03_3 = C02_temp * 02_temp * k_b(15) + M_temp * 02_temp * 0_temp * k_f(13) - M_temp
* 03_temp * k_b(13) + 02_temp**2 * k_b(16) + 02_temp * 0_ad_temp * k_b(24) - 03_temp
* 0_temp * k_f(15) - 03_temp * 0_temp * k_f(16) - 03_temp * S_temp * k_f(24)

786 dC02_plus_3 = -C02_temp * C02_plus_temp * k_f(17) + C02_temp * C0_temp * 0_plus_temp
* k_b(17) + C02_temp * 02_plus_temp * k_b(18) + C02_temp * 0_temp * k_b(21) +
C02_temp * e_temp * k_f(2) - C02_plus_temp * 02_temp * k_f(18) - C02_plus_temp *
0_minus_temp * k_f(21) - C02_plus_temp * e_temp**2 * k_b(2)

787 dC0_plus_3 = C02_temp * e_temp * k_f(3) - C0_plus_temp * 0_temp * e_temp**2 * k_b(3)

788 d03_plus_3 = 02_temp * 02_plus_temp * k_f(19) - 03_plus_temp * 0_temp * k_b(19)

789 d02_plus_3 = -C02_temp * 02_plus_temp * k_b(18) + C02_plus_temp * 02_temp * k_f(18)
- 02_temp * 02_plus_temp * k_f(19) + 02_temp * e_temp * k_f(6) - 02_plus_temp *
e_temp**2 * k_b(6) + 03_plus_temp * 0_temp * k_b(19)

790 d0_plus_3 = C02_temp * C02_plus_temp * k_f(17) - C02_temp * C0_temp * 0_plus_temp *
k_b(17) + 02_temp * 0_temp * k_b(20) - 02_minus_temp * 0_plus_temp * k_f(20)

791 d02_minus_3 = 02_temp * 0_temp * k_b(20) - 02_minus_temp * 0_plus_temp * k_f(20) +
02_temp * e_temp * k_f(7) + 02_temp * e_temp * k_f(5)

792 d0_minus_3 = C02_temp * 0_temp * k_b(21) - C02_plus_temp * 0_minus_temp * k_f(21) +
M_temp * 0_temp * e_temp * k_f(9) - M_temp * 0_minus_temp * k_b(9) + 0_temp * e_temp
* k_f(8) - 0_minus_temp * e_temp * k_b(8)

793 dC02_exc_3 = -C02_temp * C02_exc_temp * k_f(30) + C02_temp * e_temp * k_f(4) -
C02_exc_temp * e_temp * k_b(4) - C02_exc_temp * k_f(29) + C0_temp**2 * 02_temp * k_b
(30) + C0_temp * 0_temp * k_b(29)

794 d02_exc_3 = 02_temp * e_temp * k_f(5) - 02_exc_temp * e_temp * k_b(5)

795 d0_ad_3 = -02_temp * 0_ad_temp * k_b(24) + 2 * 02_temp * k_b(23) + 03_temp * S_temp
* k_f(24) + 0_temp * S_temp * k_f(22) - 2 * 0_ad_temp**2 * k_f(23) - 0_ad_temp * k_b
(22)

796 dM_3 = 0

797 dS_3 = 02_temp * 0_ad_temp * k_b(24) - 03_temp * S_temp * k_f(24) - 0_temp * S_temp
* k_f(22) + 0_ad_temp * k_b(22)

798 de_3 = C02_temp * e_temp * k_f(2) + C02_temp * e_temp * k_f(3) - C02_plus_temp *
e_temp**2 * k_b(2) - C0_plus_temp * 0_temp * e_temp**2 * k_b(3) - M_temp * 0_temp *
e_temp * k_f(9) + M_temp * 0_minus_temp * k_b(9) + 02_temp * e_temp * k_f(6) -
02_temp * e_temp * k_f(7) + 02_minus_temp * 0_temp * k_b(7) - 02_plus_temp * e_temp
**2 * k_b(6)

799 C02_temp = C02 + 0.5 * dC02_3 * dt
800 C0_temp = C0 + 0.5 * dC0_3 * dt
801 C_temp = C + 0.5 * dC_3 * dt
802 C2_temp = C2 + 0.5 * dC2_3 * dt
803 O_temp = O + 0.5 * dO_3 * dt
804 O2_temp = O2 + 0.5 * d02_3 * dt
805 O3_temp = O3 + 0.5 * d03_3 * dt
806 C02_plus_temp = C02_plus + 0.5 * dC02_plus_3 * dt
807 C0_plus_temp = C0_plus + 0.5 * dC0_plus_3 * dt
808 O3_plus_temp = O3_plus + 0.5 * d03_plus_3 * dt
809 O2_plus_temp = O2_plus + 0.5 * d02_plus_3 * dt
810 O_plus_temp = O_plus + 0.5 * d0_plus_3 * dt
811 O2_minus_temp = O2_minus + 0.5 * d02_minus_3 * dt

```

```

813 O_minus_temp = O_minus + 0.5 * dO_minus_3 * dt
814 C02_exc_temp = C02_exc + 0.5 * dC02_exc_3 * dt
815 O2_exc_temp = O2_exc + 0.5 * dO2_exc_3 * dt
816 O_ad_temp = O_ad + 0.5 * dO_ad_3 * dt
817 M_temp = M + 0.5 * dM_3 * dt
818 S_temp = S + 0.5 * dS_3 * dt
819 e_temp = e + 0.5 * de_3 * dt
820
821 dC02_4 = -2 * C02_temp**2 * k_f(14) - C02_temp * C02_exc_temp * k_f(30) - C02_temp *
822   02_temp * k_b(15) - C02_temp * O2_plus_temp * k_b(18) - C02_temp * O_temp * k_b(21)
823   - C02_temp * O_temp * k_f(10) - C02_temp * e_temp * k_f(1) - C02_temp * e_temp *
824   k_f(2) - C02_temp * e_temp * k_f(3) - C02_temp * e_temp * k_f(4) + C02_exc_temp *
825   e_temp * k_b(4) + C02_plus_temp * O2_temp * k_f(18) + C02_plus_temp * O_minus_temp *
826   k_f(21) + C02_plus_temp * e_temp**2 * k_b(2) + 2 * C0_temp**2 * O2_temp * k_b(14) +
827   C0_temp**2 * O2_temp * k_b(30) + C0_temp * O2_temp * k_b(10) + C0_temp * O_temp *
828   e_temp * k_b(1) + C0_plus_temp * O_temp * e_temp**2 * k_b(3) + O3_temp * O_temp *
829   k_f(15)
830 dC0_4 = 2 * C2_temp * O2_temp * k_f(28) + C2_temp * O_temp * k_b(27) + 2 * C02_temp *
831   **2 * k_f(14) + 2 * C02_temp * C02_exc_temp * k_f(30) + C02_temp * C02_plus_temp *
832   k_f(17) - C02_temp * C0_temp * O_plus_temp * k_b(17) + C02_temp * O_temp * k_f(10) +
833   C02_temp * e_temp * k_f(1) + C02_exc_temp * k_f(29) - 2 * C0_temp**2 * O2_temp *
834   k_b(14) - 2 * C0_temp**2 * O2_temp * k_b(30) - 2 * C0_temp**2 * k_b(28) - C0_temp *
835   C_temp * k_f(27) - C0_temp * O2_temp * k_b(10) - C0_temp * O_temp * e_temp * k_b(1)
836   - C0_temp * O_temp * k_b(29) - C0_temp * O_temp * k_f(11) - C0_temp * k_b(25) +
837   C_temp * O2_temp * k_b(11) + C_temp * O_temp * k_f(25)
838 dC_4 = C2_temp * O_temp * k_b(27) + 2 * C2_temp * k_b(26) - C0_temp * C_temp * k_f(
839   27) + C0_temp * O_temp * k_f(11) + C0_temp * k_b(25) - 2 * C_temp**2 * k_f(26) -
840   C_temp * O2_temp * k_b(11) - C_temp * O_temp * k_f(25)
841 dC2_4 = -C2_temp * O2_temp * k_f(28) - C2_temp * O_temp * k_b(27) - C2_temp * k_b(
842   26) + C0_temp**2 * k_b(28) + C0_temp * C_temp * k_f(27) + C_temp**2 * k_f(26)
843 dO_4 = -C2_temp * O_temp * k_b(27) + C02_temp * O2_temp * k_b(15) - C02_temp *
844   O_temp * k_b(21) - C02_temp * O_temp * k_f(10) + C02_temp * e_temp * k_f(1) +
845   C02_temp * e_temp * k_f(3) + C02_exc_temp * k_f(29) + C02_plus_temp * O_minus_temp *
846   k_f(21) + C0_temp * C_temp * k_f(27) + C0_temp * O2_temp * k_b(10) - C0_temp *
847   O_temp * e_temp * k_b(1) - C0_temp * O_temp * k_b(29) - C0_temp * O_temp * k_f(11) +
848   C0_temp * k_b(25) - C0_plus_temp * O_temp * e_temp**2 * k_b(3) + C_temp * O2_temp *
849   k_b(11) - C_temp * O_temp * k_f(25) - M_temp * O2_temp * O_temp * k_f(13) + 2 *
850   M_temp * O2_temp * k_b(12) + M_temp * O3_temp * k_b(13) - 2 * M_temp * O_temp**2 *
851   k_f(12) - M_temp * O_temp * e_temp * k_f(9) + M_temp * O_minus_temp * k_b(9) +
852   O2_temp**2 * k_b(16) + O2_temp * O2_plus_temp * k_f(19) - O2_temp * O_temp * k_b(20)
853   + O2_temp * e_temp * k_f(7) - O2_minus_temp * O_temp * k_b(7) + O2_minus_temp *
854   O_plus_temp * k_f(20) - O3_temp * O_temp * k_f(15) - O3_temp * O_temp * k_f(16) -
855   O3_plus_temp * O_temp * k_b(19) - O_temp * S_temp * k_f(22) - O_temp * e_temp * k_f
856   (8) + O_ad_temp * k_b(22) + O_minus_temp * e_temp * k_b(8)
857 dO2_4 = -C2_temp * O2_temp * k_f(28) + C02_temp**2 * k_f(14) + C02_temp *
858   C02_exc_temp * k_f(30) - C02_temp * O2_temp * k_b(15) + C02_temp * O2_plus_temp *
859   k_b(18) + C02_temp * O_temp * k_f(10) - C02_plus_temp * O2_temp * k_f(18) - C0_temp *
860   **2 * O2_temp * k_b(14) - C0_temp**2 * O2_temp * k_b(30) + C0_temp**2 * k_b(28) -
861   C0_temp * O2_temp * k_b(10) + C0_temp * O_temp * k_f(11) - C_temp * O2_temp * k_b
862   (11) - M_temp * O2_temp * O_temp * k_f(13) - M_temp * O2_temp * k_b(12) + M_temp *
863   O3_temp * k_b(13) + M_temp * O_temp**2 * k_f(12) - 2 * O2_temp**2 * k_b(16) -
864   O2_temp * O2_plus_temp * k_f(19) - O2_temp * O_temp * k_b(20) - O2_temp * O_ad_temp *
865   * k_b(24) - O2_temp * e_temp * k_f(5) - O2_temp * e_temp * k_f(6) - O2_temp * e_temp *
866   * k_f(7) - O2_temp * k_b(23) + O2_exc_temp * e_temp * k_b(5) + O2_minus_temp *
867   O_temp * k_b(7) + O2_minus_temp * O_plus_temp * k_f(20) + O2_plus_temp * e_temp**2 *
868   k_b(6) + O3_temp * O_temp * k_f(15) + 2 * O3_temp * O_temp * k_f(16) + O3_temp *
869   S_temp * k_f(24) + O3_plus_temp * O_temp * k_b(19) + O_ad_temp**2 * k_f(23)
870 dO3_4 = C02_temp * O2_temp * k_b(15) + M_temp * O2_temp * O_temp * k_f(13) - M_temp
871   * O3_temp * k_b(13) + O2_temp**2 * k_b(16) + O2_temp * O_ad_temp * k_b(24) - O3_temp
872   * O_temp * k_f(15) - O3_temp * O_temp * k_f(16) - O3_temp * S_temp * k_f(24)
873 dC02_plus_4 = -C02_temp * C02_plus_temp * k_f(17) + C02_temp * C0_temp * O_plus_temp *
874   * k_b(17) + C02_temp * O2_plus_temp * k_b(18) + C02_temp * O_temp * k_b(21) +
875   C02_temp * e_temp * k_f(2) - C02_plus_temp * O2_temp * k_f(18) - C02_plus_temp *
876   O_minus_temp * k_f(21) - C02_plus_temp * e_temp**2 * k_b(2)
877 dC0_plus_4 = C02_temp * e_temp * k_f(3) - C0_plus_temp * O_temp * e_temp**2 * k_b(3)
878 dO3_plus_4 = O2_temp * O2_plus_temp * k_f(19) - O3_plus_temp * O_temp * k_b(19)
879 dO2_plus_4 = -C02_temp * O2_plus_temp * k_b(18) + C02_plus_temp * O2_temp * k_f(18)
880   - O2_temp * O2_plus_temp * k_f(19) + O2_temp * e_temp * k_f(6) - O2_plus_temp *
881   e_temp**2 * k_b(6) + O3_plus_temp * O_temp * k_b(19)
882 dO_plus_4 = C02_temp * C02_plus_temp * k_f(17) - C02_temp * C0_temp * O_plus_temp *
883   k_b(17) + O2_temp * O_temp * k_b(20) - O2_minus_temp * O_plus_temp * k_f(20)
884 dO2_minus_4 = O2_temp * O_temp * k_b(20) - O2_minus_temp * O_plus_temp * k_f(20) +
885   O2_temp * e_temp * k_f(7) + O2_temp * e_temp * k_f(5)

```

---

```

834 d0_minus_4 = CO2_temp * 0_temp * k_b(21) - CO2_plus_temp * 0_minus_temp * k_f(21) +
M_temp * 0_temp * e_temp * k_f(9) - M_temp * 0_minus_temp * k_b(9) + 0_temp * e_temp
* k_f(8) - 0_minus_temp * e_temp * k_b(8)
835 dCO2_exc_4 = -CO2_temp * CO2_exc_temp * k_f(30) + CO2_temp * e_temp * k_f(4) -
CO2_exc_temp * e_temp * k_b(4) - CO2_exc_temp * k_f(29) + CO2_temp**2 * 02_temp * k_b
(30) + CO2_temp * 0_temp * k_b(29)
836 d02_exc_4 = 02_temp * e_temp * k_f(5) - 02_exc_temp * e_temp * k_b(5)
837 d0_ad_4 = -02_temp * 0_ad_temp * k_b(24) + 2 * 02_temp * k_b(23) + 03_temp * S_temp
* k_f(24) + 0_temp * S_temp * k_f(22) - 2 * 0_ad_temp**2 * k_f(23) - 0_ad_temp * k_b
(22)
838 dM_4 = 0
839 dS_4 = 02_temp * 0_ad_temp * k_b(24) - 03_temp * S_temp * k_f(24) - 0_temp * S_temp
* k_f(22) + 0_ad_temp * k_b(22)
840 de_4 = CO2_temp * e_temp * k_f(2) + CO2_temp * e_temp * k_f(3) - CO2_plus_temp *
e_temp**2 * k_b(2) - CO2_plus_temp * 0_temp * e_temp**2 * k_b(3) - M_temp * 0_temp *
e_temp * k_f(9) + M_temp * 0_minus_temp * k_b(9) + 02_temp * e_temp * k_f(6) -
02_temp * e_temp * k_f(7) + 02_minus_temp * 0_temp * k_b(7) - 02_plus_temp * e_temp
**2 * k_b(6)
841
842 CO2 = CO2 + (dt / 6.0) * (dCO2_1 + 2 * dCO2_2 + 2 * dCO2_3 + dCO2_4)
843 CO = CO + (dt / 6.0) * (dCO_1 + 2 * dCO_2 + 2 * dCO_3 + dCO_4)
844 C = C + (dt / 6.0) * (dC_1 + 2 * dC_2 + 2 * dC_3 + dC_4)
845 C2 = C2 + (dt / 6.0) * (dC2_1 + 2 * dC2_2 + 2 * dC2_3 + dC2_4)
846 0 = 0 + (dt / 6.0) * (d0_1 + 2 * d0_2 + 2 * d0_3 + d0_4)
847 02 = 02 + (dt / 6.0) * (d02_1 + 2 * d02_2 + 2 * d02_3 + d02_4)
848 03 = 03 + (dt / 6.0) * (d03_1 + 2 * d03_2 + 2 * d03_3 + d03_4)
849 CO2_plus = CO2_plus + (dt / 6.0) * (dCO2_plus_1 + 2 * dCO2_plus_2 + 2 * dCO2_plus_3
+ dCO2_plus_4)
850 CO_plus = CO_plus + (dt / 6.0) * (dCO_plus_1 + 2 * dCO_plus_2 + 2 * dCO_plus_3 +
dCO_plus_4)
851 03_plus = 03_plus + (dt / 6.0) * (d03_plus_1 + 2 * d03_plus_2 + 2 * d03_plus_3 +
d03_plus_4)
852 02_plus = 02_plus + (dt / 6.0) * (d02_plus_1 + 2 * d02_plus_2 + 2 * d02_plus_3 +
d02_plus_4)
853 0_plus = 0_plus + (dt / 6.0) * (d0_plus_1 + 2 * d0_plus_2 + 2 * d0_plus_3 +
d0_plus_4)
854 02_minus = 02_minus + (dt / 6.0) * (d02_minus_1 + 2 * d02_minus_2 + 2 * d02_minus_3
+ d02_minus_4)
855 0_minus = 0_minus + (dt / 6.0) * (d0_minus_1 + 2 * d0_minus_2 + 2 * d0_minus_3 +
d0_minus_4)
856 CO2_exc = CO2_exc + (dt / 6.0) * (dCO2_exc_1 + 2 * dCO2_exc_2 + 2 * dCO2_exc_3 +
dCO2_exc_4)
857 02_exc = 02_exc + (dt / 6.0) * (d02_exc_1 + 2 * d02_exc_2 + 2 * d02_exc_3 +
d02_exc_4)
858 0_ad = 0_ad + (dt / 6.0) * (d0_ad_1 + 2 * d0_ad_2 + 2 * d0_ad_3 + d0_ad_4)
859 M = M + (dt / 6.0) * (dM_1 + 2 * dM_2 + 2 * dM_3 + dM_4)
860 S = S + (dt / 6.0) * (dS_1 + 2 * dS_2 + 2 * dS_3 + dS_4)
861 e = e + (dt / 6.0) * (de_1 + 2 * de_2 + 2 * de_3 + de_4)
862
863 CO2 = CO2
864 CO = CO * 0.5
865 C = C
866 C2 = C2
867 0 = 0 * 1E-51_8
868 02 = 02 * (-1.25E-3)
869 03 = 03
870 CO2_plus = CO2_plus * (-1)
871 CO_plus = CO_plus * 1E16
872 03_plus = 03_plus * (-1E36_8)
873 02_plus = 02_plus * 1E14
874 0_plus = 0_plus * 1E-9
875 02_minus = 02_minus * 1E-29
876 0_minus = 0_minus * 1E-9
877 CO2_exc = CO2_exc * 1E15
878 02_exc = 02_exc * 1E38
879 0_ad = 0_ad
880 M = M
881 S = S
882 e = e
883
884 if (t > t_discharge) then
885     if ((CO2 /= CO2) .or. CO2 < 0.0 .or. CO2 > n_CO2) then
886         CO2 = CO2_old

```

---

```

887     end if
888
889     if ((CO /= CO) .or. CO < 0.0 .or. CO > n_CO2) then
890         CO = CO_old
891     end if
892
893     if ((C /= C) .or. C < 0.0 .or. C > n_CO2) then
894         C = C_old
895     end if
896
897     if ((C2 /= C2) .or. C2 < 0.0 .or. C2 > n_CO2) then
898         C2 = C2_old
899     end if
900
901     if ((O /= O) .or. O < 0.0 .or. O > n_CO2) then
902         O = O_old
903     end if
904
905     if ((O2 /= O2) .or. O2 < 0.0 .or. O2 > n_CO2) then
906         O2 = O2_old
907     end if
908
909     if ((O3 /= O3) .or. O3 < 0.0 .or. O3 > n_CO2) then
910         O3 = O3_old
911     end if
912
913     if ((CO2_plus /= CO2_plus) .or. CO2_plus < 0.0 .or. CO2_plus > n_CO2) then
914         CO2_plus = CO2_plus_old
915     end if
916
917     if ((CO_plus /= CO_plus) .or. CO_plus < 0.0 .or. CO_plus > n_CO2) then
918         CO_plus = CO_plus_old
919     end if
920
921     if ((O3_plus /= O3_plus) .or. O3_plus < 0.0 .or. O3_plus > n_CO2) then
922         O3_plus = O3_plus_old
923     end if
924
925     if ((O2_plus /= O2_plus) .or. O2_plus < 0.0 .or. O2_plus > n_CO2) then
926         O2_plus = O2_plus_old
927     end if
928
929     if ((O_plus /= O_plus) .or. O_plus < 0.0 .or. O_plus > n_CO2) then
930         O_plus = O_plus_old
931     end if
932
933     if ((O2_minus /= O2_minus) .or. O2_minus < 0.0 .or. O2_minus > n_CO2) then
934         O2_minus = O2_minus_old
935     end if
936
937     if ((O_minus /= O_minus) .or. O_minus < 0.0 .or. O_minus > n_CO2) then
938         O_minus = O_minus_old
939     end if
940
941     if ((CO2_exc /= CO2_exc) .or. CO2_exc < 0.0 .or. CO2_exc > n_CO2) then
942         CO2_exc = CO2_exc_old
943     end if
944
945     if ((O2_exc /= O2_exc) .or. O2_exc < 0.0 .or. O2_exc > n_CO2) then
946         O2_exc = O2_exc_old
947     end if
948
949     if ((O_ad /= O_ad) .or. O_ad < 0.0 .or. O_ad > n_CO2) then
950         O_ad = O_ad_old
951     end if
952
953     if ((M /= M) .or. M < 0.0 .or. M > n_CO2) then
954         M = M_old
955     end if
956
957     if ((S /= S) .or. S < 0.0 .or. S > n_CO2) then
958         S = S_old
959     end if

```

---

```
960      if ((e /= e) .or. e < 0.0 .or. e > n_CO2) then
961          e = e_old
962      end if
963  end if
964 end subroutine kinetics_step
```